Temperatures inside SKB and Posiva type disposal canisters for spent fuel

Kari Ikonen

Temperatures inside SKB and Posiva type disposal canisters for spent fuel

Kari Ikonen, VTT Nuclear Safety

This report concerns a study which was conducted for Svensk Kärnbränslehantering AB (SKB) and Posiva Oy. The conclusions and viewpoints presented in the report are those of the author. SKB or Posiva may draw modified conclusions, based on additional literature sources and/or expert opinions.

This report is published on www.skb.se and www.posiva.fi.

Abstract

The objective of this study was to evaluate the temperature inside spent fuel canisters, when they are disposed of at the vertical KBS-3V-type spent nuclear fuel repository in Forsmark, Sweden or in Olkiluoto, Finland in crystalline bedrock. Four canister types, SKB-BWR, SKB-PWR, Posiva-BWR and Posiva-VVER-440, were studied. The main goal of the study was to determine the temperatures of the cast iron inserts, however, the analyses also obtained the temperatures of the spent fuel assemblies and pellets. The target maximum temperature of the cast iron was set to 125 °C because of the availability of existing material test data.

The structure inside a canister has numerous features: the cast iron insert, steel tubes and fuel assemblies having hundreds of fuel rods and many gas-filled gaps. Heat transfer occurs by conduction in solid materials and gas and by thermal radiation over gas-filled gaps. Very detailed 2D analyses using a quarter model of a canister cross-section were performed. Using the 2D model, the effective thermal conductivity through the fuel rods and surrounding gas in the transverse direction was also determined. This enabled the homogenisation of the fuel assemblies in the thermal modelling, which makes subsequent 2D and 3D analyses easier to perform.

The main target of the study was to investigate the effect of varying decay heat powers of the fuel assemblies in a canister on the temperatures of the cast iron and fuel pellets. This was first studied with 2D models in the full cross-section of a canister at the location, at which the longitudinal decay heat profile of a fuel assembly obtains its maximum value and using the effective thermal conductivity for the homogenized fuel rod array. Cast iron and fuel pellet temperatures with other boundary temperatures are presented in the end of the report. The total power was 1700 W in the BWR and SKB-PWR fuel-type canister and 1370 W in the VVER-440-type canister, corresponding to the heat powers at the moment of disposal. These 2D analyses gave the maximum temperature for the cast iron inserts of 112.7–118.1 °C in the nine analysed cases, and the maximum temperatures of the fuel pellets were 143.4–203.0 °C. The highest fuel pellet temperatures naturally occur only in those assemblies that greatly exceed the average heat power. For uniform decay power assemblies the fuel pellet temperatures varied between 143.5 °C and 165.4 °C. The temperatures inside a canister were also calculated in such cases when the canister surface temperature varies between 60 °C and 140 °C. The results are given in Figure 5-17, in Section 5.6.

One task of the study was to calculate the evolution of the best estimate temperatures of the cast iron and fuel pellets for long periods of time as realistically as possible while also considering the effects of all other canisters in a repository panel. The global repository temperatures were previously determined for the SKB and Posiva repositories in Hökmark et al. (2010) and Ikonen and Raiko (2012). The temperature evolution of the maximum temperature at the lowest point of a canister, which is always in contact with the bentonite buffer, was taken from the global temperature analyses referenced above and used as a boundary condition for the 3D analyses. The temperature distribution on the external canister surface was determined by axisymmetric models, wherein the canister, the surrounding air-filled and pellet-filled gaps, the bentonite buffer and the host rock were considered. Varying heat powers of the fuel assemblies in a canister were studied in the same manner as in the 2D analyses for the nine pre-defined cases.

The 3D analyses corresponding to circumstances in the repositories for long durations gave the maximum temperature of the cast iron inserts of 103.9–108.9 °C for different canister types and varying decay heat powers of the fuel assemblies in a canister and the maximum temperatures of the fuel pellets were 134.4–182.7 °C. The maximum temperatures of the cast iron appear after 10–12 years, and those of the fuel pellets are obtained after 4 years or earlier following the disposal of the canister at the repository. The 3D analyses gave clearly lower temperatures than did the 2D analyses. The main reason for this is, that in the 2D, the temperature of the outer radius of the canister was conservatively set to a constant, 100 °C, and the decay heat was set to correspond to the power at the moment of canister disposal, in contrast, in the 3D analyses, the actual evolution of the outer surface temperature and the decreasing decay heat power of the individual fuel assemblies were considered. In addition, in 3D modelling, part of the decay heat escapes through the top and bottom ends of the canister.

Various sensitivity analyses were performed, e.g., concerning the geometric eccentricity between the copper shell and the cast iron insert, the eccentricity of the fuel assembly in the compartment and the effect of an unintended hollow in the cast iron insert material. These studies showed that the target maximum temperature of 125 °C for the cast iron is not reached in any investigated case. One sensitive parameter is the average gap width between the insert and the cylindrical copper wall. The nominal average gap width is 1.5 mm; however, if the average gap width were approximately 3.5 mm, the target maximum temperature of 125 °C for the cast iron could be reached. This emphasizes the importance of maintaining strict tolerances for gap measures.

As a conclusion, the analyses show that the variation of the decay power of the fuel assembly does not, remarkably, change the cast iron temperature, as far as the sum decay power for a canister is constant. Further, the simulation of the evolution of the temperatures in the repository showed that the temperatures of 104 – 109 °C in the cast iron remain below the target maximum temperature of 125 °C in the analysed cases under given assumptions. The maximum temperature in the copper shell is about 97 °C.

Sammanfattning

Målet med den här forskningen var att undersöka kärnbränsle kapslarnas innertemperatur, när kapslarna deponeras enligt KBS-3V-lösningen i upprätt riktning i de kärnbränsleförvar som planeras i Forsmark och i Olkiluoto. Fyra olika kapseltyper undersöktes, SKB-BWR, SKB-PWR, Posiva-BWR and Posiva-VVER-440. Undersökningens huvudmål var att bestämma temperaturen på kapselns gjutjärn insats, men undersökningen inkluderar också analyser på temperaturen av använda bränsle-elementen i kapseln. Maximala tillåtna innertemperaturen sätts till 125 °C, på grund av att det inte finns bakgrundsdata på mekaniska egenskaper för högre temperaturer.

Slutförvaring kapselns uppbyggnad är komplex. Kapseln består av en gjutjärninsats, stålrör och bränsleelement bestående av hundratals bränslestavar, och mellanrummet fylld med gas. Värmen sprids i de fasta materialen och i gaser via värmeledning, och värmen sprids över mellanrummen fyllda med gas via värmestrålning. Temperaturen på kapselns tvärsnitt analyserades noggrant med en detaljerad fjärdedels 2D modell. En 2D modell användes också till att beräkna den effektiva värmeledningen genom bränslestavarna och omgivande gasen i transversell riktning. Den här metoden möjliggör homogenisationen av bränsleelementen, vilket underlättar där på följande 2D och 3D analyser.

Undersökningens huvuduppgift var att studera bränsleelement med olika värmeeffekt och deras inverkan på gjutjärnets och bränslets temperatur. Värmeeffektens inverkan undersöktes först med hela 2D-tvärsnitts modeller av kapseln där snitten lagts där den longitudinella värmeeffekt profilen av ett bränsleelement uppnår sitt maximala värde. Totala effekten var 1700 W för BWR och SKB-PWR och 1370 W för Posiva-VVER-kapseltypen. Dessa värmeeffekter motsvarar kapselns värmeeffekt under installeringen av kapslarna. Beräkningarna i 2D gav en maximitemperatur mellan 112,7 och 118,1 °C för gjutjärnet och bränslets maximitemperatur var mellan 143,4 och 203,0 °C. Nio olika fall beräknades i 2D analysen. De högsta temperaturerna för bränslet förekommer endast då det finns bränsleelement med onormalt hög värmeeffekt. Bränslets maximitemperatur varierar mellan 143,5 och 165,4 °C för element med likformig värmeeffekt. Temperaturerna inne i kapsel beräknades också i sådana fall, i vilka kapselhöljets temperatur varierade mellan 60 °C och 140 °C. Resulterande temperaturer ges i figur 5-17 i kapitel 5.6.

En annan uppgift av undersökningen var att så realistiskt som möjligt beräkna temperaturen av gjutjärnet och bränslet över en lång tidsperiod genom att också i beaktande inverkan av andra kapslar. Värmehistorien för slutförvaring i Forsmarks och Olkiluoto har bestämts tidigare i Hökmark et al. (2010) och Ikonen och Raiko (2012), och användes till 3D modellens kontaktyta. Bentonitens temperatur är som högst i kontaktytan mellan kapseln och bentoniten. Temperaturfördelningen på kapselns yta bestämdes med en axisymmetrisk modell, där kapseln, omgivande luften och utrymmet mellan pelletarna, bentoniten, och urberget tas i beaktande. Värmeeffektens fördelning i bränsle-elementens längdriktning bestämdes med en axisymmetrisk modell som gav ett randvillkor för ytan av 3D modell på kapseln. De nio fall som tidigare undersökts med 2D modellen analyserades med 3D modellen. 3D analyserna gav som gjutjärnets maximitemperatur 103,9 och 108,9 °C och som bränslets maximitemperatur 134,4 – 182,7 °C. Gjutjärnet uppnår de högsta temperaturerna efter 10–12 år, och bränslet före 4 år efter installeringen av kapseln.

Olika typer av känslighetsanalyser gjordes för excentriciteten av kopparhöljet och gjutjärnsinsatsen, bränsleelementens excentriska position inom stålröret, samt inverkan av tomrum i materialet som formas under tillverkningen. Undersökningen visade att gjutjärnets tillåtna maximitemperatur 125 °C inte nås i de granskade fallen. En inverkande parameter är utrymmet mellan kopparhöljet och gjutjärnsinsatsen. Utrymmets nominala bredd är 1,5 mm, men om dess bredd är 3,5 mm kan man uppnå gjutjärnets maximala temperatur på 125 °C. Det här understryker viktigheten av noggranna tillverkningstoleranser.

Sammanfattningsvis kan man från de gjorda analyserna konstatera att bränsleelement med varierande värmeeffekt inte ändrar gjutjärnets temperatur särskilt mycket, så länge som den sammanlagda värme-effekten förblir konstant. Simuleringarna av kapselns temperaturutveckling i slutförvaringstillstånd visade att gjutjärnets maximitemperatur 104 – 109 °C stannar under den tillåtna maximitemperaturen 125 °C i de undersökta fallen och med de gjorda antagandena. Den högsta temperaturen i kopparhöljet blev ungefär 97 °C.

Tiivistelmä

Tämän tutkimuksen tavoite on määrittää ydinpolttoaineen loppusijoituskapselien sisäosien lämpötilat, kun kapselit sijoitetaan KBS-3V-ratkaisun mukaisesti pystyasentoon Forsmarkin tai Olkiluodon loppusijoitustilaan peruskalliossa. Tarkastellut kapselityypit ovat SKB-BWR ja SKB-PWR sekä Posiva-BWR ja Posiva-VVER-440. Tarkastelujen päätavoite on kapselien valurautaisen sisärungon lämpötilojen määritys, mutta analyysien tuloksena saadaan myös polttoaineen lämpötilan kehittyminen pitkällä aikavälillä. Valuraudan sallituksi maksimilämpötilaksi on asetettu 125 °C, johon lämpötilaan asti valuraudan materiaalitestaustietoja on käytettävissä.

Loppusijoituskapselin rakenne on hyvin monimutkainen sisältäessään valurautarungon, teräsputket ja polttoaine-elementit ja suuren määrän kaasutäytteisiä rakoja. Lämpö siirtyy kiinteissä materiaaleissa johtumalla sekä kaasussa johtumalla ja säteilemällä rakojen yli. Kapselin poikkileikkauksen neljännestä tutkittiin hyvin yksityiskohtaisella 2D-mallilla. 2D-mallilla määritettiin myös polttoaineen efektiivinen poikittainen lämmönjohtumiskerroin. Tämä homogenisointi helpottaa varsinaisia 2D- ja 3D-analyysejä.

Tutkimuksen päätavoite oli tutkia eritehoisten polttoaine-elementtien vaikutusta valuraudan ja polttoaineen lämpötiloihin. Valuraudan ja polttoaineen maksimilämpötilat määritettiin varioimalla kapselissa olevien polttoaine-elementtien tehoja pitämällä kuitenkin summatehoa vakiona 1700 W muille kuin Posiva-VVER-kapselityypillä ja vakiona 1370 W Posiva-VVER-kapselityypille. Nämä tehot vastaavat kapselien jälkilämpötehoa sijoitushetkellä. Tehdyt 2D-tarkastelut antoivat valuraudan maksimilämpötilaksi 112,7 – 118,1 °C ja polttoaineen maksimilämpötilaksi 143,4 – 203,0 °C yhdeksässä eri analysoidussa tapauksessa. Kuumimmat lämpötilat esiintyvät vain poikkeuksellisen suuren jälkilämmön omaavissa polttoaine-elementeissä. Saman tehoisten elementtien tapauksessa polttoaineen maksimilämpötilat vaihtelivat välillä 143,5 – 165,4 °C. Kapselin sisäosien lämpötilat laskettiin myös tapauksille, jossa kapselin ulkopinnan lämpötila vaihteli välillä 60 – 140 °C. Tuloksena saadut lämpötilat on esitetty kuvassa 48 luvussa 5.6.

Yksi tehtävä tutkimuksessa oli määrittää mahdollisimman realistisesti lämpötilat valuraudassa ja polttoaineessa pitkän ajan kuluessa ottamalla myös muiden kapseleiden vaikutus huomioon. Kapselin ja bentoniitin kontaktikohtaan kapselin pohjalle, jossa bentoniitin lämpötila on korkeimmillaan, 3D-malliin annettiin aiemmin määritetyt Formarkin ja Olkiluodon loppusijoitukseen liittyvät lämpötilahistoriat (Hökmark et al. 2010, Ikonen and Raiko 2012). Lämpötilajakauma kapselin ulkopinnalla määritettiin aksisymmetrisellä mallilla ottamalla huomioon kapseli, ympäröivät ilma- ja pellettiraot, bentoniitti sekä kallio. Jälkilämpötehon jakautuminen polttoaine-elementin pituussuunnassa määritettiin aksisymmetrisellä mallilla reunaehdoksi kapselin 3D-mallin ulkopintaan. 2D-analyysejä vastaavat yhdeksän tapausta analysoitiin. 3D-tarkastelut antoivat valuraudan maksimilämpötilaksi 103,9 – 108,9 °C ja polttoaineen maksimilämpötilaksi 134,4 – 182,7 °C. Korkeimmat lämpötilat valuraudassa esiintyvät noin 10–12 vuoden jälkeen ja polttoaineessa 4 vuoden tai lyhemmän ajan kuluessa kapselin asentamisesta.

Erityyppisiä herkkyystarkasteluja tehtiin koskien mm. kuparivaipan ja valurautaisen sisustan epäkeskisyyttä, polttoaine-elementin epäkeskeistä sijaintia teräsputken sisällä sekä puutteellisesta täytöstä aiheutuvan valuonkalon vaikutusta lämpötiloihin. Tarkastelut osoittivat, että valuraudan sallittua maksimilämpötilaa 125 °C ei saavuteta missään tutkituissa tapauksissa. Yksi vaikuttava parametri on kuparivaipan ja valurautaisen sisustan keskimääräinen rako. Sen nimellisleveys on 1,5 mm, mutta jos keskimääräinen leveys olisi 3,5 mm, valuraudan maksimilämpötila 125 °C voitaisiin saavuttaa. Tämä painottaa tiukkojen asennustoleranssien tärkeyttä.

Yhteenvetona suoritetuista analyyseistä voidaan todeta, että eritehoiset polttoaine-elementit eivät muuta merkittävästi valuraudan lämpötiloja, kunhan kokonaislämpöteho pysyy vakiona. Kapseleiden lämpötilojen kehittymisen simulointi loppusijoitustilassa osoitti, että valuraudan maksimilämpötila 104 – 109 °C jää sallittavaa maksimilämpötilaa 125 °C alhaisemmaksi tarkastelluissa tapauksissa ja tehdyillä oletuksilla. Kuparivaipan maksimilämpötilaksi saatiin noin 97 °C.

Contents

List of symbols

Latin alphabet

		Unit
A	area	[m^2]
c	thermal heat capacity	[J/kg/K]
F	view factor	[-]
G	radiation flux coming to a considered surface	[W/m^2]
H	actual height of a canister	[m]
J	radiosity	[W/m^2]
P	power	[W]
R, r	radius	[m]
r_0	external radius of canister	[m]
T	temperature	[°C or K]
T_0	canister surface temperature	[°C]
T_{0b}	bentonite surface temperature	[°C]
t	time	[s]
V	volume	[m^3]
x, y, z	Cartesian co-coordinates	[m]

Greek alphabet

		Unit
α	thermal absorptivity	[-]
α	thermal expansion	[1/K]
δ	gap width, displacement	[m]
ε	emissivity	[-]
ε_{tot}	total emissivity	[-]
ϕ	thermal heat flux	[W/m^2]
Φ	volumetric heat generation	[W/m^3]
λ	thermal conductivity	[(W/m)/K]
v	thermal diffusivity, n = 1/(rc)	[m^2/s]
ρ	density	[kg/m^3]
σ	Stefan-Boltzmann constant = 5.6697×10^{-8}	[W/(m^{2}K^4)]

Special notation

BWR	boiling water reactor (ASEA BWR type reactor)
SKB-PWR	pressurized water reactor (Westinghouse type)
VVER	Russian type pressurized water reactor VVER-440 (in Loviisa)
LO1-2	Loviisa units 1 and 2 (VVER-440)
OL1-2	Olkiluoto units 1 and 2 (BWR)
2D	two-dimensional
3D	three-dimensional
SKB	Svensk Kärnbränslehantering AB, Sweden
Posiva	Posiva OY, Finland

1 Introduction

This study was performed at the Technical Research Centre of Finland (VTT) for Posiva Oy on contract.

The goal of this study was to determine the temperatures inside spent fuel canisters (Figure 1-1) that are disposed of vertically in the horizontal tunnels in bedrock. The maximum temperatures are of greatest interest, however, the long-term evolution of the temperatures is also obtained. The analyses were performed in a very detailed manner using 2D and 3D numerical models.

In BWR and VVER canisters, there are 12 fuel assemblies, and in an SKB-PWR canister, there are 4 fuel assemblies. The canister consists of two major components: the massive nodular graphite cast iron insert and the corrosion-resistant shell composed of oxygen-free copper.

The main target of the work was to investigate the effect of varying decay heat powers of fuel assemblies in a canister on the temperatures of cast iron and fuel pellets. One task of the study was to calculate the best estimate evolution of the temperatures of the cast iron and fuel pellets for long periods of time considering the effect of all the other canisters in a repository panel.

Figure 1-1. *Canister types for VVER, BWR and PWR spent fuel assemblies with 12, 12 and 4 assembly positions in each canister.*

1.1 Scope of the study

The objective of this work was to determine the temperatures inside spent fuel canisters. The structure inside a canister has numerous details: the cast iron insert, steel tubes and fuel assemblies having hundreds of fuel rods and many gas-filled gaps. In addition, the temperatures outside the canister, resulting from the other canisters in a canister panel, affect the internal temperature of the canister. To solve this problem, various analysis phases need to be combined.

This report contains the following items:

1) Initial data for the analysed cases and the principles underlying the calculation method (Chapters 2 and 3).

2) 2D analysis of the fuel canister sections (Chapter 4).
   – Detailed analysis of one quarter of a canister.
   – Calculation of the effective transverse conductivity in a fuel assembly.

3) 2D cross-sectional analyses with homogenized fuel model and using effective thermal transverse conduction (Chapter 5).
   – Study of varying fuel assembly decay heat powers in the canisters (9 cases). The total decay heat power is the initial power 1700 W in the BWR and SKB-PWR fuel type canister and 1370 W in the VVER-440 type canister.
   – The temperature of the canister outer radius was conservatively set to 100 °C. The temperatures inside a canister were also calculated in such cases when the canister surface temperature varies between 60 °C and 140 °C.

4) 3D analyses being the main results of the study (Chapter 6).
   – Determining the long-term temperatures of the cast iron and in fuel pellets as realistically as possible by considering the effect of all other canisters in a repository panel.
   – Varying the heat powers of the fuel assemblies in a canister in the same fashion as in the 2D analyses (9 cases). Varying the pre-cooling times and related decreasing decay heat power rates of the individual fuel assemblies.
   – Using the evolution of the maximum bentonite buffer temperature at the lowest point of a canister (always in contact with the buffer) as known input data and determined earlier for the SKB and Posiva repositories.

5) Sensitivity studies (Chapter 7).
   – Conducting various sensitivity analyses, e.g., concerning the thermal effect of the geometric eccentricity between the copper shell and the cast iron insert, the eccentricity of a fuel assembly in the compartment and the effect of an unintended hollow in the cast iron insert material.

2 Initial data

In the following, the geometry of the canister and fuel assemblies, the thermal properties of the materials, the emissivity of radiating surfaces and the decay heat power are presented.

Figure 2-1 presents typical BWR, VVER-440 and PWR fuel assemblies. For instance, in a BWR fuel assembly, there may be 8×8, 9×9, 10×10 or 11×11 fuel rods. The lattice design is changed to improve neutron economy. In a VVER-440 fuel assembly, there are 127 fuel rod positions (the central position is for a tie rod) in a hexagonal grid. Later in this text, VVER-440 is abbreviated as VVER. In a SKB-PWR fuel assembly, there are $17 \times 17 = 289$ rod positions (of which 24 positions are for the control rods) in a rectangular lattice. There are several variations for all the fuel types, but SKB and Posiva have selected typical fuel assemblies for every reactor type for design purposes; see Table 2-1.
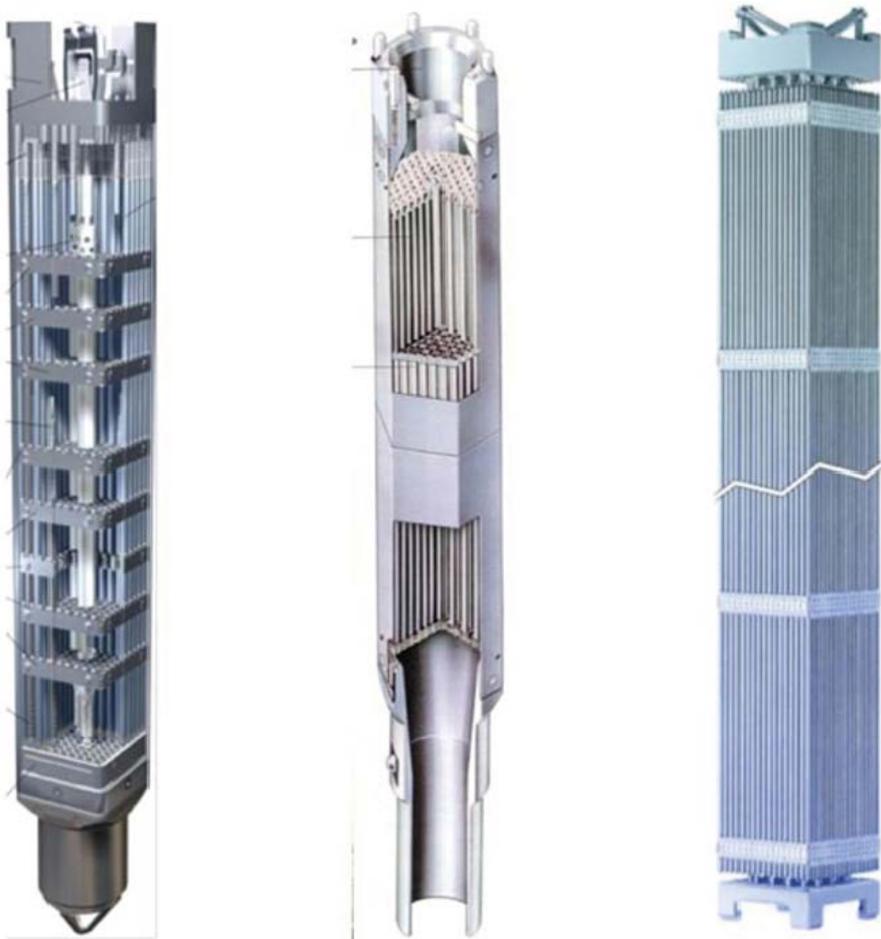
Figure 2-1. *Schematic diagrams of partly cut-open BWR, VVER and PWR fuel assemblies (Raiko 2012). Figures are schematic and not in scale.*

2.1 Geometry of canisters and spent fuel assemblies

Figure 2-2 shows the nominal cross-sectional dimensions of the canister inserts. The insert is made of nodular graphite cast iron in one piece. The fuel assemblies are inserted into holes dimensioned and formed either for Posiva-BWR or Posiva-VVER fuel assemblies. The openings in the insert are formed with square or circular steel tubes set in the mould before casting. Figure 2-3 shows the SKB-PWR insert.

SKB and Posiva have so far more than 20 slightly variable versions of BWR fuel assemblies. And future years are to produce even more versions, most probably. There are several fuel assembly manufacturers who all have their own detailed designs and, in addition, in time of several decades, the fuel rod array has changed from 8×8 through 9×9 and 10×10 up to 11×11 designs. However, the main dimensions of the BWR fuel assemblies have been practically the same through all decades, because physically the space for each individual fuel assembly in the reactor core has been the same.

From earlier respective analysis experience it is concluded that the thermal effect outside the fuel channel is not dependent on the fuel rod array but only the sum of decay heat power. The inside details of the fuel assemblies are modelled, however, in detail for typical generic geometry to introduce also the maximum temperature of the fuel pellets in the central area of the fuel assembly in cooling conditions existing in canister insert with shield gas environment. To make all the thermal analyses with reasonable number of fuel assembly variations, typical modern fuel assembly designs are introduced by the customer to be used for each reactor type (BWR, PWR and VVER).
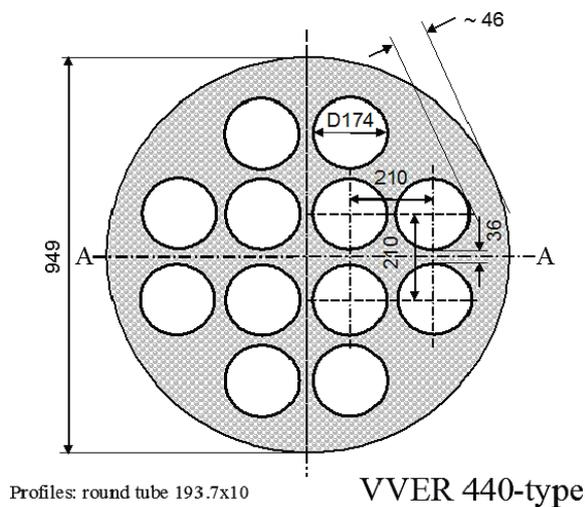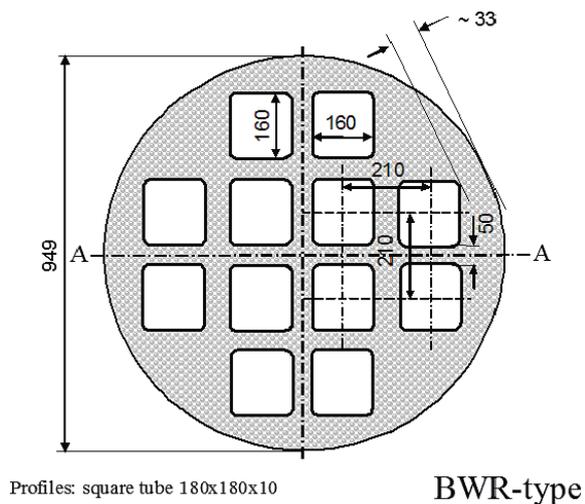
Figure 2-2. Cross-sectional dimensions of the Posiva-BWR and Posiva-VVER canister inserts (Raiko 2012).
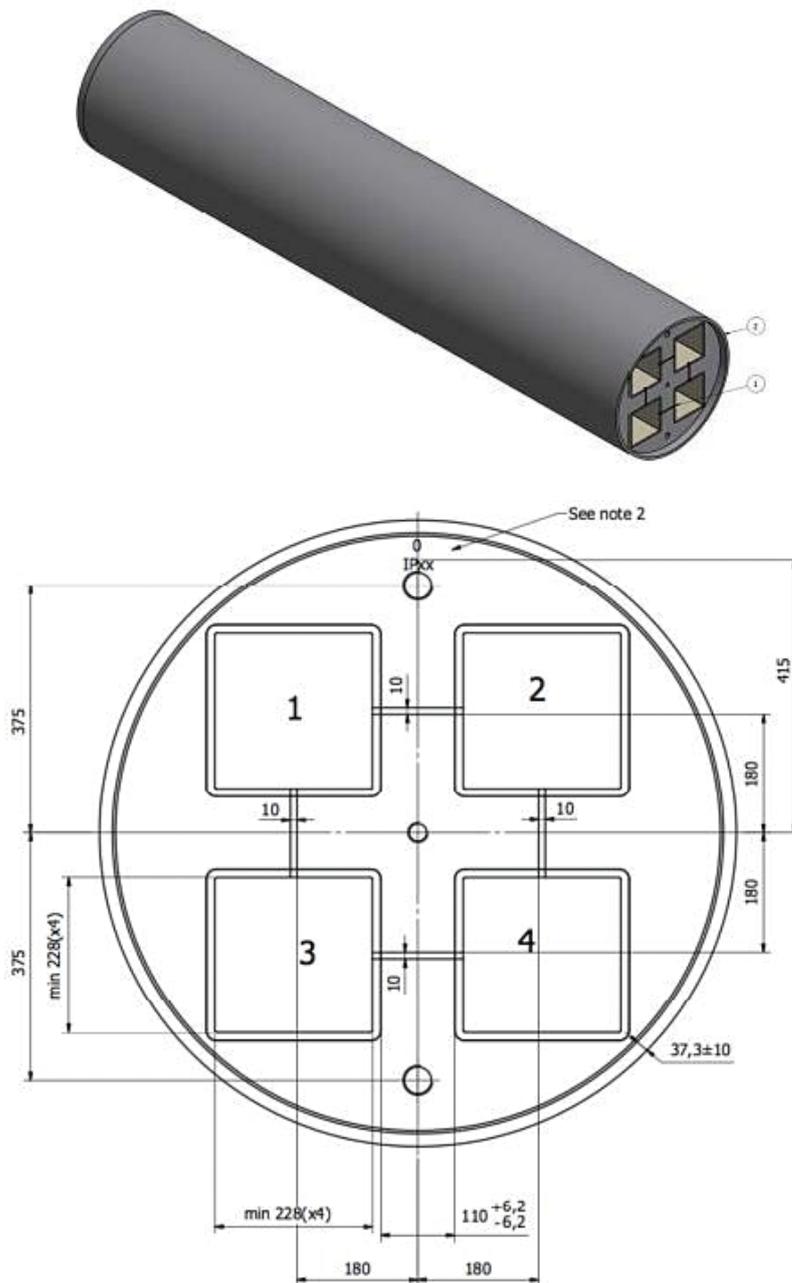
Figure 2-3. *Cross-sectional dimensions of the SKB-PWR canister insert. The current specified minimum size of the compartment channel is 229.9 x 229.9 mm.*

The number of existing design variations for actual PWR and VVER type fuel assemblies are less and the differences between them are minor than for BWR fuel assemblies.

SKB introduced (Jonsson and Junéll 2017) the GE14 type BWR fuel assembly and for variation calculation an older AA 8 × 8 BWR fuel assembly. For PWR fuel analyses the F17 × 17 type fuel assembly was introduced.

Posiva has earlier (Ikonen and Raiko 2012) introduced generic fuel assemblies for BWR and VVER type fuel assemblies for thermal analyses and the same types are used in this study.

The initial data of the SKB-BWR, SKB-PWR, Posiva-BWR and Posiva-VVER fuel canisters used in the analyses are given in Tables 2-1 and 2-2. Details in the longitudinal direction of the canisters are shown later in Figures 6-16 to 6-18.

Table 2-1. Dimensions of the typical SKB fuel assemblies (Jonsson and Junéll 2017, SKB 2010, Table A-3) used in the analyses and of the Posiva reference fuels (Raiko 2012, (Nuclear Engineering International 2011). All dimensions are nominal and given in units of mm.

	SKB-BWR GE14	SKB-BWR AA	SKB-PWR F17×17	Posiva-BWR	Posiva-VVER
Fuel rod array	10×10	8×8	17×17	10×10	127 HEX
Rod external diameter	10.3	12.3	9.5	10.3	9.1
Rod cladding thickness	0.66	0.8	0.57	0.605	0.65
Fuel rod pitch	13	16.3	12.6	13	12.3
Fuel channel ext. width	137	139	-	139	144
Fuel channel plate thickness	1.65	2.3	-	2.5	2
Active length of fuel rod	3680	3712	3658	3700	2420

Table 2-2. Main dimensions of the SKB canisters (Raiko et al. 2010) and of the Posiva canisters (Raiko 2012). All dimensions are nominal and given in units of mm.

	SKB-BWR	SKB-PWR	Posiva-BWR	Posiva-VVER
Cast iron thickness between channel tubes	30	110	30	16.3
Distance between compartment centres	210	370	210	210
Compartment size (inside width)	160	235	160	173.7
Steel channel tube wall thickness	10	12.5	10	10
Inside length of cast iron insert	4463*)	4443*)	4455**)	3245**)
Total length of canister	4835*)	4835*)	4752**)	3552**)

*) Raiko et al. 2010, Tables 5-1, 5-2, 5-3, 5-4, pp 35–36.

**) Raiko 2012, Tables 3, 5, 6, pp 39–43.

The gap clearance between the pellet and the zircaloy or zirconium cladding in the spent fuel is assumed to be zero because the original gap in fresh fuel is assumed to be closed for spent fuel due to the swelling of the pellets during operation. The oxide layer thickness is very small, approximately 0.05 mm, and primarily affects the thermal emissivity of the surface.

For all the fuel canisters mentioned above in Table 2-2, the cylindrical copper shell outer diameter is 1 050 mm, the copper shell inner diameter is 952 mm (wall thickness of 49 mm in the cylindrical part and 50 mm in the lids), and the cast iron insert external diameter is 949 mm.

The nominal decay heat power at the moment of encapsulation is 1700 W for both the BWR and SKB-PWR canisters and 1370 W for the Posiva-VVER canister.

The nominal gap width of 1.5 mm between the copper and cast iron is for the cylindrical part on the canister and a gap of 2 mm is used for the upper end of the canister between the steel lid and the copper.

Figure 2-4 shows the cross-section of the reference Posiva-BWR fuel assembly, the surrounding zirconium fuel channel and the hexagonal Posiva-VVER fuel assembly cross-section with 127 rod positions surrounded by the zirconium fuel channel and the 10-mm-thick circular steel tube. The central rod in the Posiva-VVER fuel assembly is an empty tie rod. In a SKB-PWR fuel assembly there are 17×17 = 289 fuel rod positions, of which 24 are guide tubes for the control rods. The assemblies may be disposed together with the control rod clusters, when applicable.
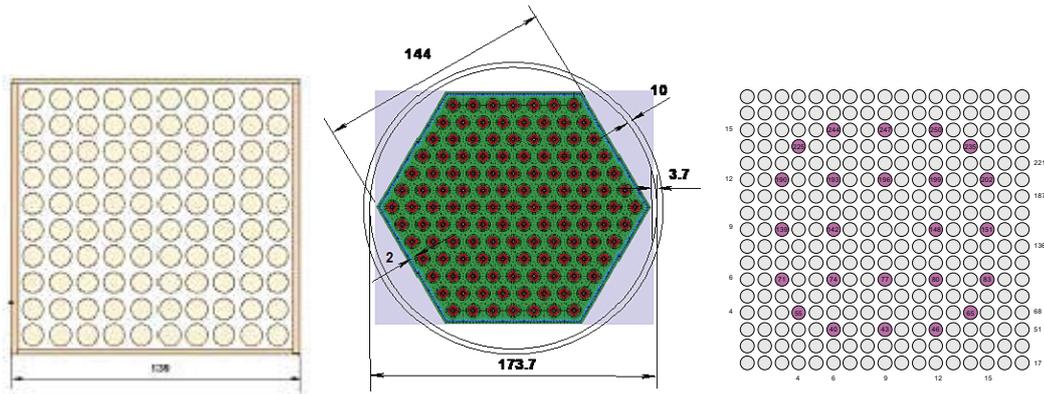
Figure 2-4. Posiva-BWR fuel assembly surrounded by the fuel channel (left), Posiva-VVER-440 fuel assembly cross section and surrounding steel tube (middle) and SKB-PWR fuel assembly (right). Figures are not in scale.

2.2 Thermal properties of the materials

The units of the thermal parameters are presented in the symbol list at the beginning of this report.

The thermal properties of the materials are taken from MATPRO (2014). The subroutine FTHCON in MATPRO (2014) was applied to calculate the thermal conductivity of the pellets. Figure 2-5 shows the temperature dependence of the thermal conductivities of the SKB-BWR, SKB-PWR, Posiva-BWR and Posiva-VVER fuel pellets (burn-up values are listed in Table 2-6). For the analyses, only conductivities below 300 °C are of interest. The fittings for the curves in Figure 2-5 were formed (λ in W/m/K and T in Celsius < 300 °C) and are for UO_2.

$$\lambda_{BWR\ and\ VVER} = 3.93 - 3.43 \times 10^{-3}\ T + 2.27 \times 10^{-6}\ T^2$$

$$\lambda_{SKB-PWR} = 3.21 - 1.93 \times 10^{-3}\ T. \tag{2-1}$$

These curves are used in the analyses of the thermal conductivity of the fuel pellets. SKB-PWR fuel pellets are characterized by, in the reference case, higher burn-up (60 MWd/kgU), which damages the pellet material and causes micro-cracking of the material and decreases the thermal conductivity.

The thermal conductivity of the fuel pellets affects the longitudinal heat transfer inside a fuel rod. Fuel pellets are assumed to be in contact vertically, although there may be some deformations and micro-cracking in the material.
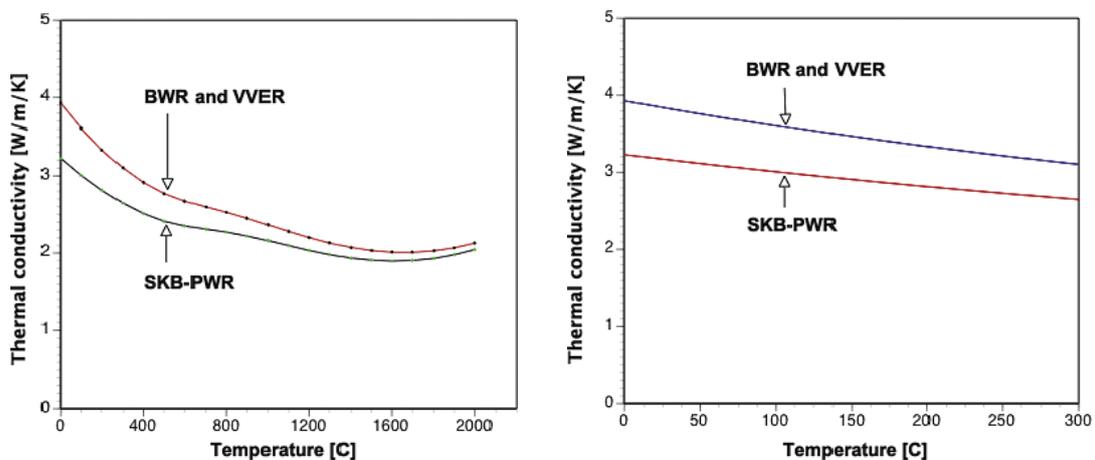
Figure 2-5. Thermal conductivity of the spent fuel pellets (MATPRO 2014).
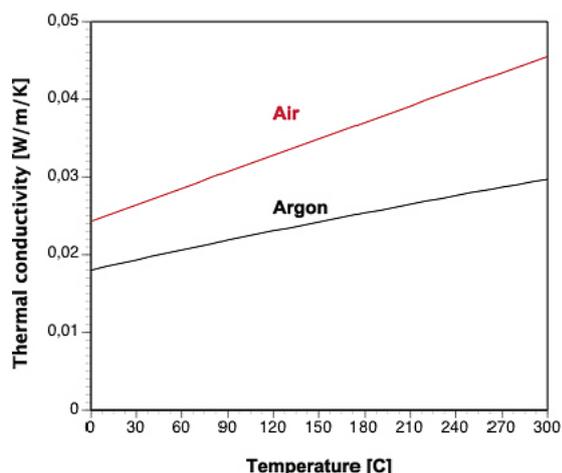
Figure 2-6. *Thermal conductivity of argon (MATPRO 2014) and air (Fletcher 1991) at atmospheric pressure.*

All voids and gaps in the canister structure are filled with argon gas. According to the current SKB requirement the air inside the canister shall be replaced by argon, so that at least 90 % of the atmosphere inside the canister consists of argon. The residual air content is thus 10 %, at maximum. The gas atmosphere of the inside of the insert is changed from air to argon as a part of the spent fuel encapsulation procedure (Raiko 2012). The gas content of the gap between the outer surface of the insert and the copper shell is assumed, according to the current plans of the friction-stir-welding process, to be changed from air to argon gas that is used as an inert shield gas during the copper-lid-welding process. The thermal conductivity of argon at atmospheric pressure (Figure 2-6) is used in the analyses and is given by the following function in MATPRO (2014) (l in W/m/K and T in Kelvin):

$$\lambda(T) = 4.092 10^{-4} \ T^{0.6748} \tag{2-2}$$

According to MATPRO (2014) the thermal conductivity of zircaloy for SKB-BWR and Posiva-BWR and the thermal conductivity of the ZrNb-1 alloy for SKB-PWR and Posiva-VVER (Zr, 1 % Nb) are (T in Kelvin)

$$\lambda_{BWR} = 7.51 + 0.0209 \cdot T - 1.45 \times 10^{-5} \ T^2 + 7.67 \times 10^{-9} \ T^3$$

$$\lambda_{SKB\text{-}PWR \text{ and } VVER} = 15.0636 \ e^{0.000461843} \ T. \tag{2-3}$$

Figure 2-7 shows the thermal conductivity of zircaloy and zirconium.

Table 2-3 shows the thermal conductivities of the other materials. The bottom and top end structures of the fuel assemblies are composed of stainless steel (Figures 6-16 to 6-21).

Table 2-3. Thermal conductivities of other materials used in the analyses.

Copper (pure) conductivity *)	390	W/m/K
Cast iron conductivity **)	35.5	W/m/K
Steel conductivity ***)	57.5	W/m/K
Stainless steel conductivity ****)	15.0	W/m/K
Zirconium oxide conductivity	2	W/m/K

*) http://www.engineeringtoolbox.com/thermal-conductivity-metals-d_858.html

**) Average of standard values (SFS3395) and (SS140717).

***) Average of (Rautaruukki 1996).

****) (Gauntt et al. 2005) (the conductivity is very specific to alloy contents).
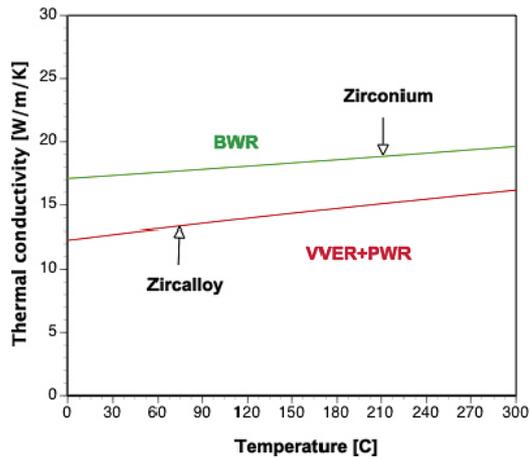
Figure 2-7. *Thermal conductivity of zircaloy and zirconium (MATPRO 2014).*

Table 2-4 shows the volumetric thermal capacities of the materials inside a canister and of the bentonite buffer that are used in the analyses.

Table 2-4. Volumetric thermal capacities used in the analyses.

Argon *)	858	$J/m^3/K$
Bentonite	2.4	$MJ/m^3/K$
Copper (pure) **)	3.45	$MJ/m^3/K$
Cast iron **)	3.22	$MJ/m^3/K$
Steel **)	3.85	$MJ/m^3/K$
Stainless steel ***)	4.06	$MJ/m^3/K$
Zirconium **)	1.97	$MJ/m^3/K$

*) http://www.engineeringtoolbox.com/specific-heat-capacity-gases-d_159.html

**) http://www.engineeringtoolbox.com/specific-heat-metals-d_152.html

***) http://www.azom.com/properties.aspx?ArticleID = 965

2.3 Emissivity of surfaces

The emissivity of a metallic surface depends strongly on the quality of the surface. A polished copper surface has an emissivity of approximately 0.02, a clean and machined surface has been tested (SKB 2004) to have an emissivity of 0.06–0.11, and the emissivity of oxidised surface is approximately 0.6. In the analyses, the emissivity of the internal copper surface in the gap between the copper and the cast iron insert is assumed to be 0.1. The external surface between the copper and bentonite buffer is oxidized in practise and a value 0.3 for the emissivity is used for the outer surface.

Table 2-5 shows the surface emissivities applied in the analyses.

Table 2-5. Surface emissivities used in the analyses.

Emissivity of fuel rod surfaces (crud)	0.7 for all except 0.6 for VVER
Emissivity of fuel channel surfaces (crud)	0.6 *)
Emissivity of steel surfaces (red rusty)	0.6 *)
Emissivity of cast iron surface	0.6 *)
Emissivity of machined copper, inner surface	0.1 *)
Emissivity of machined copper, outer surface	0.3

*) http://www.raytek.com/Raytek/en-r0/IREducation/EmissivityTableMetals.htm and http://www.omega.com/literature/transactions/volume1/emissivitya.html

Figure 2-8 shows the emissivity of the fuel cladding surface oxide layer as a function of the surface layer thickness. For the Posiva-BWR fuel, the layer thickness is approximately 50 mm. For the VVER reactor, the temperature of the coolant water is lower than the Posiva-BWR fuel; therefore, the oxide layer is thinner, and the emissivity of the Posiva-VVER cladding is assumed to be 0.6 (Table 2-4).
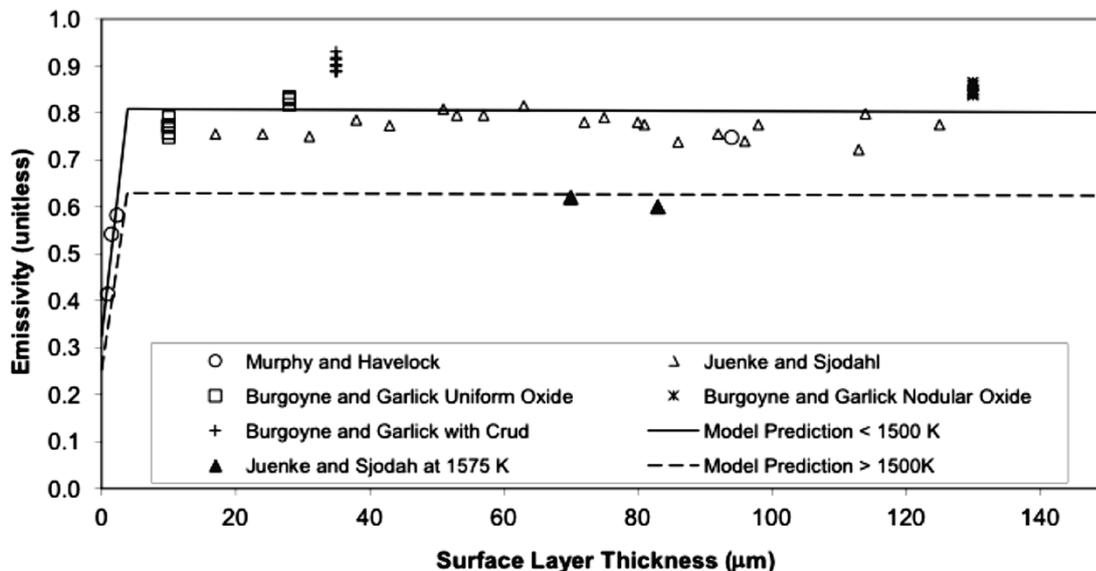
Figure 2-8. *Model-to-data comparison of cladding oxide emissivity (MATPRO 2014, p 3.13).*

2.4 Decay heat power

The decay heat power of the spent fuel was calculated by Anttila (2005) with the ORIGEN-S code (Gauld et al. 2005) of the TRITON functional module (DeHart 2005) of the SCALE programme package (ORNL 2005). Depending on burnup, the decay rate will be approximately linear and constant in a 100-year perspective after about 30–50 years. The decay rate has reached a reasonable level for encapsulation after 30 to 50 years. The decay heat level, which is reasonable, and the total decay power in the canister, will depend on the assemblies to dispose of and their distribution of burnups and ages, the starting time of encapsulation and disposal and the encapsulation and disposal rates. Figure 2-9 and Table 2-6 show the decay power densities of the spent fuels used in the long-term analyses.

The amounts of uranium in the SKB-BWR and SKB-PWR fuel canisters are 2100 kg and 1856 kg, respectively (SKB 2010, Table 2-4). The amounts of uranium in the Posiva-BWR and Posiva-VVER fuel canisters are 2110 kg and 1440 kg, respectively. (Raiko 2012, Table 29, p 129). These values are calculated from the average fuel assembly uranium masses. The thermal power of a canister at a certain time is calculated by multiplying the mass by the decay heat power density given in Table 2-6.

Table 2-6. Decay heat power densities of the SKB spent fuels (Jonsson and Junéll 2017) and of the Posiva spent fuels (Anttila 2005). The cooling time is measured from the moment, at which the fuel is removed from a reactor.

Decay heat [W/tU]

Time [years]	SKB-BWR 40 MWd/kgU	SKB-PWR 60 MWd/kgU	Posiva-BWR 40 MWd/kgU	Posiva-VVER 40 MWd/kgU
10	1340	2160	1339.0	1416.0
20	1040	1660	1036.0	1107.0
30	854	1350	854.4	927.5
40	714	1050	713.8	787.6
50	603	933	602.7	675.9
60	514	787	514.0	586.6
70	443	674	443.0	514.6
80	386	562	386.1	456.5
90	340	515	340.1	409.2
100	303	457	303.1	370.9
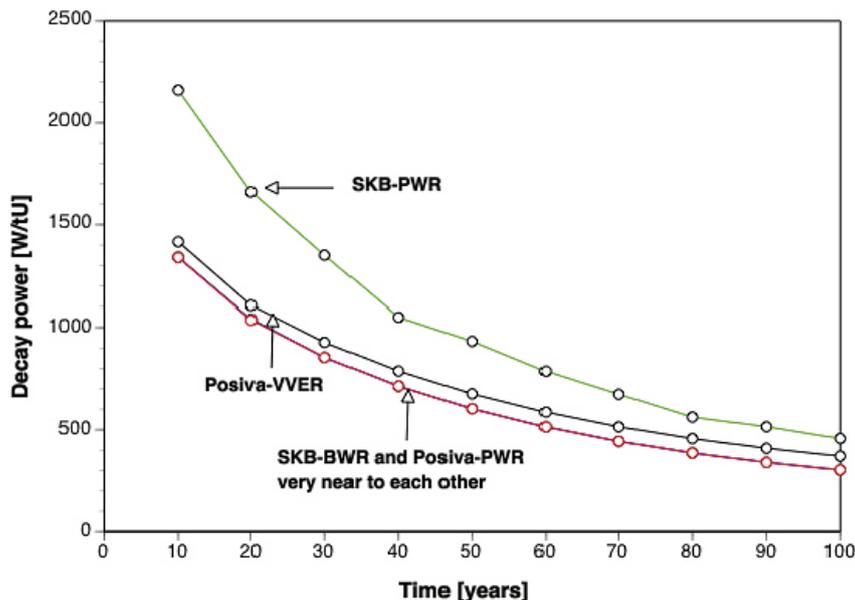
Figure 2-9. *Decay heat power densities of the SKB-BWR and SKB-PWR spent fuel and of the Posiva-BWR and Posiva-VVER spent fuel. The cooling time is measured from the moment, at which the fuel is removed from a reactor. The decay heat is calculated for an equivalent ton of uranium in fresh fuel.*

2.5 Decay heat power density along fuel assemblies

Figures 2-10 to 3-1 show typical conservative decay heat power densities along the fuel assemblies, which are applied in subsequent analyses. These curves were obtained from SKB and from Finnish nuclear power companies.

Table 2-7. Axial decay heat distributions along the SKB-BWR and SKB-PWR spent fuel rods (Viertel and Runevall 2014, Table 2 on page 14 and Table 8 on page 19).

SKB-BWR			SKB-PWR		
TOP	14.85 cm	1.60 %	TOP	46 cm	10.25 %
	93.35 cm	21.41 %		276 cm	79.50 %
	124.00 cm	35.99 %	BOT	46 cm	10.25 %
	124.15 cm	38.86 %			
BOT	14.85 cm	2.04 %			
Total		100.00 %			100.00 %

For all the fuel types the decay heat is expressed as the relative decay heat distribution in Table 2-8. For instance, for the SKB-PWR fuel and in the TOP part, the relative decay heat distribution is 10.25 % × 1700 W/46 cm/(1700 W/(46 cm + 276 cm + 46 cm)) = 0.82.

Table 2-8 summarises the relative decay heat power density distributions.

Table 2-8. Relative decay heat power density ϕ distributions at a distance d measured from the lower end of a fuel rod.

SKB-BWR		SKB-PWR		Posiva-BWR		Posiva-VVER	
d [cm]	ϕ_{rel} [-]	d [cm]	ϕ_{rel} [-]	d [cm]	ϕ_{rel} [-]	d [cm]	ϕ_{rel} [-]
0	0.51	0	0.82	7.36	0.311	13.5	0.665
14.85	0.51	46	0.82	22.08	0.775	38.5	1.044
14.85	1.16	46	1.06	36.8	0.989	88.5	1.125
139	1.16	322	1.06	51.52	1.091	113.5	1.118
139	1.08	322	0.82	66.24	1.149	138.5	1.107
263	1.08	368	0.82	80.96	1.173	163.5	1.094
263	0.86			95.68	1.182	188.5	1.064
356.35	0.86			110.4	1.177	213.5	0.960
356.35	0.4			125.12	1.183	238.5	0.704
371.2	0.4			139.84	1.183		
				154.56	1.182		
				169.28	1.171		
				184.00	1.173		
				198.72	1.167		
				213.44	1.149		
				228.16	1.123		
				242.88	1.110		
				257.6	1.090		
				272.32	1.065		
				287.04	1.027		
				301.76	0.975		
				316.48	0.891		
				331.2	0.762		
				345.92	0.585		
				360.64	0.318		
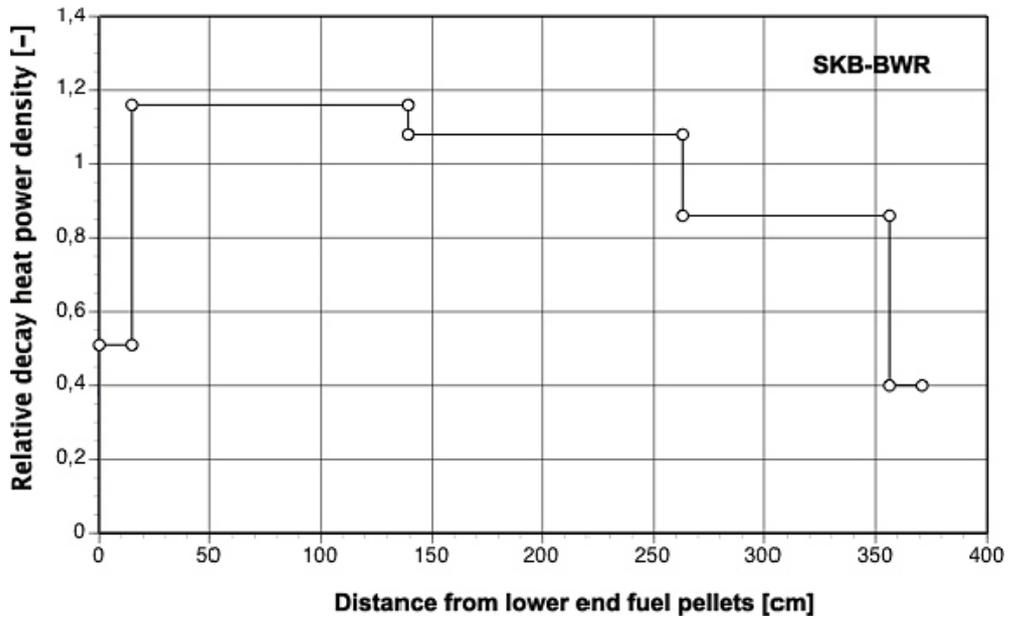
Figure 2-10. *Decay heat power density distribution along the SKB-BWR fuel assembly length.*
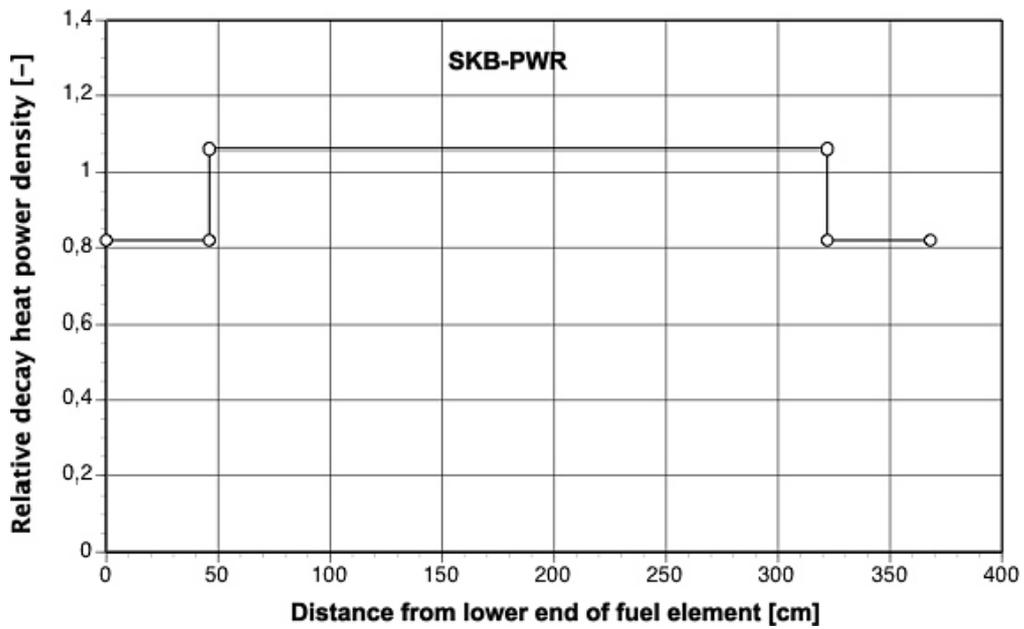
Figure 2-11. *Decay heat power density distribution along the SKB-PWR fuel assembly length.*
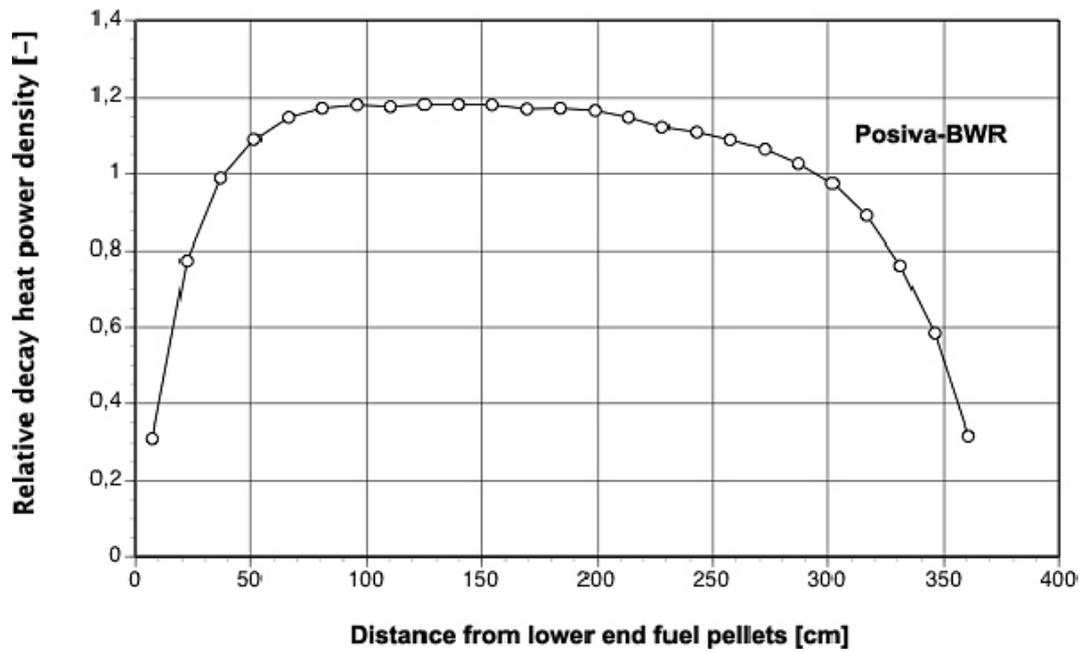
Figure 2-12. *Decay heat power density distribution along the Posiva-BWR fuel assembly length. The active length of the fuel rod is 370 cm.*
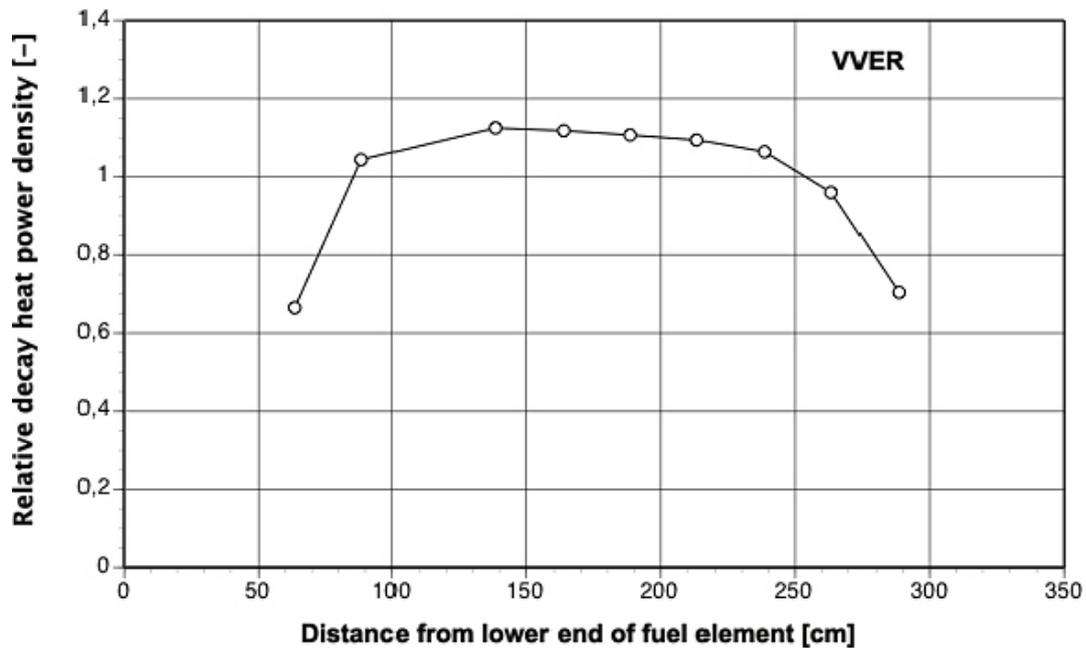
Figure 2-13. *Decay heat power density distribution along the Posiva-VVER fuel assembly length. The active length of the fuel rod is 242 cm.*

3 Calculation method

For the thermal analyses of this research work, 2D, axisymmetric and 3D computer codes are applied with, e.g., numerous special mesh generators. In addition, several auxiliary programmes related to, e.g., visualization, are used. Heat transfer inside a canister is a combination of conduction, radiation and convection. The effect of convection is conservatively neglected because the canisters are closed and because the gaps are relatively narrow. Spacers supporting the fuel rods also hinder the longitudinal vertical gas flows inside the fuel assemblies.

3.1 Control volume modelling of thermal heat transfer

Numerical thermal heat conduction analyses are performed using the control volume method. To this end, in-house 2D and 3D computer codes have been developed. These codes use 4- and 8-node control volumes, respectively. The codes have many special features and are tailored to this research. The programmes are developed for transient analyses. Without going into the details, the equation for a control volume (Figure 3-1) is

$$c_v \frac{\partial T}{\partial t} = \frac{1}{V} \oint_S \lambda \frac{\partial T}{\partial n} \, dS + \Phi, \tag{3-1}$$

where c_v is the volumetric heat capacity ($c_v = \rho c$), T is the temperature of the control volume centre, t is time, V is the volume of the control volume, λ is the thermal conductivity, n is the outward co-ordinate from the surface, S is the surface area and Φ is the volumetric decay heat generation. The fully implicit principle is applied everywhere, an iterative solution method for solving the unknowns is applied, and special mesh generators are developed. The operation of the code is verified through numerous test cases (Ikonen 2006, 2009, 2013), and some test cases are presented in the appendix. The visualization codes were also developed in-house. These codes include features suited for this type of analysis, increase the reliability of different phases of the calculation process, and represent a suitable tool for quality control.
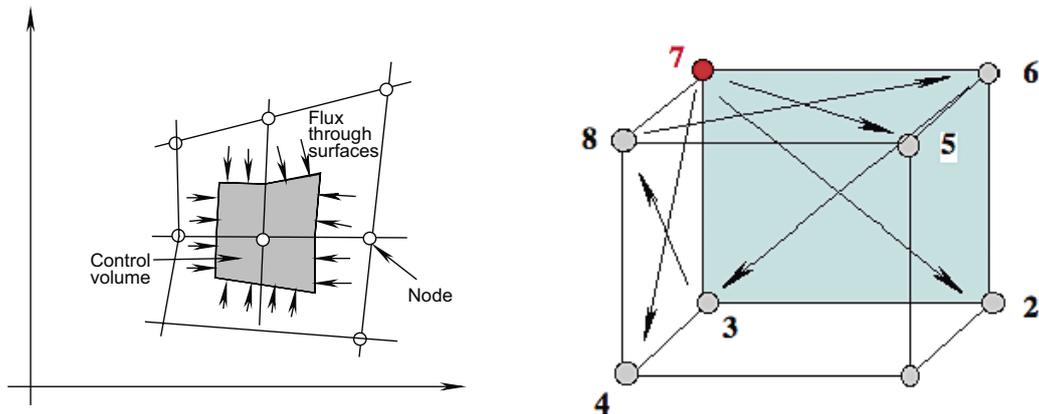
Figure 3-1. Heat fluxes to a planar control volume (left) and 8-node control volume (right).

3.2   Thermal radiation modelling

Thermal radiation between surfaces is an essential heat transfer mechanism inside a canister. Unlike heat conduction electromagnetic waves do not require a medium for their propagation. A black surface is defined as a surface that absorbs all incident radiation. Consequently, all the radiation leaving a black surface is emitted by the surface and is given by the Stefan-Boltzmann law as

$$\phi_b = \sigma T^4, \tag{3-2}$$

where T is the absolute temperature and σ is the Stefan-Boltzmann constant ($\sigma = 5.6697 \times 10^{-8}$ W/m^2/K^4). A black body is an ideal surface. Real surfaces (Figure 3-2) emit or absorb less radiation than do black surfaces and the emittance is given by

$$\phi = \varepsilon \phi_b = \varepsilon \sigma T^4, \tag{3-3}$$

The fraction of incident radiation absorbed is called the absorptivity α. A widely used model of a real surface is the grey surface, which is defined as a surface for which α is a constant, irrespective of the spectrum of the incident radiation. A rigorous definition of a grey surface is the following (Bejan 2003): "Grey surface is a surface for which the spectral radiation properties are independent of wavelength". The fraction of incident radiation reflected is the reflectivity, ρ. If an object is opaque, that is, it is not transparent to electromagnetic radiation, then $\rho = 1 - \alpha$. It will be assumed herein that all surfaces are grey and that they are diffuse emitters, absorbers, and reflectors. Under these conditions $\varepsilon = \alpha = 1 - \rho$. It is further assumed that conduction and radiation through gas produces no interaction. This assumption of transparency is valid for gases such as argon and air (but not, e.g., for steam).

In analysing thermal heat transfer in complicated geometries it is useful to introduce a quantity called the radiosity J:

$$J = \varepsilon \sigma T^4 + \rho G = \varepsilon \sigma T^4 + (1-\varepsilon)G. \tag{3-4}$$

where G is the radiation flux incident onto a considered surface. The radiosity is the net heat flux, which the surface sends towards other surfaces. The details for applying the radiosity in the calculation process are presented in Ikonen (2013).

Basic formulae for the view factor in 2D case and crossed-strings method (Mills 1999) are applied in view factor evaluation. Figure 3-3 demonstrates view factor determination.
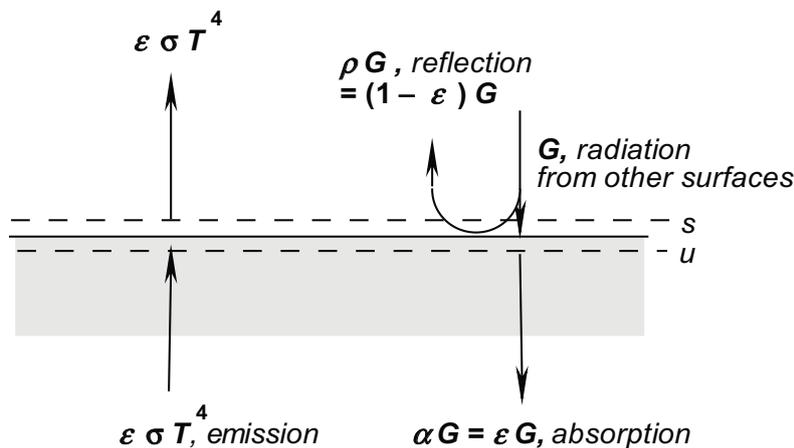
Figure 3-2. *Thermal radiation near a grey surface. It is assumed that the emission and absorption coefficients of a surface are equal, i.e., $\varepsilon = \alpha$.*
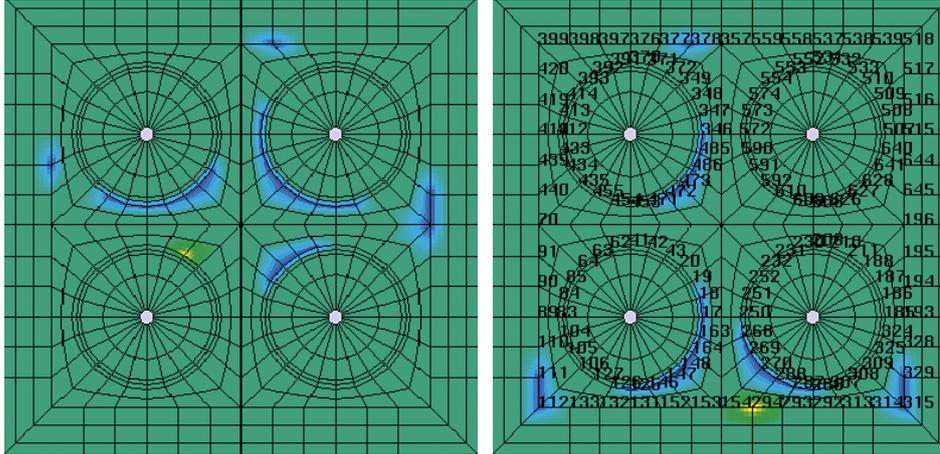
Figure 3-3. *Demonstration of a view factor determination (the yellow point on a cylinder "sees" the blue areas on other cylinders and fuel channel plates).*

3.2.1   Thermal radiation through a narrow gas-filled gap

In a narrow gap, such as the 1.5 mm gap between the copper cylinder and the insert, the thermal radiation is assumed to be in the transverse direction, and the view factor can be set to one. The radiation heat flux ϕ_{rad} between two surfaces close to each other having surface temperatures of T_1 and T_2 is calculated from

$$\phi_{rad} = \varepsilon_{tot}\,\sigma(T_1^4 - T_2^4)\,, \tag{3-5}$$

where the total emissivity is calculated from the formula (Ikonen 2013)

$$\varepsilon_{tot} = \frac{1}{\dfrac{1}{\varepsilon_1} + \dfrac{1}{\varepsilon_2} - 1} = \frac{\varepsilon_1\,\varepsilon_2}{\varepsilon_1 + \varepsilon_2 - \varepsilon_1\,\varepsilon_2}\,, \tag{3-6}$$

where ε_1 and ε_2 are the emissivities of the surfaces. If the emissivity of the copper is, for instance, 0.1 and the emissivity of cast iron 0.6, the total emissivity is 0.094.

Heat transfer by thermal radiation can also be described by the effective thermal conductivity in the transverse direction as follows:

$$\lambda_{eff} \approx \lambda_{argon} + 4\,\delta_{local}\,\varepsilon_{tot}\,\sigma T_{mean}^3\,, \tag{3-7}$$

where δ_{local} is the local gas gap width and T_{mean} is the mean temperature in the gap (the average of the surface temperatures). The effective thermal conductivity increases proportionally to the local gas gap width δ_{local} and increases proportionally to the third power of T_{mean}. In the longitudinal direction only the shield gas thermal conductivity needs to be applied thus indicating a need for orthotropic conduction modelling. The use of the effective thermal conductivity simplifies computer programs; however, it must be noted that heat conduction in 3D is orthotropic (a tensor matrix).

4 Detailed 2D Analysis of fuel canisters and effective transverse conductivity between fuel rods

Thermal heat transfer in the transverse direction through fuel rods is rather weak, especially at low temperature. In the following, initially, one quarter of a canister is analysed; and then, the effective transverse conductivity for homogenized fuel assembly models is determined.

4.1 Analysis of one quarter of a canister

Thermal heat transfer in the cross-section of a canister was studied in a very detailed manner by modelling one quarter of the canister (Figure 4-1). Thermal radiation between surface elements was modelled by considering the interaction of all radiant surfaces. A special computer program, based on the control volume method and using, e.g., the radiosity (Equation 3-4) in treating thermal radiation, was written previously to solve the problem.

An estimate of the extension of the radiation heat effect from a rod to neighbouring rods is obtained from Howell (2001). In that reference, an infinitely large group of cylindrical rods in a square grid is considered and all the rods are at equal temperatures, except of the considered rod (denoted as "1" in Figure 4-2), which, we assume, is at a lower temperature. In a BWR fuel assembly, the distance between fuel rods (pitch) is 13 mm, and the rod external diameter is 10.3 mm. The contribution of the four closest rods in the horizontal and vertical directions (denoted as "2") is 54.4 % of the total heating effect on the considered rod. A total of 35.0 % of the heating effect is caused by four rods in diagonal directions (denoted as "3") and the contribution of eight rods (denoted as "5") is 9.1 %. The remaining 1.5 % of the heating effect is caused by all the other rods located farther away. In the analyses, such rods are ignored.
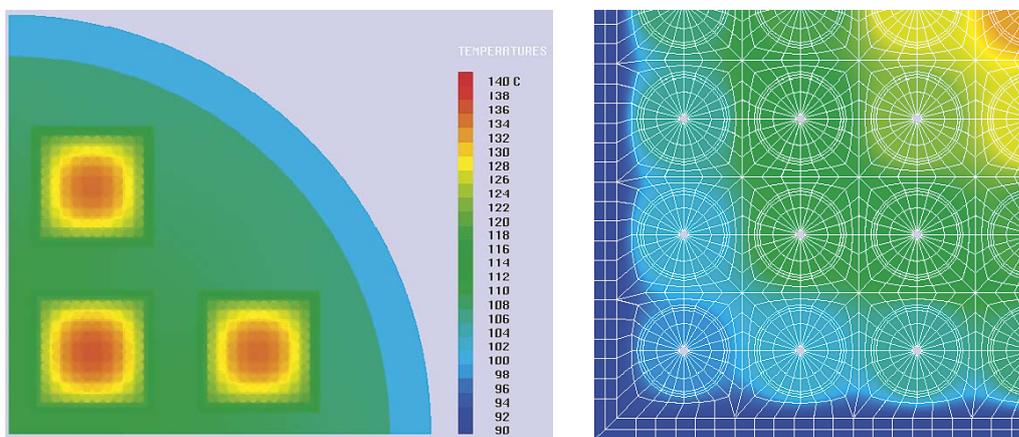
Figure 4-1. *Detailed analysis of the Posiva-BWR canister (Ikonen 2006). The quarter model has approximately 50 000 control volumes.*
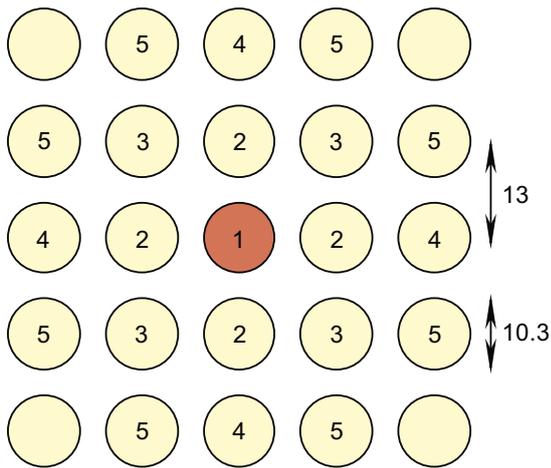
Figure 4-2. *BWR rods and estimation of the radiation heat effect from neighbouring rods on the rod denoted as "1".*

Figure 4-3 demonstrates temperature distributions on a horizontal (or vertical) line passing through the middle points of two fuel assemblies in the Posiva-BWR canister.

The temperature of the outer radius of the canister is set to 100 °C. The internal heat generation of a pellet was calculated by dividing the total decay power of the pellets by the total pellet volume. The active length of the Posiva-BWR fuel rod is 3.7 m. There are $12 \times 10 \times 10 = 1200$ fuel rods in a single canister. The volumetric decay heat generation of Posiva-BWR fuel pellets, when using the dimensions in Table 2-1, is obtained from the equation $\Phi_{BWR} \times 1200$ rods $\times 3.7$ m $\times \pi \times (0.0103/2$ m $- 0.000605$ m$)^2 = 1700$ W, giving $\Phi_{BWR} = 5\,932$ W/m^3.

Figure 4-4 shows the temperature distribution along 45 degrees line in the SKB-PWR canister.

In this case it was assumed that all fuel assemblies are identical, thereby generating equal amounts of decay heat power. Thus it was sufficient to model one quarter of the cross section of a canister when adiabatic (due to symmetry) boundary conditions on the symmetry planes were applied.
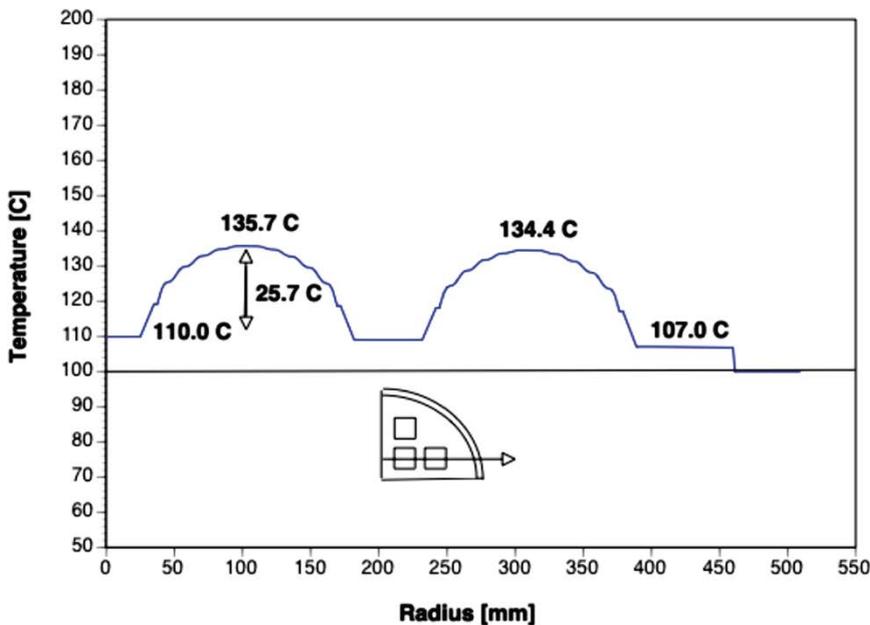
Figure 4-3. *Temperature distributions along horizontal line passing through the middle point of two fuel assemblies in the Posiva-BWR canister.*
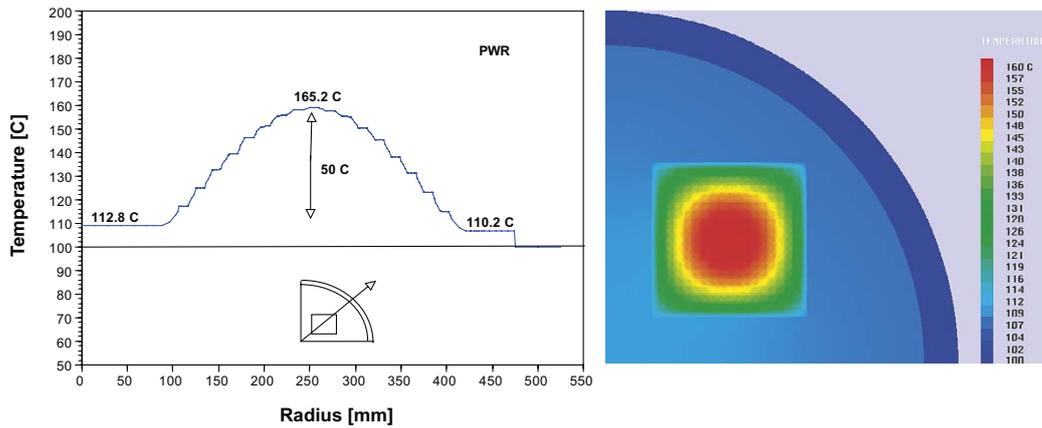
Figure 4-4. *Temperature distribution along 45 degrees line in SKB-PWR canister. The radius denotes the distance from the centre of the canister.*

4.2   Effective transverse conductivity

Detailed thermal radiation in the 3D modelling of an actual fuel assembly would be very complicated. Therefore, the effective thermal conductivity in the transverse direction for homogenized models is determined using detailed 2D models. The idea is to take one fuel assembly, apply a constant temperature at the edges of the model and calculate the temperatures using both a detailed model (Figure 4-5) and a homogenized model formed on the same fuel rod array area. In the homogenized model the effective conductivity is adjusted so that equal maximum temperatures in the middle are obtained by both models. In the homogenized model the heat generation is assumed to be uniformly distributed across the fuel rod array area. The calculation is started from a high edge temperature because temperature differences in the homogenized fuel rod array area are the smallest, and conductivities at lower temperature have no effect on the calculation. Then, applying the lower edge temperature, due to decay heat generation, the temperatures in the middle of the homogenized area are higher and their conductivities are already determined.

Figure 4-5 presents analyses of one Posiva-BWR fuel assembly when the temperature of the outer edges is 100 °C. For the homogenized model, the effective volumetric decay heat generation, assumed to be uniformly distributed, is obtained, when applying the dimensions in Table 2-1, from the equation $\Phi \times 12 \times 3.7$ m $\times (0.139$ m $- 2 \times 0.0025$ m$)^2 = 1700$ W giving $\Phi = 2132$ W/m^3.
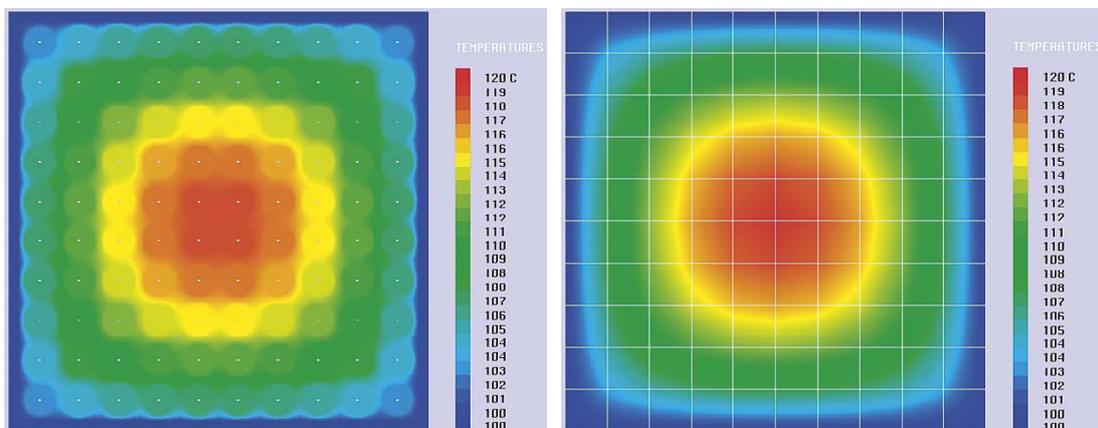
Figure 4-5. *Detailed model of a Posiva-BWR fuel assembly (left) and homogenized model (right).*

Figure 4-6 shows the temperature distribution along the diagonal at 45 degrees. In the example case above, the temperature along the whole edge was set to a constant of 100 °C. How well the determined effective conductivity performs, if the temperature deviates from the constant temperature, as is the case of the actual canister, was determined. Figure 4-7 shows the temperature distribution in the case where the temperature on the edges changes linearly in the diagonal direction from 120 °C in the lower-left lower corner to 220 °C in the upper-right corner. Figure 4-8 shows the temperature distribution along the diagonal. Good agreement between the solutions is obtained.
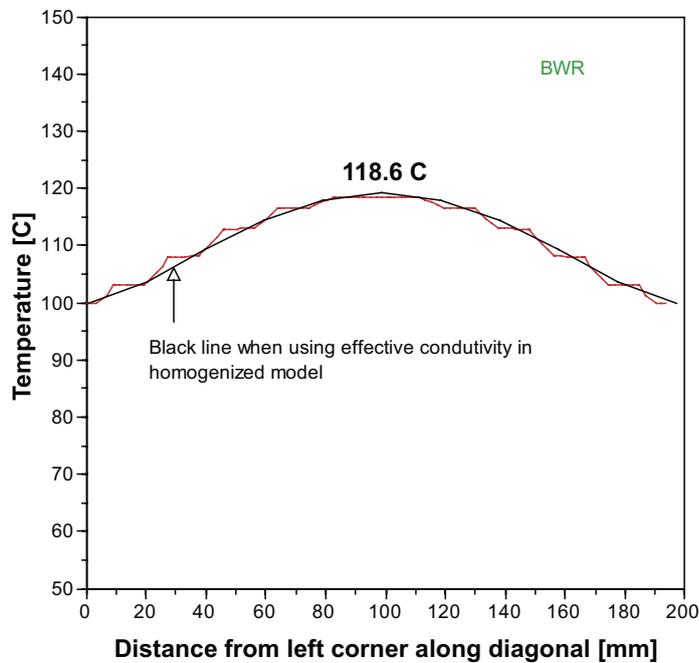
Figure 4-6. Temperature distribution along the diagonal at 45 degrees angles starting from the lower-left corner and ending at the upper-right corner and passing through a BWR fuel pellet obtained under a detailed model and under the homogenized model. Temperature on the outer edges is 100 °C.
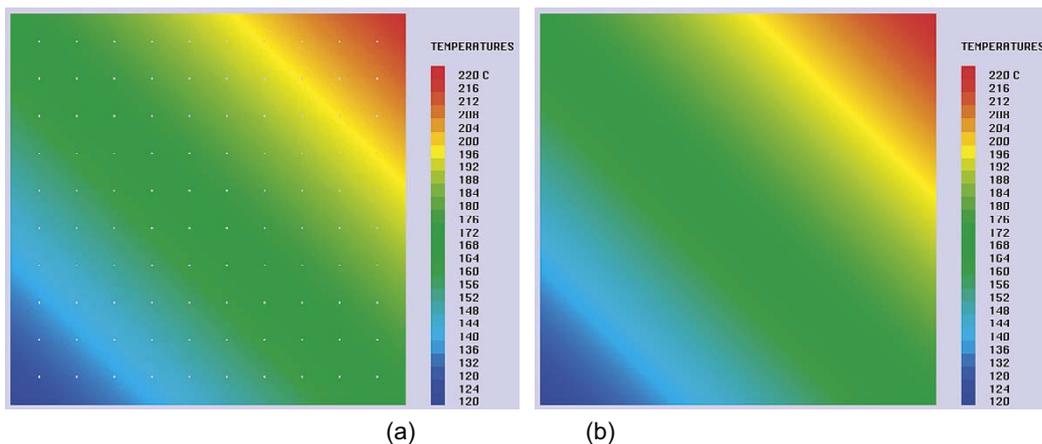
Figure 4-7. Temperature distribution in the case where the temperature on the edges changes linearly in the diagonal direction from 120 °C in the lower-left corner to 220 °C in the upper-right corner obtained under a detailed model (a) and under a homogenized model (b).
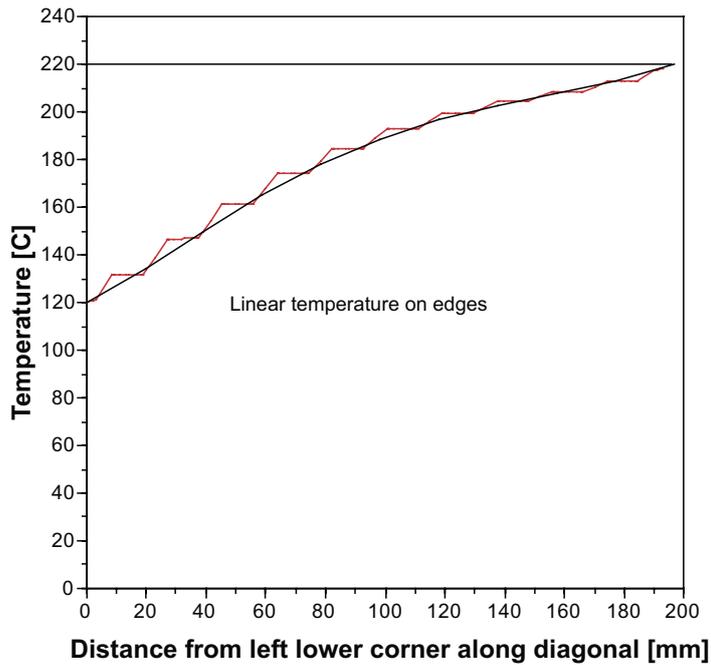
Figure 4-8. *Temperature distribution along the diagonal starting from the lower-left corner and ending at the upper-right corner and passing through the BWR fuel assembly pellets.*

Figure 4-9 shows the temperature distributions of one SKB-PWR fuel assembly. The temperature on the outer edge is 100 °C. In the detailed analysis, the fuel rod array area of the assembly (0.222 m x 0.222 m) is modelled as surrounded by 12.5 mm steel plate (compartment tube) having good conductivity (57.5 W/m/K). In the homogenized model, the 0.222 m x 0.222 m fuel rod array area (Table 2-1) is divided into a 10×10 grid. Figure 4-10 shows the temperature distribution along the diagonal.

Figure 4-11 is related to the analyses of the Posiva-VVER fuel assembly.
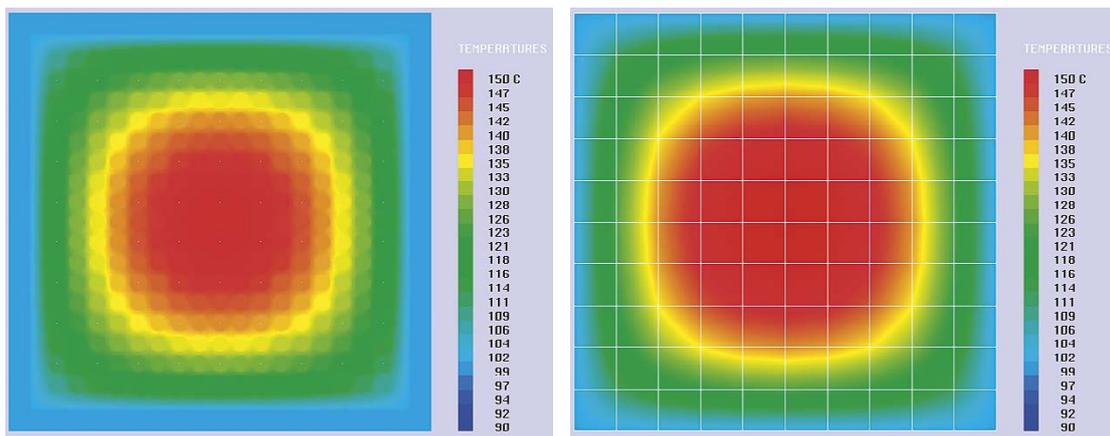
Figure 4-9. *One SKB-PWR fuel assembly. On the left, the temperature distribution under the detailed model, and on the right, that under the homogenized fuel model. The maximum temperature in the middle is 153.5 °C.*
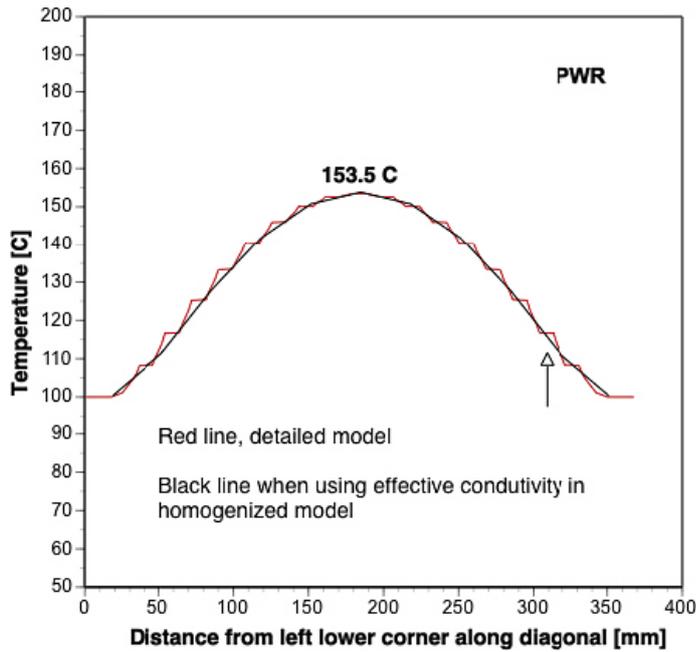
Figure 4-10. *Temperature profile along a 45 degrees line through the SKB-PWR fuel rod array area. The temperature on the outer edges is 100 °C.*
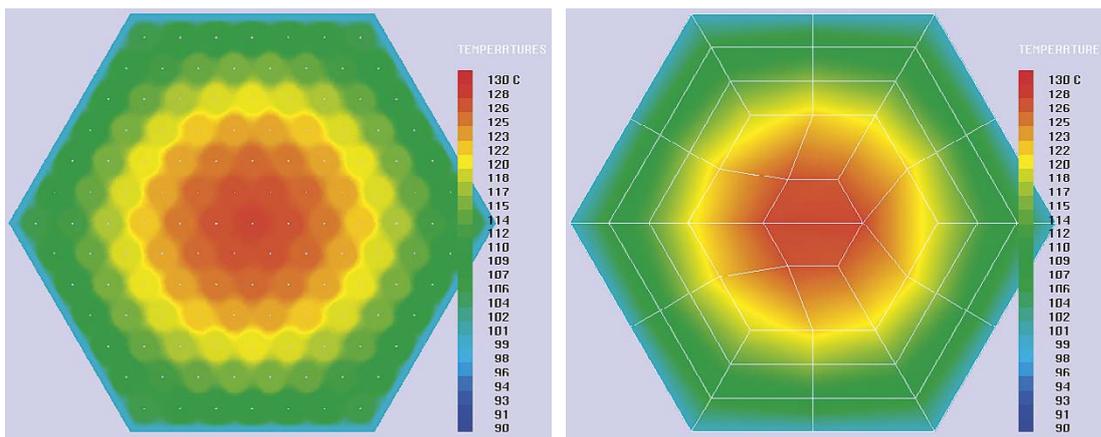
Figure 4-11. *One VVER fuel assembly surrounded by a 2 mm zirconium fuel channel tube and analysed using a detailed model (left). The homogenized model only for the fuel rod array area (right). The temperature on the outer edges is 100 °C.*

Table 4-1 presents the results for the SKB fuel rod arrays and Table 4-2 presents the results for the Posiva fuel rod arrays. The calculation was started from a highest edge temperature of 1300 °C. For instance, for the SKB-PWR fuel rod array, first, the detailed model gave a maximum temperature of 1301.7 °C. Then, under the homogenized model, the effective conductivity was adjusted to give the same temperature of 1301.7 °C, giving an effective conductivity of 5.0 W/(m·K). After this, the edge temperature of 1000 °C was treated in the same manner. The process was repeated to the edge temperature of 0 °C. At low temperature the effective conductivity is very low due to weak thermal radiation.

In the analyses the decay heat density corresponds to a nominal power of 1700 W or 1370 W in a canister. It was also demonstrated in the case of the SKB-PWR fuel assemblies that the decay heat density does not affect the obtained effective conductivity when applying, e.g., a two times higher decay power.

Table 4-1. Effective conductivity of homogenized SKB-fuel rod arrays in transverse direction.

Temperature on edge [°C]	SKB-BWR-10×10		SKB-BWR-8×8		SKB-PWR	
	Temperature on centre [°C]	λ [W/(m·K)]	Temperature on centre [°C]	λ [W/(m·K)]	Temperature on centre [°C]	λ [W/(m·K)]
0	31.6	0.081	20.26	0.130	88.3	0.068
50	74.3	0.108	65.1	0.179	118.8	0.102
100	118.9	0.143	111.4	0.241	153.6	0.134
150	164.7	0.19	158.7	0.317	191.8	0.183
200	211.6	0.24	206.7	0.41	232.9	0.237
300	307.5	0.37	304.3	0.66	321.0	0.384

Table 4-2. Effective conductivity of homogenized Posiva-fuel rod arrays in transverse direction.

Temperature on edge [°C]	Posiva-BWR		Posiva-VVER	
	Temperature on centre [°C]	λ [W/(m·K)]	Temperature on centre [°C]	λ [W/(m·K)]
0	32.5	0.079	42.5	0.099
50	75.0	0.105	84.1	0.126
100	119.4	0.138	127.5	0.159
150	165.1	0.180	172.4	0.199
200	211.9	0.230	218.3	0.246
300	307.7	0.360	312.5	0.364

Figure 4-12 shows the effective thermal conductivity in the transverse direction up to 300 °C.

In the case of SKB-BWR-8×8 (dimensions in Table 2-1), having 8×8 fuel rods, the effective transverse conductivity is higher than that for other fuel types because thermal radiation can more easily penetrate the coarser fuel rod lattice (Figure 4-13).
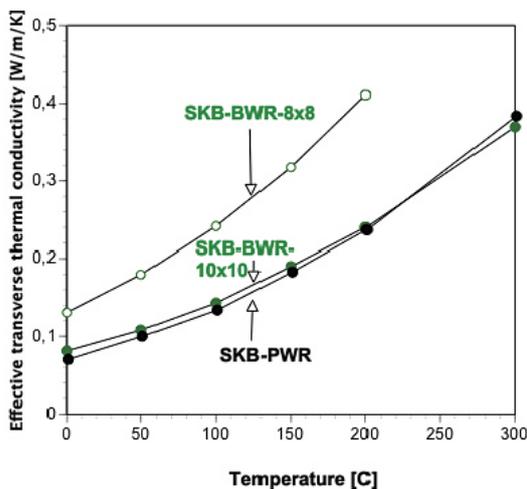
Figure 4-12. Effective thermal conductivity of SKB-fuel rod arrays in the transverse (horizontal) direction.
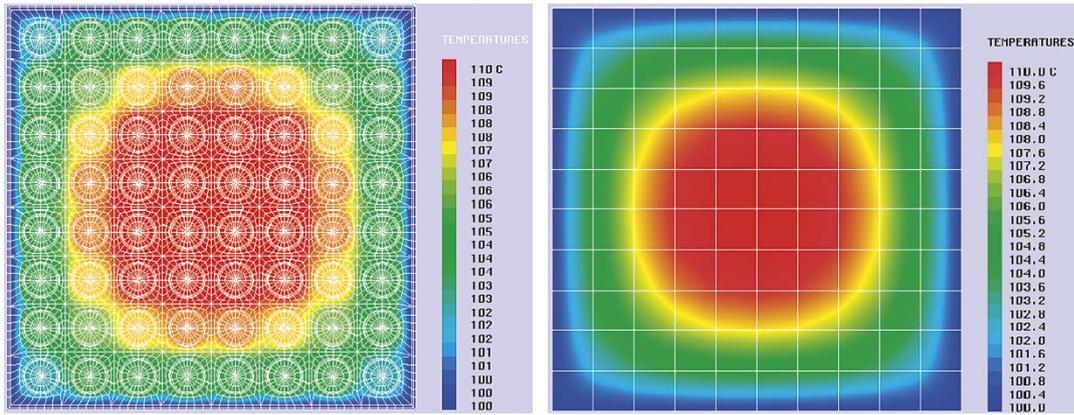
Figure 4-13. *Detailed model of a SKB-BWR-8 × 8 fuel assembly (left) and the homogenized model (right). A fuel rod array surrounded by a zirconium fuel channel. In this case, in both models, the temperature of the outer edges is 100 °C.*

The following polynomial fittings for the curves in Figures 4-12 and 4-14 were formed for the transverse thermal conductivity (at low temperatures < 300 °C, l in W/m/K and *T* in Celsius):

$$\lambda_{SKB\text{-}BWR,\,transverse} = 0.0806 + 4.70 \times 10^{-4}T + 1.65 \times 10^{-6}T^2$$

$$\lambda_{SKB\text{-}BWR\text{-}8 \times 8} = 0.1304 + 8.13 \times 10^{-4}T + 2.91 \times 10^{-6}T^2$$

$$\lambda_{SKB\text{-}PWR,\,transverse} = 0.0711 + 4.34 \times 10^{-4}T + 2.02 \times 10^{-6}T^2$$

$$\lambda_{Posiva\text{-}BWR,\,transverse} = 0.0796 + 4.03 \times 10^{-4}T + 1.77 \times 10^{-6}T^2$$

$$\lambda_{Posiva\text{-}VVER,\,transverse} = 0.0995 + 4.47 \times 10^{-4}T + 1.45 \times 10^{-6}T^2 \,. \tag{4-1}$$

These effective transverse (horizontal) thermal conductivity fittings for the homogenized fuel rod areas are used in later analyses. These curves are applied in the analysis, in which the emissivity equals 0.7 for the BWR and SKB-PWR zirconium cladding and 0.6 for the VVER zirconium cladding and shield gas exists between the rods.

Although the effective transverse conductivity is low at 100 – 150 °C, it still remains approximately seven times greater than the conductivity of the shield gas (Figure 2-6).
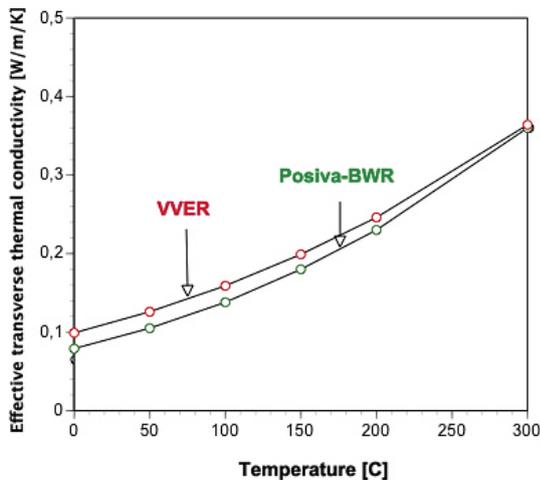
Figure 4-14. *Effective thermal conductivity of Posiva-fuel rod arrays in the transverse (horizontal) direction.*

5 Two-dimensional analyses with homogenized fuel rod arrays conductivity model in a cross-section

In this chapter the task is to study the effect of varying decay heat powers of the fuel assemblies in a canister on cast iron temperatures. This effect is studied via 2D model of the whole cross-section of the canister. A slice from the canister is separated by two planes perpendicular to the axis of the canister from the location, at which the longitudinal decay heat profile of a fuel assembly obtains its maximum value (Table 2-8). Adiabatic boundary conditions are applied in those planes. The temperature on the canister outer radius is set to 100 °C, which is the highest design temperature of the bentonite buffer. The decay heat power is set as the decay heat power at the moment of disposal. This model gives a conservative estimate for the maximum temperature in the cast iron. In the end of this chapter, in Section 5.5, it is shown that the boundary condition set to 100 °C is not a restriction factor, but the cast iron temperature and fuel pellet temperature can be calculated also with other boundary temperatures than 100 °C (see Section 5.6).

The Posiva-BWR, SKB-PWR and Posiva-VVER canister types are studied, with three cases for each type. The cases were defined in the order of the work. The effective thermal temperature-dependent conductivity of the homogenized fuel rod array is applied (the fittings in (11)). The 2D model corresponds to the detailed homogenized model presented in Chapter 4, and both models have identical gas-filled gaps outside the fuel rod lattice area.

5.1 Posiva-BWR fuel canister

Figure 5-1 shows the mesh of the homogenized 2D model of the Posiva-BWR fuel canister, and Figure 5-2 shows the material types and the gas-filled gaps.
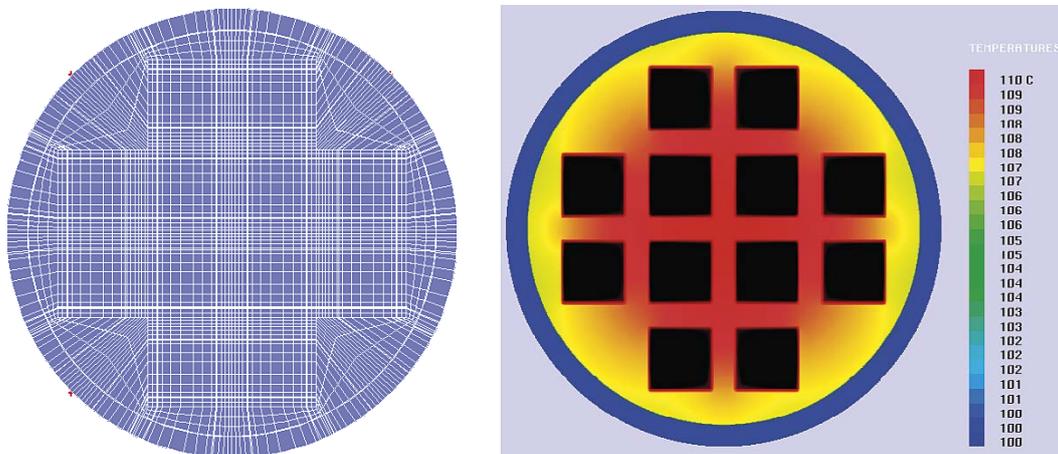
Figure 5-1. *Mesh of the homogenized cross-section 2D model of the Posiva-BWR fuel canister.*
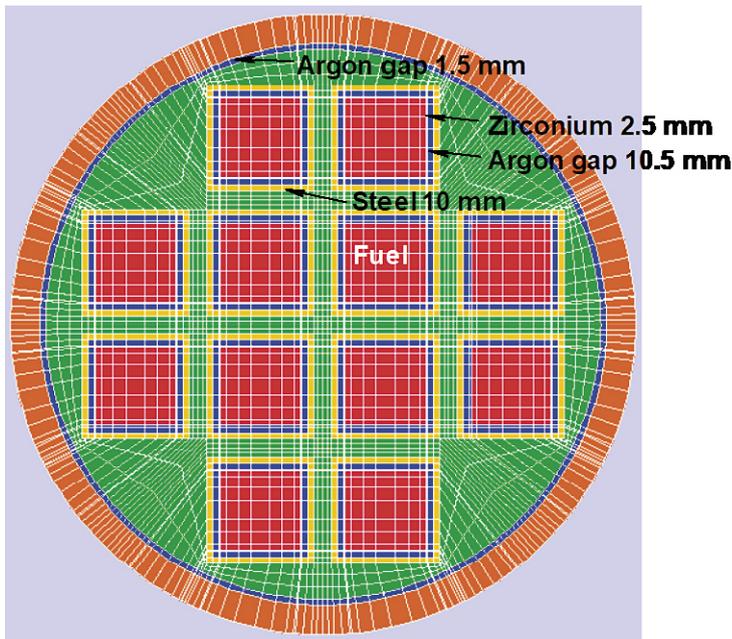
Figure 5-2. *Materials of the homogenized 2D model of the Posiva-BWR fuel canister.*

Table 2-2 shows the dimensions of the cross-section. Table 2-3 shows the thermal conductivity of the copper and of the cast iron. Equation (2-2) shows the thermal conductivity of the argon and the upper Equation (2-3) the applied conductivity for the zirconium flow channel material. The first of the Equations (4-1) shows the thermal conductivity of the homogenized fuel rod array. Table 2-5 shows the applied emissivities of the surfaces.

The stationary state is searched via iteration. The applied thermal capacities in Table 2-4 have no effect on the stationary temperatures. The iteration is stopped when the maximum temperature difference between two consecutive iteration cycles is less than 0.001 °C.

5.1.1 Reference case 0

The total decay heat power of the canister is 1700 W. All 12 fuel assemblies have equal decay heat power:

	141.67 W	141.67 W	
141.67 W	141.67 W	141.67 W	141.67 W
141.67 W	141.67 W	141.67 W	141.67 W
	141.67 W	141.67 W	

These powers are multiplied by 1.183 to consider the situation at the location of the maximum of the longitudinal decay heat distribution (Table 2-8). At the outer radius of the cast iron the temperature varies by 0.2 °C.

Figure 5-3 shows the temperature distribution along the cross-section and the maximum and minimum temperatures in the cast iron. The upper temperature scale shows the temperatures higher than 116.5 °C (primarily in the fuel rod array area), and the lower scale shows temperatures below 116.5 °C (primarily in the cast iron insert). The temperature in the copper wall is plotted in black.
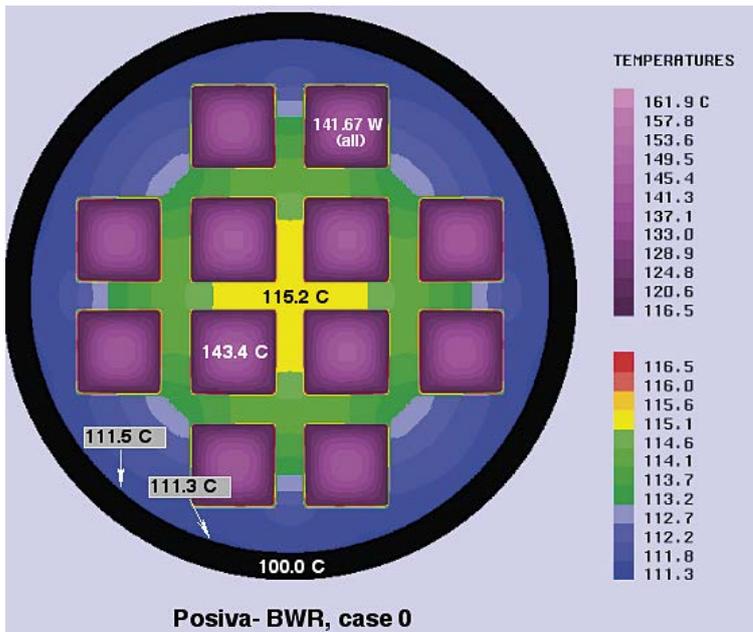
Figure 5-3. *Temperatures inside the Posiva-BWR fuel canister in reference case 0.*

5.1.2 Case 1

In this case, the decay heat powers in the fuel assemblies are

	92.5 W	92.5 W	
92.5 W	240.0 W	240.0 W	92.5 W
92.5 W	240.0 W	240.0 W	92.5 W
	92.5 W	92.5 W	

Figure 5-4 shows the temperature distribution along the cross-section and the maximum and minimum temperatures in the cast iron.
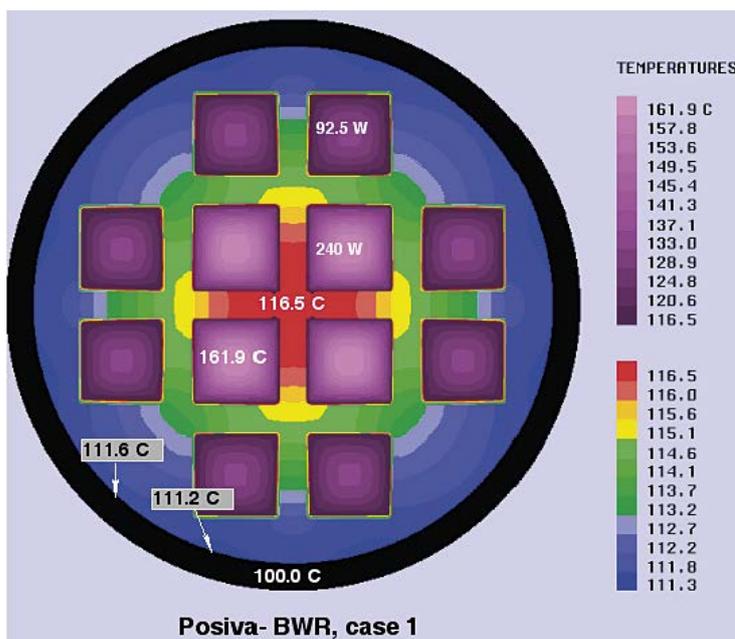
Figure 5-4. *Temperatures inside the Posiva-BWR fuel canister in case 1.*

5.1.3 Case 2

The decay heat powers in the fuel assemblies are

	182.14 W	182.14 W	
182.14 W	60.71 W	60.71 W	182.14 W
182.14 W	60.71 W	60.71 W	182.14 W
	182.14 W	182.14 W	

	1.5 x	1.5 x	
1.5 x	0.5 x	0.5 x	1.5 x
1.5 x	0.5 x	0.5 x	1.5 x
	1.5 x	1.5 x	

Figure 5-5 shows the temperature distribution in the cross-section and the maximum and minimum temperatures in the cast iron.
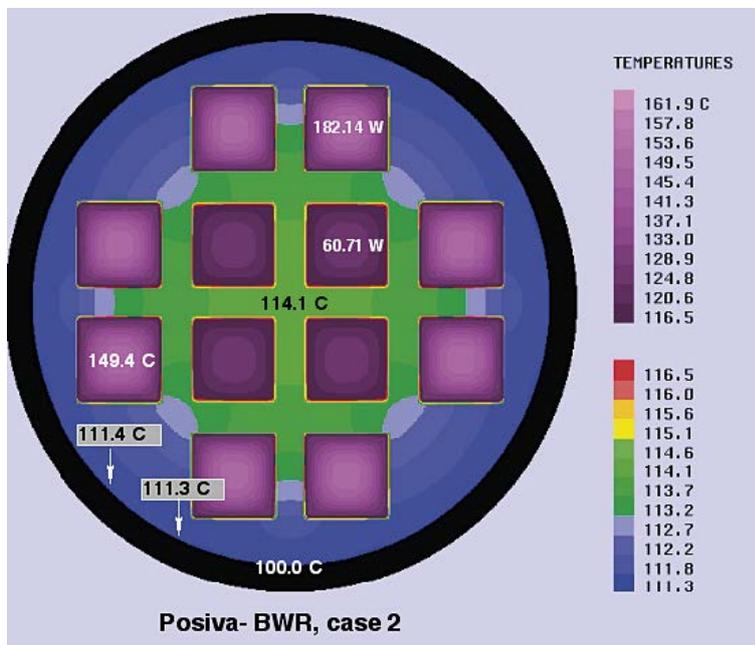
Figure 5-5. *Temperatures inside the Posiva-BWR fuel canister in case 2.*

5.2   SKB-PWR fuel canister

Figure 5-6 shows the mesh of the homogenized 2D model of the SKB-PWR fuel canister, and Figure 5-7 shows the material types.

Table 2-2 shows the dimensions of the cross-section. Table 2-3 shows the thermal conductivity of the copper and of the cast iron. Equation (2-2) shows the thermal conductivity of the argon and the upper Equation (2-3) the applied conductivity for the zirconium flow channel material. The third of the Equations (4-1) shows the thermal conductivity of the homogenized fuel rod array. Table 2-5 shows the applied emissivities of the surfaces.
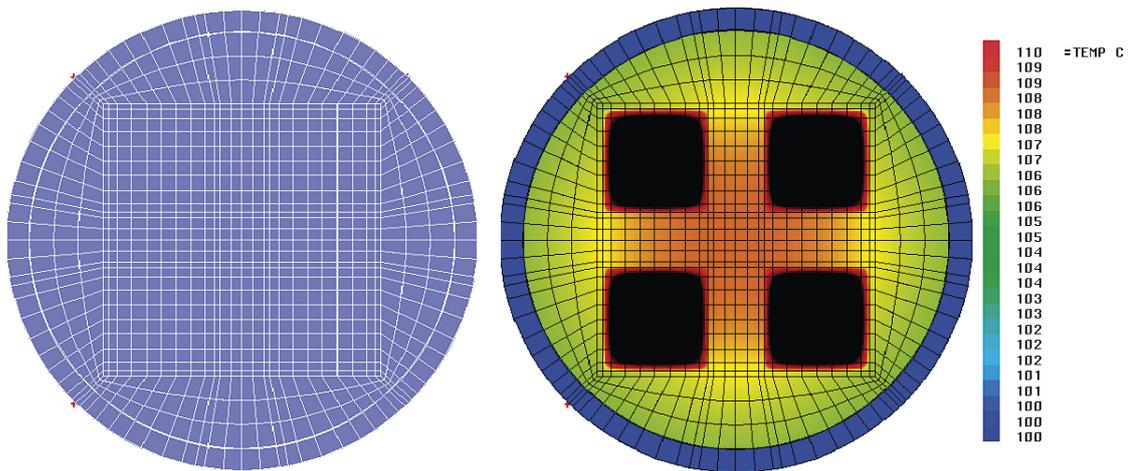
Figure 5-6. *Mesh of the homogenized 2D cross-section model of the SKB-PWR fuel canister.*
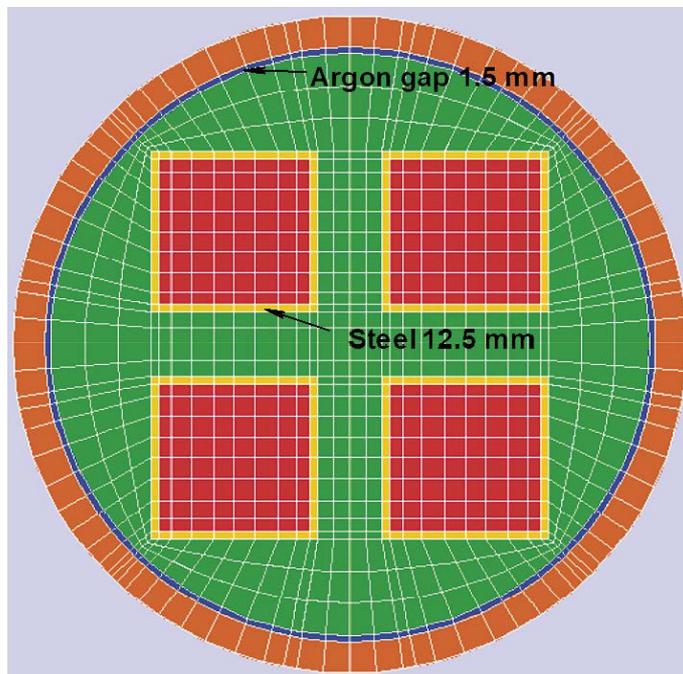
Figure 5-7. *Materials of the homogenized 2D model of the SKB-PWR fuel canister.*

5.2.1 Reference case 1

In this symmetric reference case, the total decay heat power of 1700 W is evenly distributed as follows:

425 W	425 W
425 W	425 W

These powers are multiplied by 1.06 to consider the situation at the location of the maximum of the longitudinal decay heat distribution (Table 2-8). Figure 5-8 shows the results.
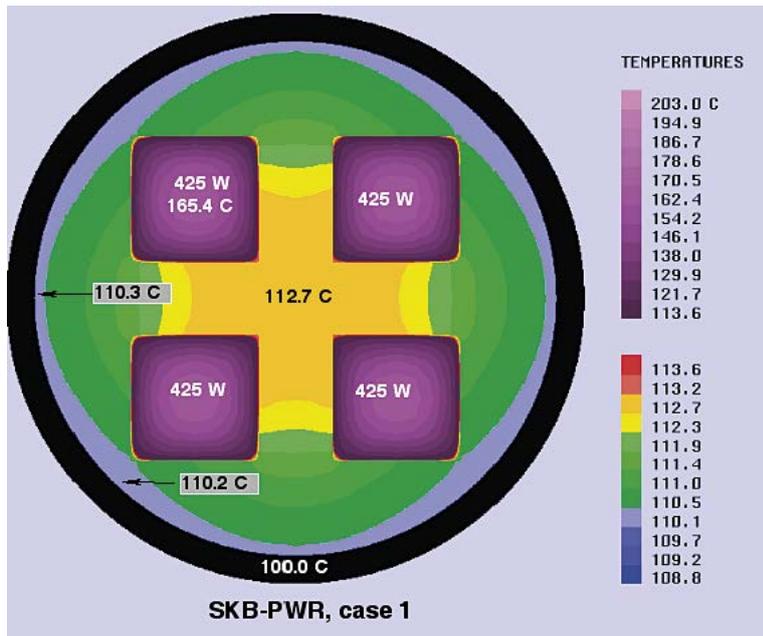
Figure 5-8. *Temperatures inside the SKB-PWR fuel canister in case 1.*

5.2.2   Case 2

In this asymmetric case, there is one "very hot" fuel assembly and three "cold" fuel assemblies (totalling 1700 W):

800 W	300 W
300 W	300 W

Figure 5-9 shows the results.
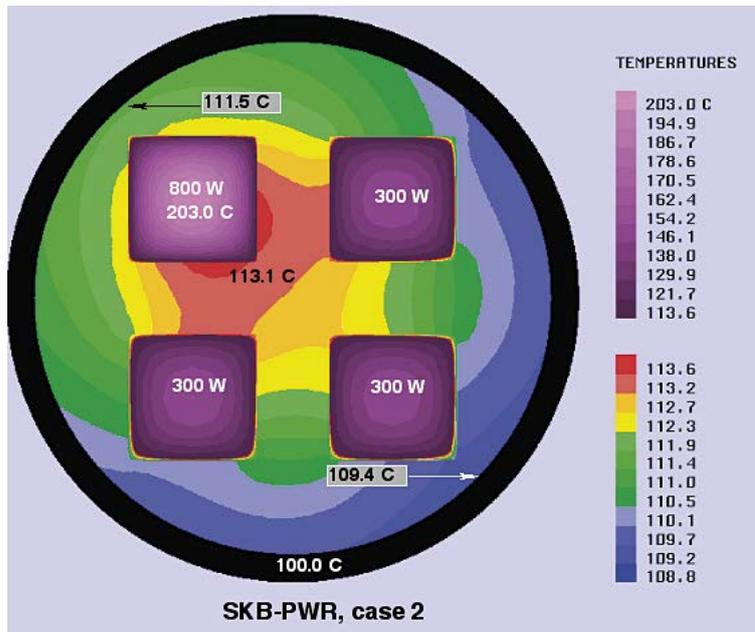
Figure 5-9. *Temperatures inside the SKB-PWR fuel canister in case 2.*

5.2.3 Case 3

In this asymmetric case there are two "hot" and two "cold" fuel assemblies (totalling 1700 W):

700 W	700 W
150 W	150 W

Figure 5-10 shows the results.
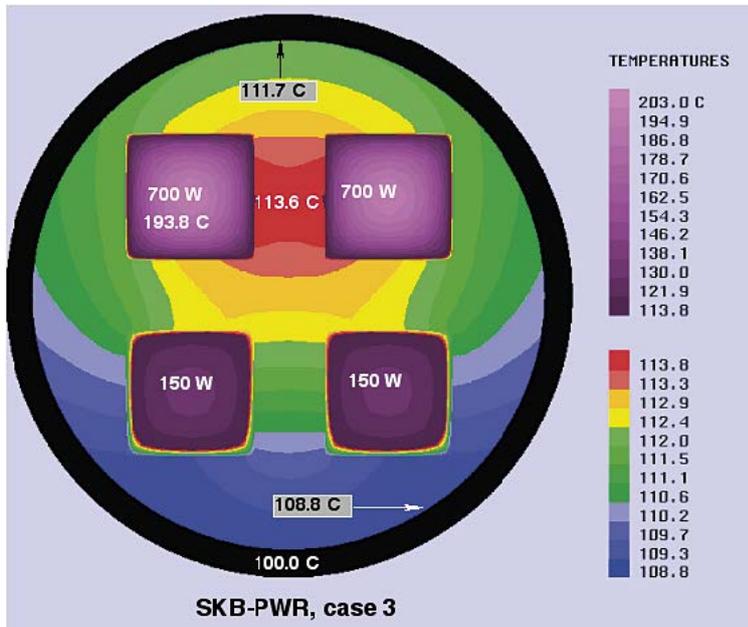
Figure 5-10. *Temperatures inside the SKB-PWR fuel canister in case 3.*

5.3   Posiva-VVER fuel canister

Figure 5-11 shows the mesh of the homogenized 2D model of the Posiva-VVER fuel canister and Figure 5-12 shows the material types and the gas-filled gaps.

Table 2-2 shows the dimensions of the cross-section. Table 2-3 shows the thermal conductivity of the copper and of the cast iron. Equation (2-2) shows the thermal conductivity of the argon and the upper Equation (2-3) the applied conductivity for the zirconium flow channel material. The fifth of the Equations (4-1) shows the thermal conductivity of the homogenized hexagonal fuel rod array. Table 2-5 shows the applied emissivities of the surfaces.
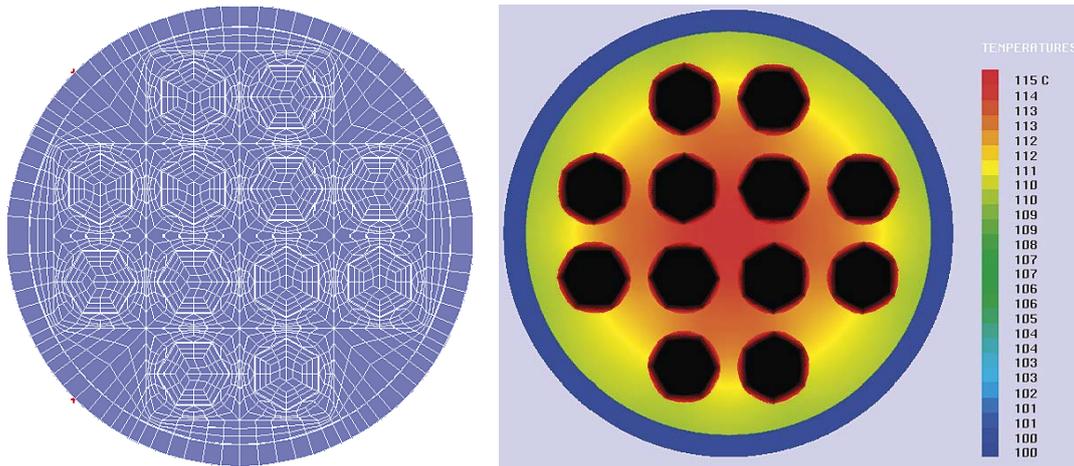
Figure 5-11. *Mesh of the homogenized 2D cross-section model of the Posiva-VVER fuel canister.*
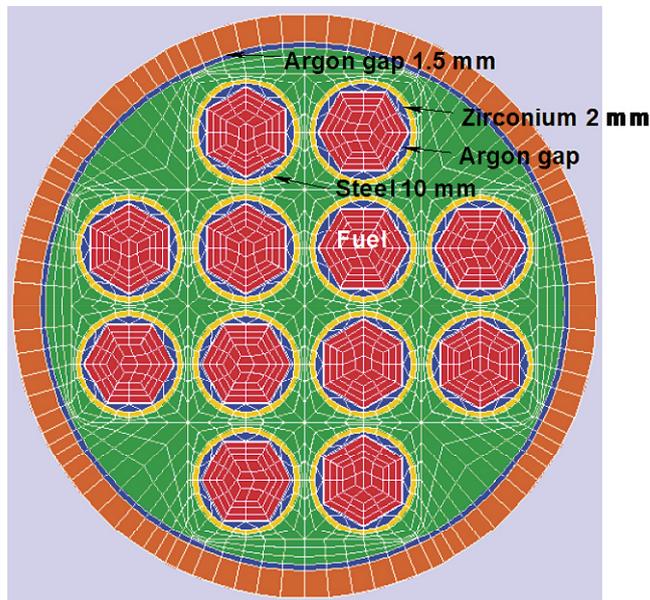
Figure 5-12. *Materials of the homogenized 2D model of the Posiva-VVER fuel canister.*

5.3.1 Reference case 0

The total decay heat power of the canister is 1370 W. In this reference case, all 12 fuel assemblies have equal decay heat powers:

	114.17 W	114.17 W	
114.17 W	114.17 W	114.17 W	114.17 W
114.17 W	114.17 W	114.17 W	114.17 W
	114.17 W	114.17 W	

These powers are multiplied by 1.125 to consider the situation at the location of the maximum of the longitudinal decay heat distribution (Table 2-8). Figure 5-13 shows the results.
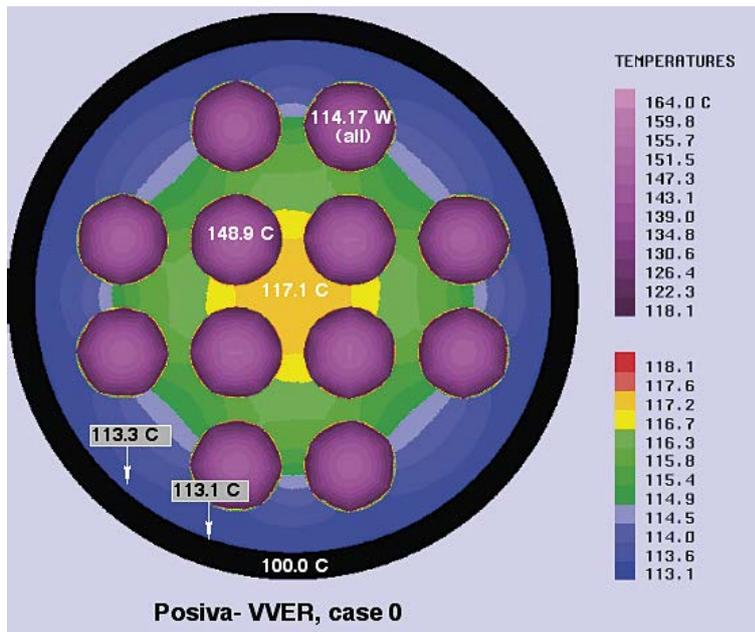
Figure 5-13. *Temperatures inside the Posiva-VVER fuel canister in reference case 0.*

5.3.2 Case 1

The decay heat powers in the fuel assemblies are as follows:

	142.71 W	142.71 W	
142.71 W	57.08 W	57.08 W	142.71 W
142.71 W	57.08 W	57.08 W	142.71 W
	142.71 W	142.71 W	

In this case, the decay heat is 25 % higher in the outer channels and 50 % lower in the inner channels compared to the nominal decay heat (114.2 W), and the γ-radiation level is higher near the outer surface. Figure 5-14 shows the results.
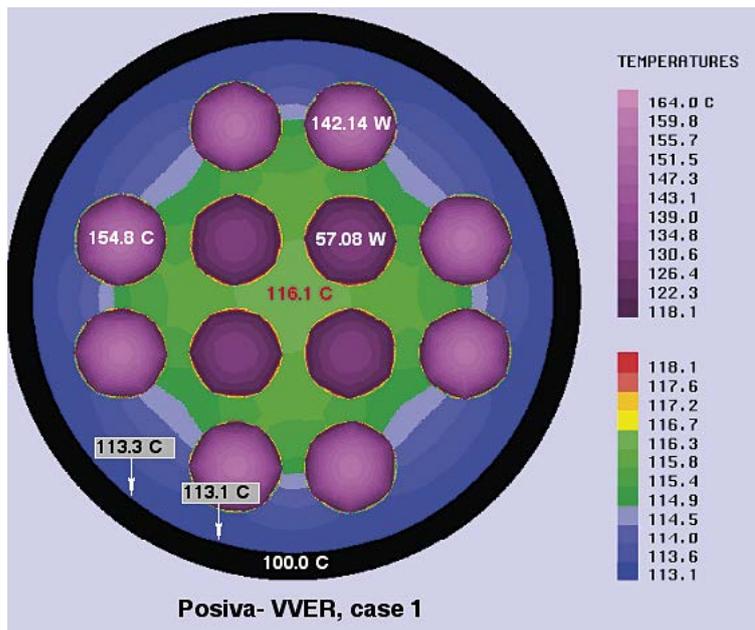
Figure 5-14. *Temperatures inside the Posiva-VVER fuel assemblies in case 1.*

5.3.3 Case 2

The decay heat powers in the fuel assemblies are as follows:

	85.63 W	85.63 W	
85.63 W	171.25 W	171.25 W	85.63 W
85.63 W	171.25 W	171.25 W	85.63 W
	85.63 W	85.63 W	

In this case, the decay heat is 25 % lower on the outer channels and 50 % higher on the inner channels compared to the nominal decay heat (114.2 W). Figure 5-15 shows the results.
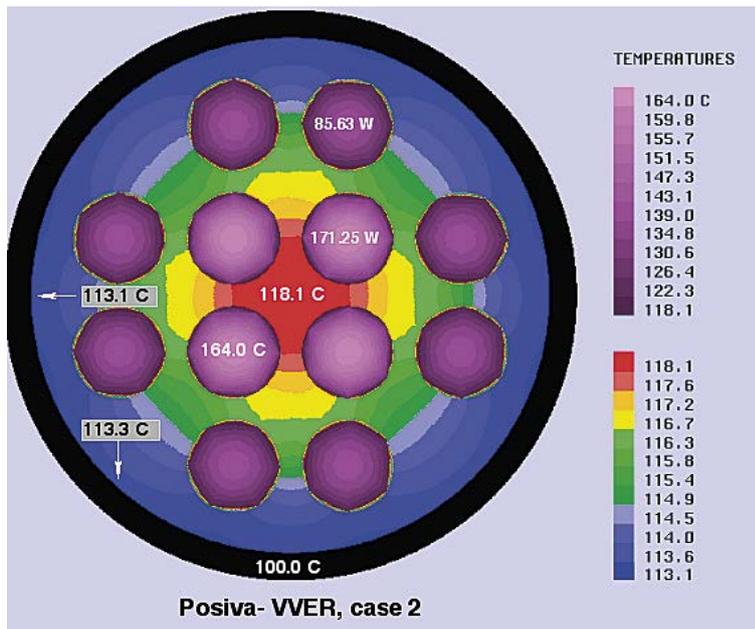
Figure 5-15. *Temperatures inside the Posiva-VVER fuel canister in case 2.*

5.4   SKB-BWR-8×8 fuel canister

In this additional case the fuel assemblies have equal decay heat powers (12×141.67 W = 1700 W). These powers are multiplied by 1.16 to consider the situation at the location of the maximum of the longitudinal decay heat distribution (Table 2-8). Figure 5-16 shows the results. The maximum temperature in the fuel pellets is approximately 8 °C lower than in the case of the SKB-BWR because the effective conductivity is better for the 8×8 lattice than for the 10×10 lattice (Figures 4-12 and 4-14). The fuel assembly type (8×8 or 10×10) does not affect the cast iron temperature, see Table 5-1.
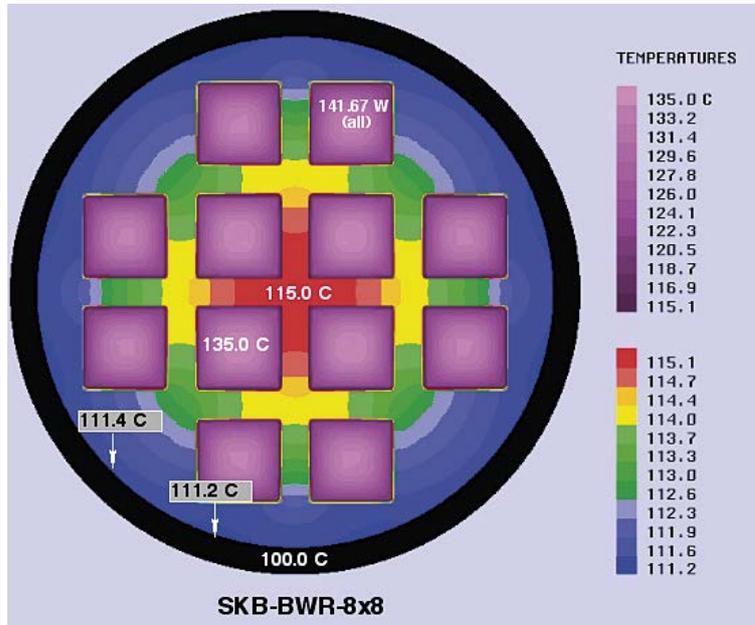
Figure 5-16. *Temperatures inside the SKB-BWR-8 × 8 fuel canister (equal heat powers of 141.67 W in all fuel assemblies).*

5.5　Summary of analysed 2D cases

Table 5-1 summarizes the analysed 2D cases. The 2D model is set at the location, at which the longitudinal decay heat profile of a fuel assembly obtains its maximum value (Table 2-8). The temperature on the canister outer radius is set to 100 °C, which is the highest design temperature of the bentonite buffer. The total decay heat power is set as the decay heat power at the moment of disposal (1700 W for the BWR and PWR canisters and 1370 W for the VVER canister). This model gives a conservative estimate for the maximum temperature in the cast iron.

In general, the calculation for the BWR case was performed by using the 10×10 lattice. There are also other BWR lattices (e.g. 8×8, 9×9, 10×10, 11×11), but the lattice type does not, in practice, affect the maximum temperature of the cast iron as far as the decay power in the fuel assembly is the same.

Table 5-1. Summary of 2D analyses showing maximum and minimum temperatures in the cast iron and maximum temperatures in the fuel pellets. In all cases, the boundary temperature of the outer surface of the canister is 100 °C. The second column shows the local decay heat factor in the longitudinal direction. The fuel assemblies and the burn-up values are according to Tables 2-1 and 2-6, respectively. Additional analyses are repeated for BWR cases with SKB fuel data.

Case ( )	$P_{Max}/P_{Average}$ [-]	$T_{Max\ in\ cast\ iron}$ [°C]	$T_{Min\ in\ cast\ iron}$ [°C]	$T_{Max\ in\ fuel}$ [°C]
Posiva-BWR (0)	1.183	115.2	111.3	143.4
Posiva-BWR (1)	1.183	116.5	111.2	161.9
Posiva-BWR (2)	1.183	114.1	111.3	149.4
SKB-PWR (1)	1.060	112.7	110.2	165.4
SKB-PWR (2)	1.060	113.1	109.4	203.0
SKB-PWR (3)	1.060	113.6	108.8	193.8
Posiva-VVER (0)	1.125	117.1	113.1	148.9
Posiva-VVER (1)	1.125	116.1	113.1	154.8
Posiva-VVER (2)	1.125	118.1	113.1	164.0
SKB-BWR-8 × 8 (0)	1.160	115.0	111.2	135.0
Additional analyses				
SKB-BWR (0)	1.160	115.0	111.2	143.3
SKB-BWR (1)	1.160	116.3	111.1	161.7
SKB-BWR (2)	1.160	114.0	111.2	149.3

The temperature on the outer surface was set to 100 °C in all the cases in Table 5-1. The Posiva-BWR (0) case has been analysed with variable outer surface temperatures. The results are given in Figure 5-17.

Analytical checking of the temperature along the outer edge of the cast iron

The purpose of the following is to calculate the temperature difference over the gap between the inner surface of the copper cylinder and the outer surface of the cast iron analytically. Due to exceptionally high conductivity of copper (390 W/m/K), the temperature is practically constant over the copper. That is why a constant temperature can be set along the whole external surface of the canister. The actual temperature variation in the circumferential direction is studied later in Section 6.4.2. The Posiva-BWR fuel canister in case (0) is considered. As Figure 5-3 shows, the temperature of the cast iron area is also nearly constant because of the relatively good conductivity of cast iron. The temperature distribution in the cast iron near the 1.5 mm gap is nearly axisymmetric. Then, the temperature difference over the gap between the copper and the cast iron insert can be calculated from the heat flux continuity over the gap:

$$\phi_{over\ gap} = \frac{P}{\pi DL} = \lambda_{gas}\frac{T_1 - T_2}{\Delta r} + \varepsilon_{tot}\sigma(T_1^4 - T_2^4)\,. \tag{5-1}$$

By setting the following values (the maximum of the axial decay heat profile is 1.183, Table 2-8) into Equation (5-1) we get the estimate for the temperature T_1:

- $P = 1.183 \times 1700$ W decay heat power of the canister

- $L = 3.7$ m active length of the fuel assembly

- $D = 0.9505$ m mean diameter of the gap

- $\Delta r = 0.0015$ m gap width

- $T_2 = 100$ °C copper surface temperature

- $\varepsilon_{tot} = 0.094$ copper and iron emissivities 0.1 and 0.6 (Equation 3-3)

- λ_{gas} argon conductivity calculated from the fitting (2)

Equation (5-1) gives the cast iron outer edge temperature $T_1 = 111.3$ °C whereas the numerical analysis gave $T_1 = 111.9$ °C (Figure 5-3). Thus the temperature on the edge of cast iron can be estimated from the Equation (5-1) quite accurately.

5.6   Variation of boundary condition temperature

In the final stage of the analyses, a question was arisen; how does the temperature behave inside a canister, if the temperature in the surrounding bentonite buffer varies. As the heat transfer models were temperature dependent, a set of simulations were made with variable postulated bentonite temperatures (60 °C – 140 °C). The result is given in Figure 5-17. The fuel pellet and cast iron maximum temperatures increase as the surrounding temperature increases.

One task of the study was to calculate the evolution of the best estimate temperatures of the cast iron and fuel pellets for long periods of time while also considering the effects of all other canisters in a repository panel. The global repository temperatures were previously determined for the SKB and Posiva repositories in Hökmark et al. (2010) and Ikonen and Raiko (2012). The temperature evolution of the maximum temperature at the lowest point of a canister, which is always in contact with the bentonite buffer, was taken from the global temperature analyses referenced above. The temperature distribution on the external canister surface was determined by axisymmetric models, wherein the canister, gaps, the bentonite buffer and the host rock were considered. Varying heat powers of the fuel assemblies in a canister were studied in the same manner as in the 2D analyses for the nine pre-defined cases.
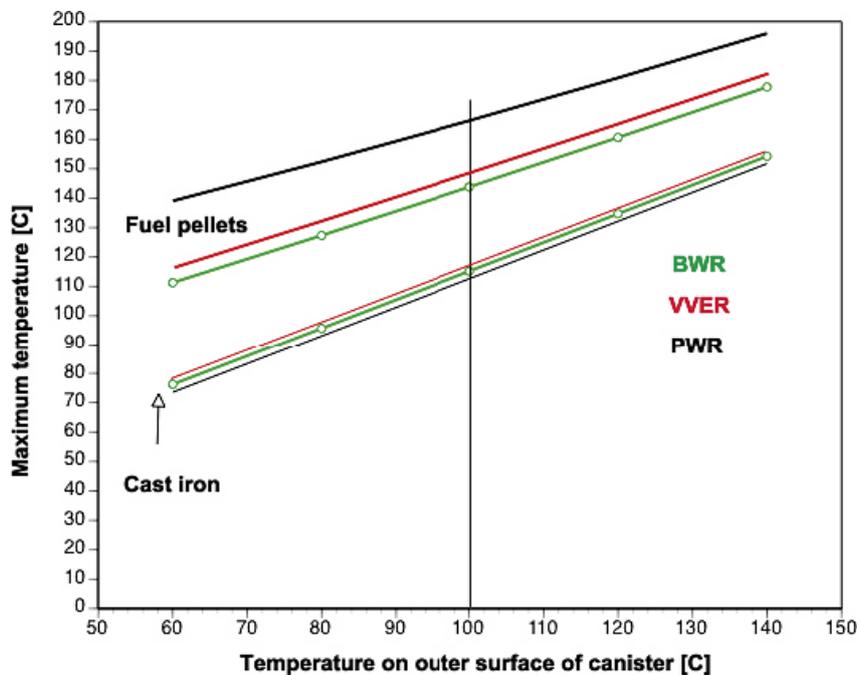
Figure 5-17. *Maximum fuel pellet and cast iron temperatures as a function of the canister outer surface temperature.*

6 Three-dimensional analyses

In this chapter, three-dimensional thermal analyses of considered three canister types are performed to obtain temperatures inside the canister and especially in the cast iron insert, but also in the fuel pellets. These analyses give long-term best estimate evolution of the temperatures, when the conservatively dry installation conditions in the repository are assumed.

3D modelling of the details inside a canister and extending the modelling further over the air filled gap (in the current design), over the surrounding bentonite blocks, over the pellet filled gap and over a large volume of host rock would lead to an impractically large 3D model. That is why the 3D model is extended over the canister volume only, and on the outer surface of the copper shell the boundary conditions (temperature distributions) obtained from axisymmetric modelling are applied. Due to high conductivity of copper the temperature on the outer surface of the copper shell is locally constant in the circumferential direction as is shown in Section 7.1 (concentric case), but varies a little in longitudinal direction of the shell.

The longitudinal temperature distribution of the outer copper surface is determined by using an axisymmetric model as presented in Section 6.1. To make axisymmetric analysis possible, the insert thermal properties are homogenized, and thus thermal properties are also axisymmetric. This homogenization can be done, because, due to the high conductivity of copper, mainly the internal total heat power, not the internal details, effects the temperature distribution in the copper cylinder. The temperature in the copper cylinder, in the circumferential direction, is locally practically constant also with the varying heat powers of the fuel assemblies in the canister as is shown in Section 7.1 (concentric case).

In the next, at first, the external longitudinal canister surface temperature distribution is solved numerically by the axisymmetric model. Thereafter, the internal structure of the canister is described in more details. Then, the effective longitudinal conductivity in the fuelled, lower and upper parts of the fuel assemblies, is derived. Finally, the evolution of the long-term temperatures inside the canister are determined. In these 3D analyses, also the global effect of the other canisters in the repository needs to be taken into account. The temperature increase caused by the other canisters was determined by the analytic method as described in Ikonen and Raiko (2012). The 3D analyses in this chapter concern the situation, where the insert and the copper cylinder are concentric. In the eccentric case, the temperature varies some degrees in the circumferential direction on the outer surface of the copper cylinder. The eccentricity increases the maximum temperature in the copper cylinder, but decreases the maximum temperature in the cast iron as can be seen from the curves in Figures 7-2 and 7-3.

6.1 Temperature distribution on the outer surface of a single canister

In the next section, the goal is to determine the temperature distribution for 3D analyses along the outer surface of various canister types. The temperature on the outer surface of the copper canister is nearly constant; however, in this section, the temperature distribution is determined by an axisymmetric model, where the canister, the surrounding air-filled and pellet-filled gaps, the bentonite buffer and the homogenous host rock, but not the neighbouring canisters, are considered.

For Olkiluoto repository, the dimensions and layout of the disposal hole and tunnel for the BWR and VVER fuel canisters are presented in Figure 6-1.

Figure 6-2 shows the applied axisymmetric model. The initial data for the analysis of the Posiva-BWR type canister are presented in Table 6-1. Figure 6-3 shows the material types.
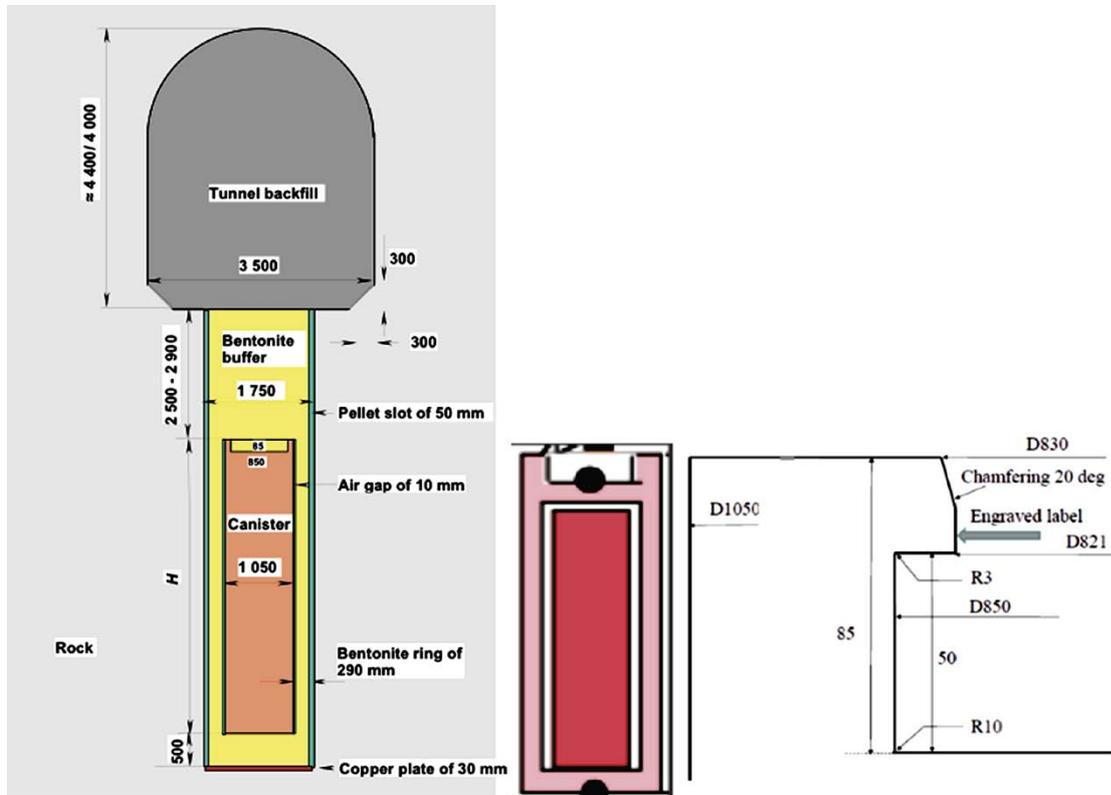
Figure 6-1. *Nominal dimensions of the disposal hole and tunnel. For the Posiva-BWR type, H = 4752 mm, and for the VVER type, H = 3552 mm. For the SKB canister, the total height is H = 4835 mm due to different bottom end design of the copper shell.*
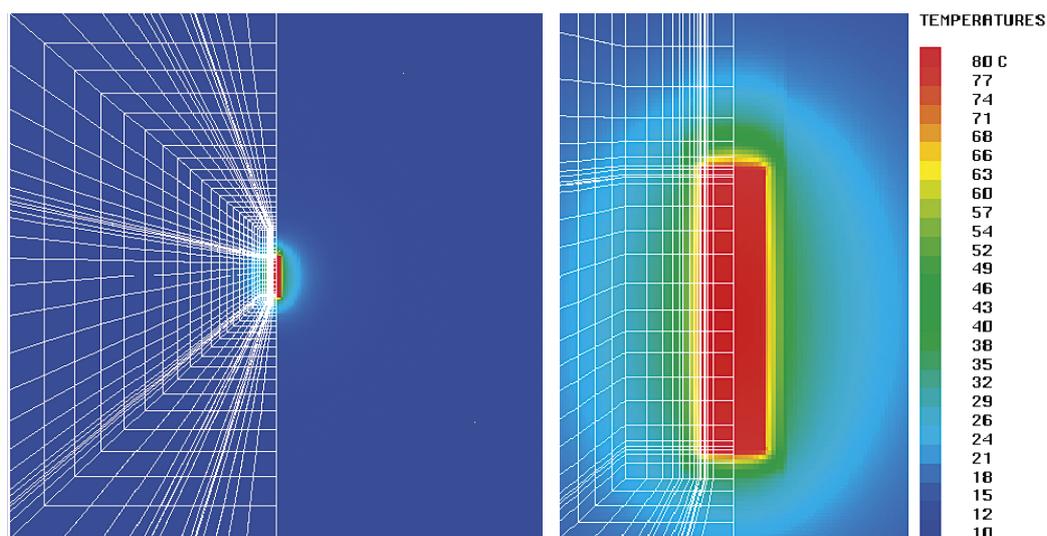
Figure 6-2. *Example of the mesh and temperature distribution after 1.3 years for a Posiva-BWR model. Left: the whole model. Right: zooming in for the near-field.*

Table 6-1. Initial values for the referenced global repository analyses (Hökmark et al. 2009, 2010, Ikonen and Raiko 2012).

	SKB	Posiva
Ambient rock temperature [°C]	11.2	10.5
Rock conductivity [(W/m)/K]	2.55–2.9	2.82
Rock volumetric heat capacity [MJ/m³/K]	2.06–2.12	2.10
Radius of the disposal hole [mm]	875	875
Bentonite below canister [mm]	500	500
Bentonite height above canister [mm]	1500	2900
Bentonite block conductivity [(W/m)/K]	-	1.0
Effective bentonite buffer conductivity [(W/m)/K]	1.0	-
Volumetric capacity of bentonite [MJ/m³/K]	2.4	2.4
Width of air gap on copper cylinder [mm]	10	10
Width of pellet slot [mm]	50	50
Conductivity in pellet slot [(W/m)/K]	-	0.2
Volumetric capacity of pellet slot [MJ/m³/K]	-	1.34
Effective conductivity in air gap around canister [(W/m)/K]	0.04	0.046–0.061
Canister spacing in tunnels [m] (BWR or PWR)	6.0–6.8	8.9
Tunnel spacing [m]	40	25

The internal parts of the canister (Figure 6-3) were modelled by considering 1.5 mm gas-filled gaps along the cylindrical shell and 2.0 mm gaps in the upper end and different materials. The materials inside the outer radius of the cast iron were homogenized, and thus thermal properties are also axisymmetric. The decay heat distribution profiles in Table 2-8 were applied. In the longitudinal direction, the homogenization is applied only for the length of the compartments.
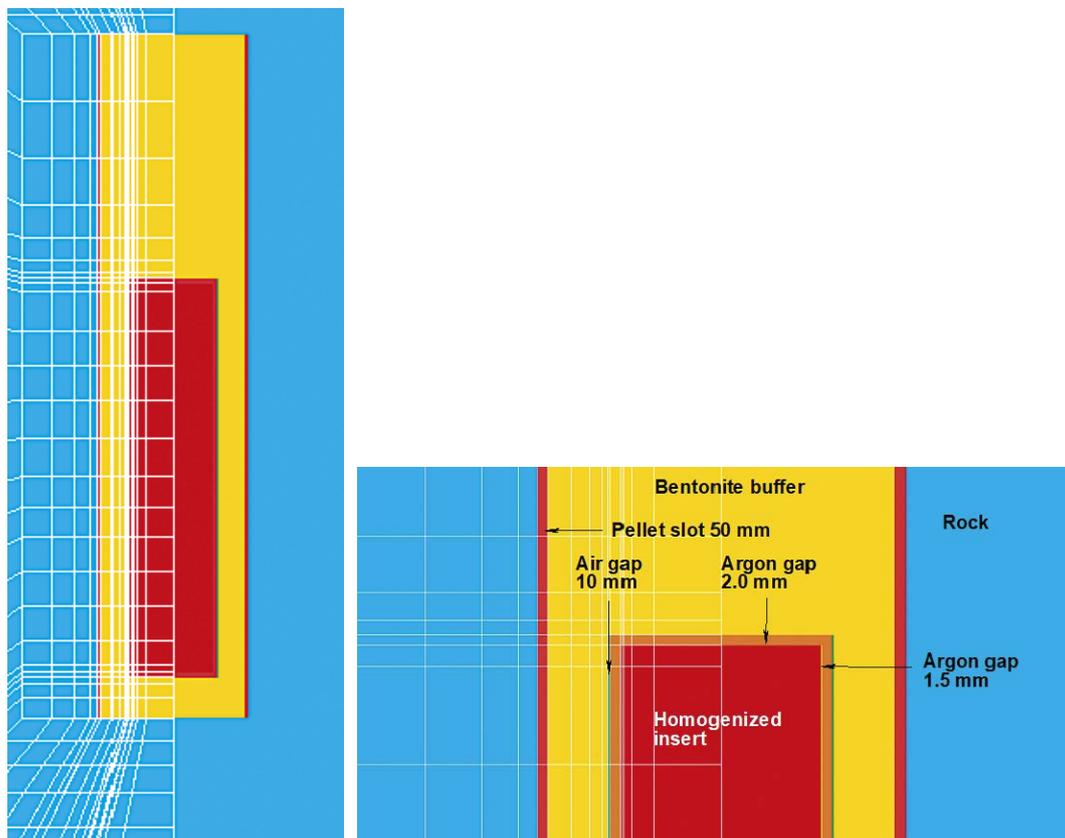
***Figure 6-3.** Material types of the axisymmetric model of the Posiva-BWR fuel canister.*

As Figure 6-4 shows, there are quite large differences in size between the "elements" of the mesh. In these analyses, one question concerns the size of the effect of the mesh density and the reliability of the calculation process. Different methods of verifying the calculation process have been studied. In the appendix, three test cases are presented. The last of these cases demonstrates that even a quite course mesh and large differences in the size between "elements" in the control volume method can give accurate results.

By applying the respective model as the detailed cross-sectional 2D model in Figure 6-15, where the grid is extended to the host rock, the temperature variation in the copper cylinder is only 0.024 °C. As shown later in Section 6.1.2, the temperature in the copper and on the outer layers of the cast iron is practically constant in the circumferential direction also in case that the decay heats of the fuel assemblies differ considerably from each other. From this it follows that insert can be homogenized and only the decay heat affects the temperature on the outer surface of the copper, whose longitudinal distribution only is of interest now. Geometric eccentricities have greater influence as it is demonstrated later in Section 6.1.2.

For determining the effective conductivity and thermal capacity for the axisymmetric model, the conductivity and capacity of different materials are calculated by weighting them by their relative sectional portions (Table 2-1, Table 2-2 and thermal properties from Section 2.2). In the cross-section the relative areas of cast iron, steel, zirconium, UO_2 and argon are 0.444, 0.115, 0.023, 0.305 and 0.113, respectively. The effective longitudinal conductivity for the Posiva-BWR insert is 0.444 × 35.5 W/m/K + 0.115 × 57.5 W/m/K + 0.023 × 15.0 W/m/K + 0.305 × 3.0 W/m/K (3.0 W/m/K from Figure 6-20) + 0.113 × 0.02 W/m/K = (15.7 + 6.6 + 0.3 + 0.913 + 0.002) W/m/K = 23.6 W/m/K. The conductivity of cast iron is dominating (67 %). The radial effective conductivity is approximately 0.444 × 35.5 W/m/K + 0.115 × 57.5 W/m/K + 0.023 × 15.0 W/m/K + 0.305 × 0.1 W/m/K + 0.113 × 0.02 W/m/K (0.1 W/m/K from Figure 4-12) = 22.8 W/m/K. The decay heat was assumed to be uniformly distributed in a circle of the effective radius 0.3 m. Assumptions done above cannot give detailed temperatures in the insert, but it predicts quite well longitudinal temperatures along the outer copper surface. A case was studied, where the radial effective conductivity was set to 15 W/m/K. This thermally orthotropic analysis caused only 0.1 °C increase in the maximum temperature on the outer copper surface. Corresponding calculation gives of the longitudinal conductivity of the canister internals of the Posiva-VVER canister 27.9 W/m/K and the SKB-PWR canister internals of 26.9 W/m/K.
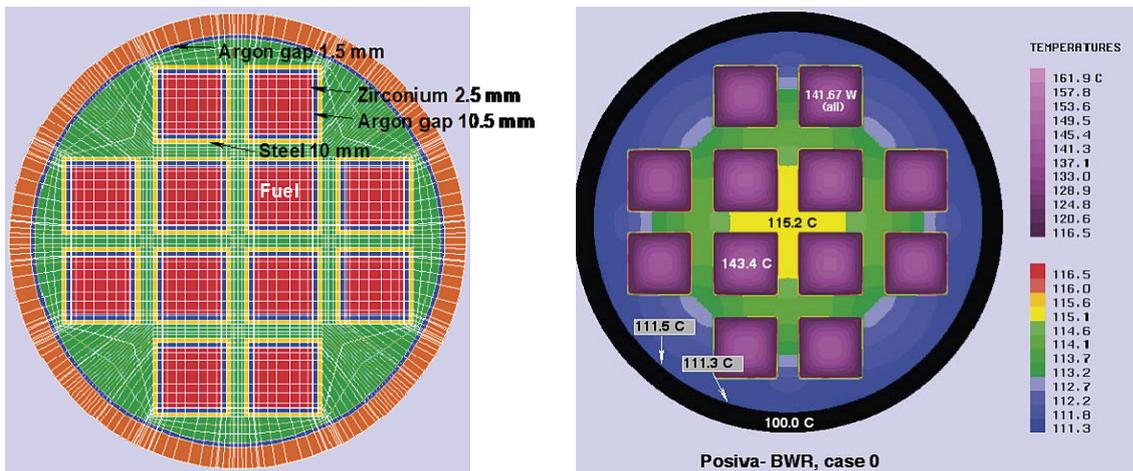
Figure 6-4. *Materials and gaps in the detailed 2D mesh of the Posiva-BWR fuel canister cross-section (left) and temperature distribution in the Posiva-BWR (0) case (right).*

The volumetric heat capacity of the Posiva-BWR insert is 0.443×3.22 MJ/m³/K + 0.115×3.85 MJ/m³/K + 0.023×1.97 MJ/m³/K + 0.304×1.3 MJ/m³/K = 2.3 MJ/m³/K. The effective volumetric capacity of the Posiva-VVER insert was computed to be 3.1 MJ/m³/K and of the SKB-PWR canister insert 2.7 MJ/m³/K.

Figure 6-5 presents the temperature evolution in the buffer in contact with the copper and on the copper cylinder in the mid-height. The hottest point of the canister surface (at the canister mid-height) is not in contact with the buffer in the dry deposition holes because of the insulating 10 mm air-filled annular gap between the copper cylinder and the bentonite buffer. Figure 6-5 also presents the effect of the 899 other Posiva-BWR canisters in a panel. The maximum summed temperature of 95 °C in the buffer is obtained in the contact area at the middle of the bottom plate after approximately 13 years. In this analysis, the decay heat power density distribution was assumed to be uniform. The temperature difference in the mid-height of the copper wall and in the buffer is approximately 2 °C.

Figure 6-6 shows the radial temperature distributions after 13 years. The temperature change over the internal 1.5 mm gas-filled gap is approximately 10 °C. In the cast iron insert, the temperature is approximately 10 °C higher than in copper cylinder, corresponding to the temperature difference obtained by the cross-sectional model analysis shown in Figure 5-3. In Figure 6-6 the temperature distribution in the homogenized insert is only the average distribution, when the effective thermal properties are used for the insert. Actually there are significant temperature differences in the fuel pellets and in the cast iron as shown in Chapter 5. As stated earlier the temperatures outside of the insert depend only on the total thermal power inside the insert.
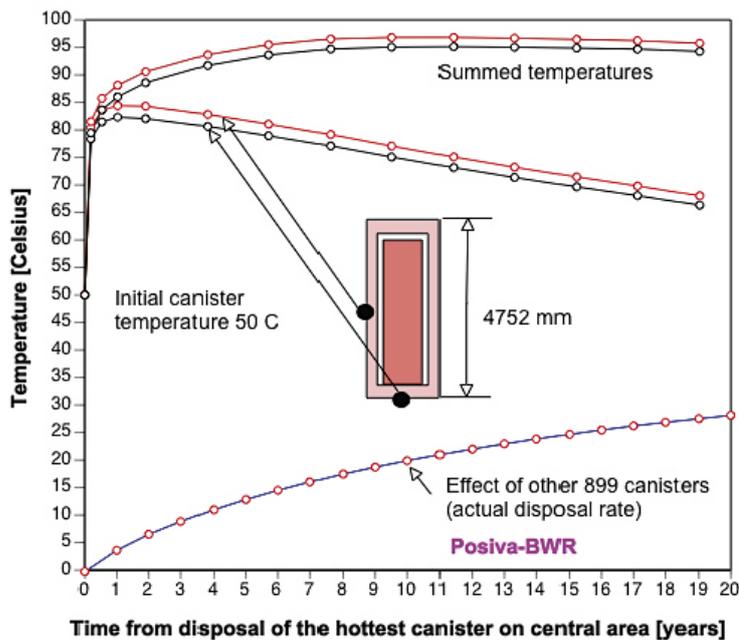
Figure 6-5. *Evolution of the maximum temperature in the buffer and in the mid-height of the copper cylinder.*
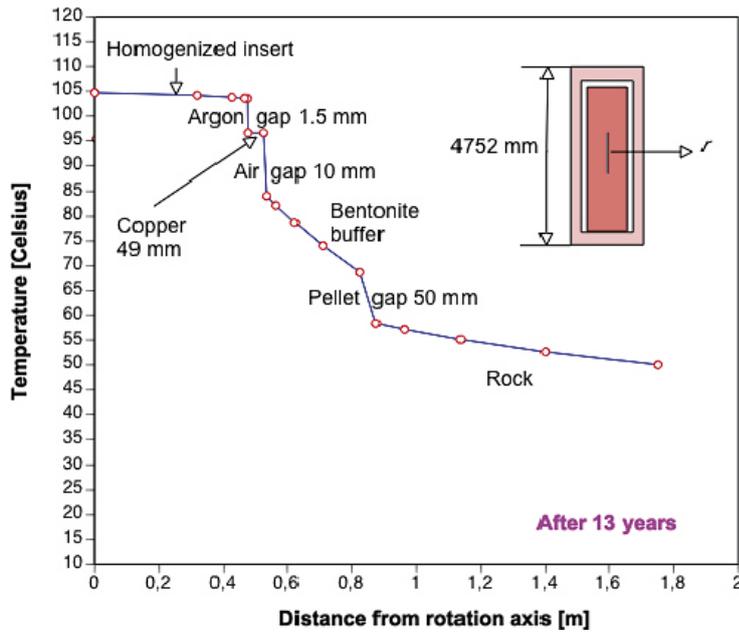
Figure 6-6. Radial temperature distribution of a single Posiva-BWR canister from the rotation axis at the mid-height of the hottest canister after 13 years including also the effect of the other 899 canisters according to Posiva-BWR global repository analysis.

6.1.1   Longitudinal temperature distribution along the canister surface

The effect of the shape of the decay heat power density distribution along the fuel assemblies on the canister surface temperature distribution was studied. Figure 6-7 shows the studied BWR density distribution shape and Figure 6-8 shows the results.

One conclusion from the curves in Figure 6-8 is that, in this case, the shape of the decay heat power density distribution has no significant effect on the maximum buffer temperature. In the upper end of the canister due to the inner gas gap of 1.5 mm, the temperature decreases by approximately 1.3 °C. In addition, other parameters inside the canister (gaps, emissivities, and shield gas) may have some effect.
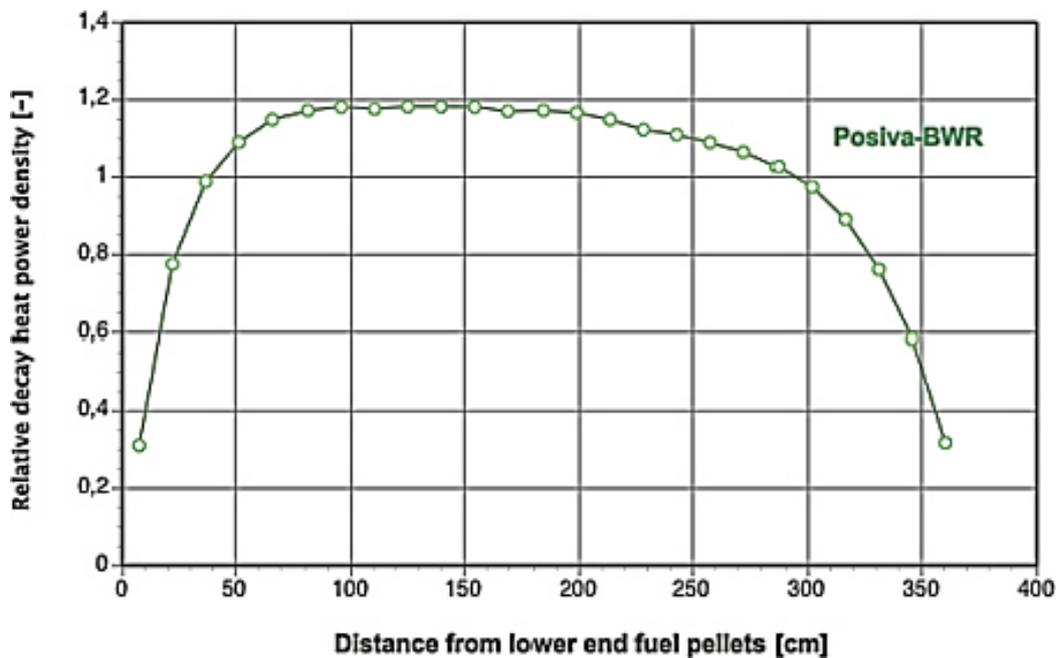
Figure 6-7. Decay heat power density distribution along the BWR fuel assembly length. The active length of the fuel rod is 370 cm.
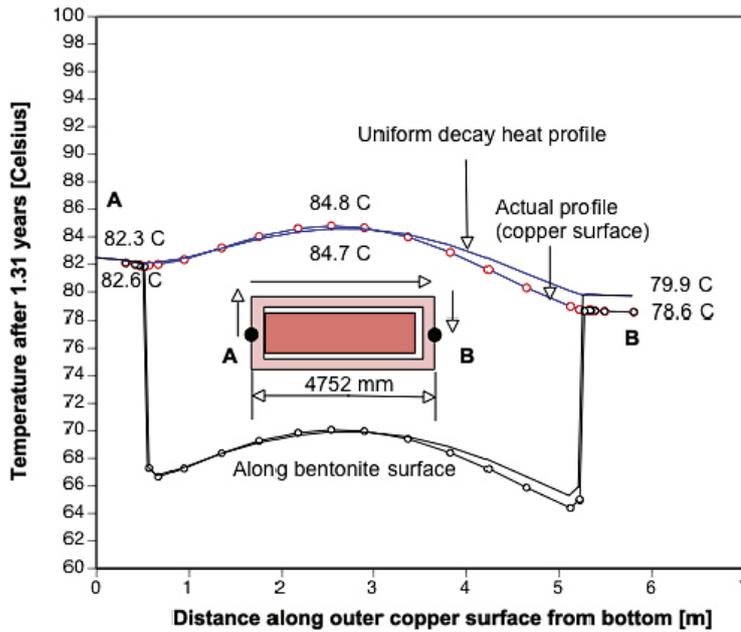
Figure 6-8. Temperature distribution along the external surface of a single Posiva-BWR canister with uniform and actual decay heat profiles after 1.3 years from disposal when the maximum temperatures in the bentonite buffer and the copper cylinder are encountered.

In an earlier analysis (Ikonen and Raiko 2012), the canister was simplified to be composed only of solid copper, and the decay heat was assumed to be uniformly distributed in the volume inside the copper walls. In that model there is only one gas gap on the outer copper surface. Figure 6-9 shows the differences between the results obtained by the solid copper model and the detailed model. Both models give practically equal maximum temperatures for the buffer temperature at point A.
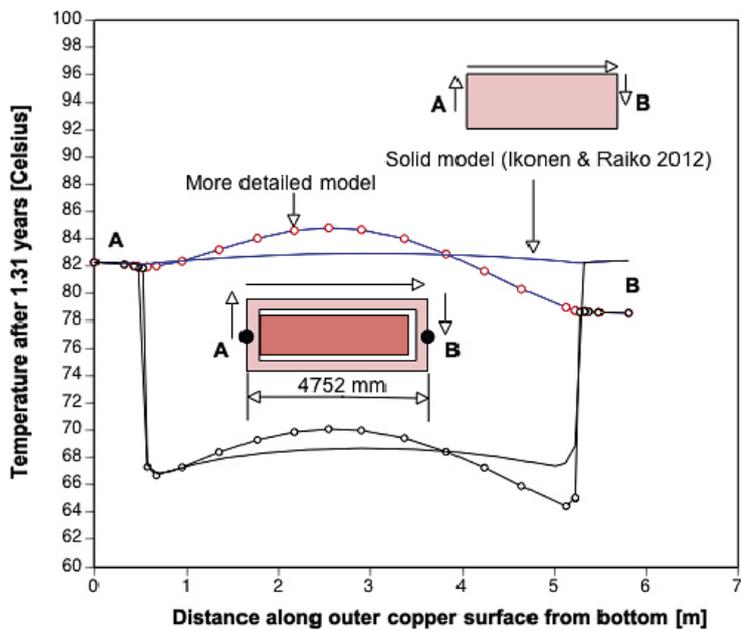
Figure 6-9. Temperature distribution along the external surface of a single Posiva-BWR canister after 1.3 years from disposal obtained by the solid homogenous modelling of the whole canister and by the more detailed canister model.

In these analyses, the effect of the collar of the copper lid was also studied (Figures 6-10 to 6-12).

It was observed that the collar can be omitted; however, the total actual length for the canister then needs to be used. If the reduced length of the canister 4752 mm − 85 mm = 4667 mm is used instead, temperatures will be overestimated by approximately 2 °C. It is important to ensure sufficient contacts between the copper and bentonite buffer in the upper end area of the canister when choosing installation tolerances for bentonite blocks. The circumstances of the upper part affect the maximum temperature of the lowest point of a canister, which is always in contact with the buffer.
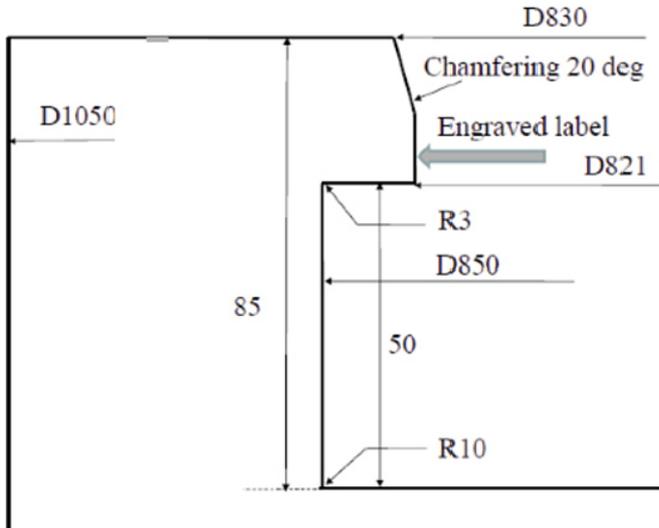
Figure 6-10. Canister copper lid. The dimensions reflect the geometry before welding deformations. Also the location of the engraved canister identification label is shown in the figure (Raiko 2012, Figure 15).
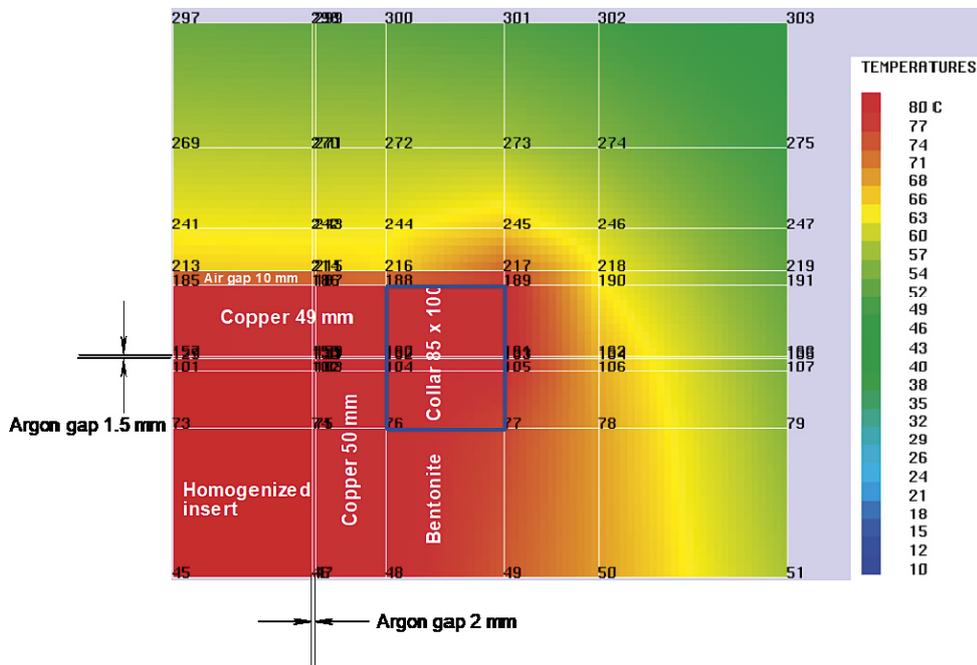
Figure 6-11. Temperature distribution in the upper corner of a canister with an 85 mm x 100 mm collar.
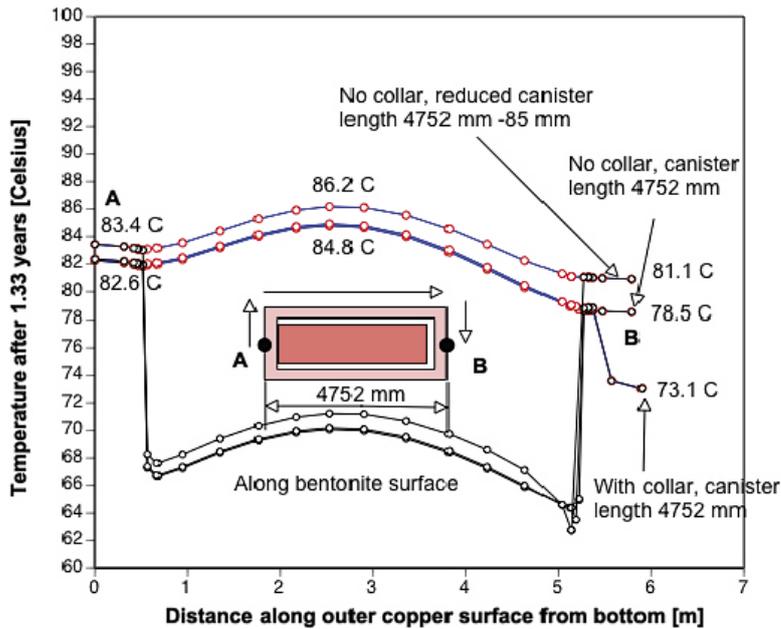
Figure 6-12. *The effect of modelling the collar in the upper end of the canister.*

Modelling of the longitudinal outer canister surface temperature distribution

The temperature distribution along the external surface was calculated for different canister types by an axisymmetric model and using the decay heat profile of the considered canister (Table 2-8). The evolution of the temperature at different moments, starting from the disposal time and extending up to many years, was obtained. The relative temperature was calculated along the canister surface, dividing by the current buffer temperature (in Kelvin) at point A (Figure 6-13). The scaled length in the horizontal axis is the distance from point A to point B along the outer surface of the canister. Apparently, the relative temperature profiles are very close to each other at different times, except for very short times (0.04 years in Figure 6-13). The differences in the beginning are caused by the initial temperatures of the model (e.g., the fuel temperature constant of 50 °C in starting the transient).

A decrease in the temperature at the top of the canister is caused by the 2 mm and 1.5 mm gas gaps and the distance to the heat-generating fuel pellets.
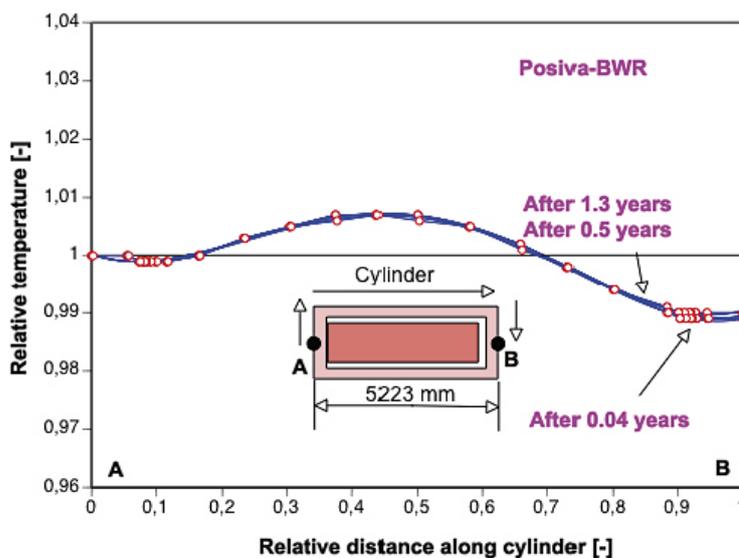
Figure 6-13. *Relative temperature distribution on the copper surface starting from the centre of the lower lid and ending at the centre of the upper lid.*

The curves in Figure 6-14 for various canister types are dependent on all the dimensions, the thermal properties, the decay heat profiles for various canister types etc but not on the time or the current decay power in a canister. The decay heat profiles in the longitudinal direction presented in Table 2-8 are assumed to be independent of the time and the decreasing decay power. On the bottom and top plate, the temperature is nearly constant, as seen from Figure 6-14.

The analysis of the whole repository gives the maximum temperature evolution (Figures 6-26 and 6-27) for the bentonite buffer at point A in Figure 6-14. Then, for the 3D analyses the longitudinal external surface temperature distribution of a canister is described by the curves in Figure 6-14. In the circumferential direction, the temperature is also very nearly constant in the case of differing heat powers of the fuel assemblies in a canister, as shown in Section 6.1.2. The effect of non-eccentricity is studied later in Section 7.1.

6.1.2 Circumferential temperature variation on the external copper wall

The goal of this section is to study, to what extent the temperature deviates from axisymmetric in the circumferential direction along the 49-mm-thick external cylindrical copper wall. For the study, the worst case of the SKB-PWR canister was chosen, where the canister has fuel assembly decay heat powers of 800 W, 300 W, 300 W and 300 W (SKB-PWR case 2). A slice of the canister was separated from the hottest place in the longitudinal direction. Then, adiabatic boundary conditions were set at the planes perpendicular to the axis of the canister. The 2D model (Figure 6-15) was extended radially over the 10 mm air gap, 290 mm bentonite layer (conductivity of 1.0 W/m/K), 50 mm pellet slot (conductivity of 0.29 W/m/K) and 875 mm to the host rock (conductivity of 2.9 W/m/K); thus, the total radius was 1750 mm from the canister centre line. The outer radius is sufficiently large that a constant temperature at the outer radius can be set. The temperature at this radius was chosen as 100 °C along the external copper wall.

Figure 6-16 shows the results. In the circumferential direction, the temperature varies by approximately 0.33 °C. If the fuel assemblies have equal powers of 425 W, the variation is only 0.0013 °C. This analysis concerned a four-assembly SKB-PWR canister. In the case of 12-fuel-assembly canisters (BWR or VVER), the temperature variation is smaller.
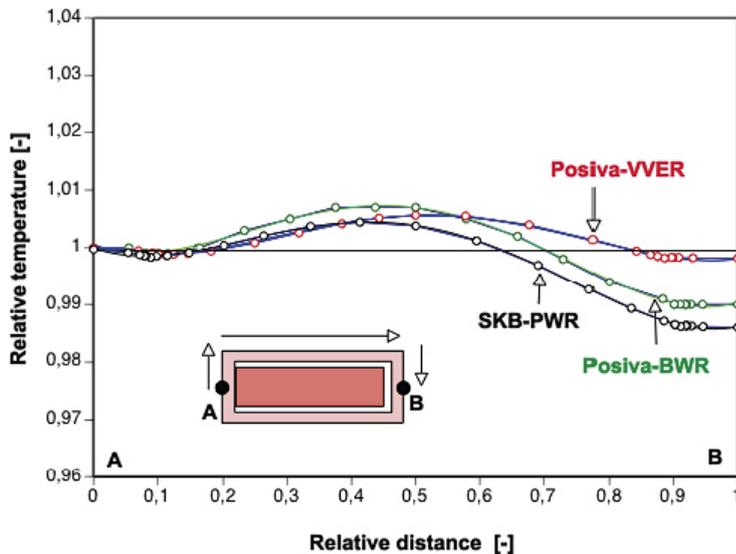
Figure 6-14. *Relative temperature distribution on the copper surface on the cylindrical part for various canister types. Points A and B are at the centre of the copper shell lids.*
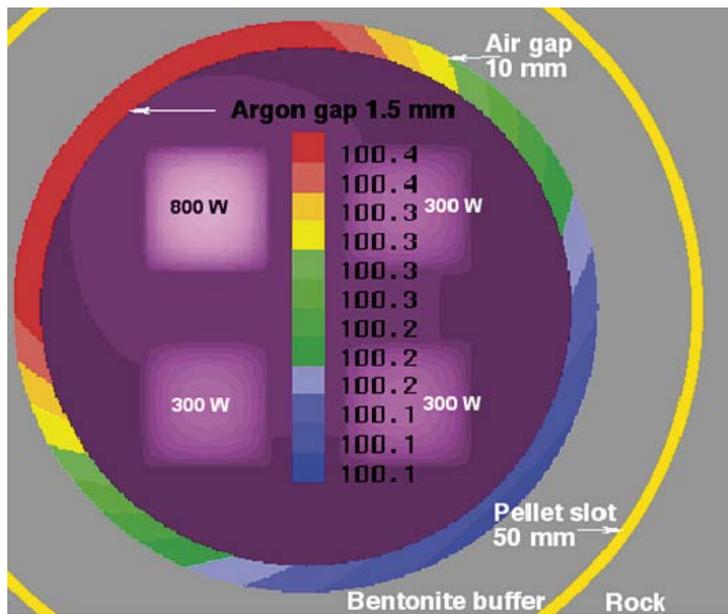
Figure 6-15. *Asymmetric decay heat power of the SKB-PWR fuel assemblies.*
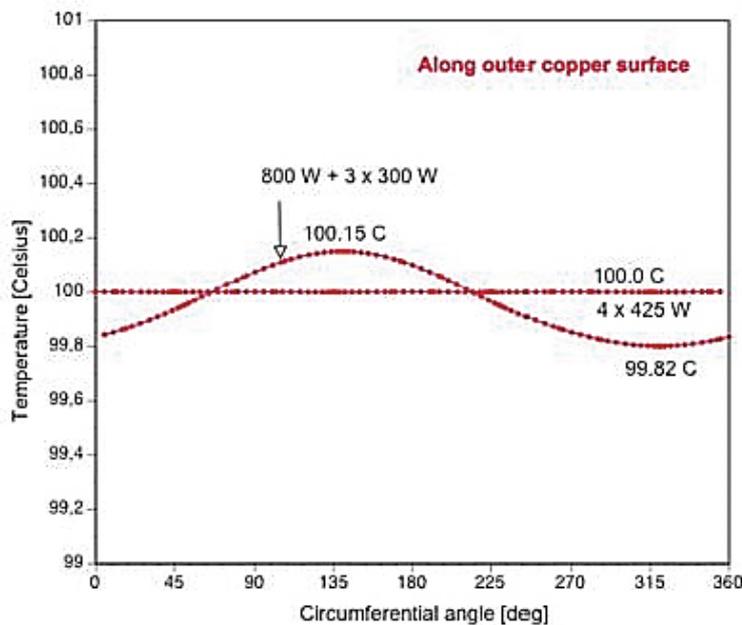
Figure 6-16. *Temperature variation in the circumferential direction along the external copper wall. Temperature distributions in the case of 800 W + 3 × 300 W = 1700 W (left) and in the case of 4 × 425 W.*

On the outer radius of the cast iron the temperature variation along the circumference is 2.1 °C (Figure 5-9). The SKB-PWR case 3 (Figure 5-10) may be a little more severe, but it can be expected that the temperature variation along the outer circumference of the copper is still negligible.

The conclusion from this study is that in 3D analyses, the temperature variation along the circumferential direction along the external surface of the copper is practically constant, also in cases when the fuel assemblies have strongly variable decay heat powers.

6.2   Internal structure of the canisters

The inserts have an integral flat bottom of cast iron and loose flat lids made of 50 mm steel plate on the top ends. Figures 6-17 to 6-19 show the principle of the modelling of the fuel assemblies and the surrounding structures.

Figure 6-18 shows the SKB fuel assemblies.
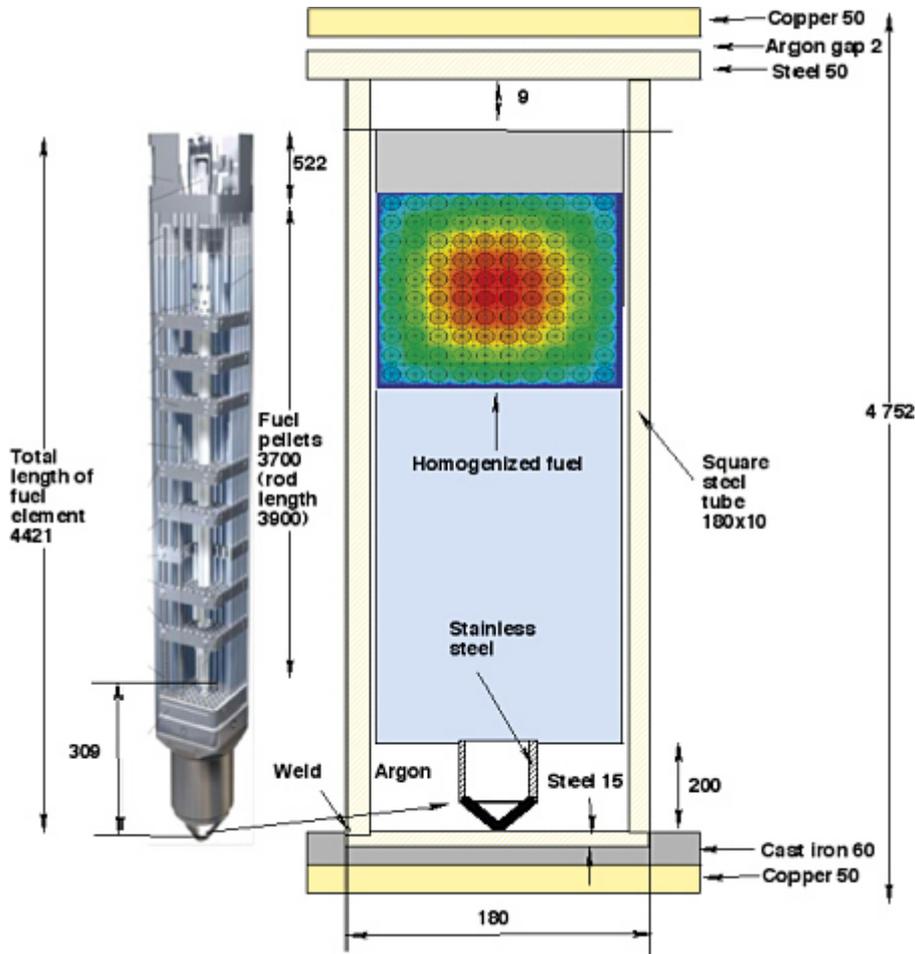
Figure 6-17. *Posiva-BWR-type fuel assembly and surrounding structures in canister (principal drawing, dimensions not to scale). Dimensions according to the Posiva-BWR canister.*
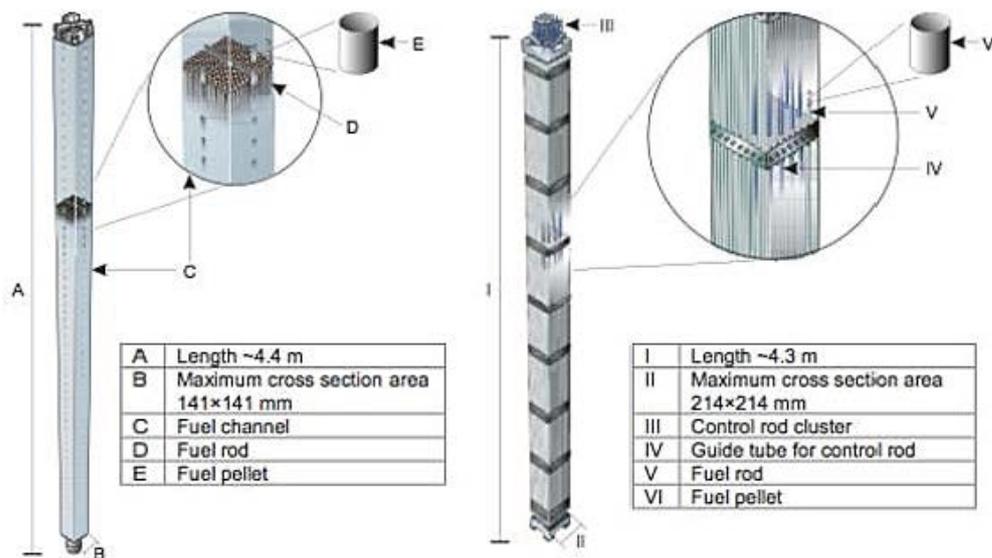
Figure 6-18. *SKB-BWR (left) and SKB-PWR fuel assemblies (right) (SKB 2010, Figure 2.5). Data based on specifications provided by the nuclear fuel suppliers.*
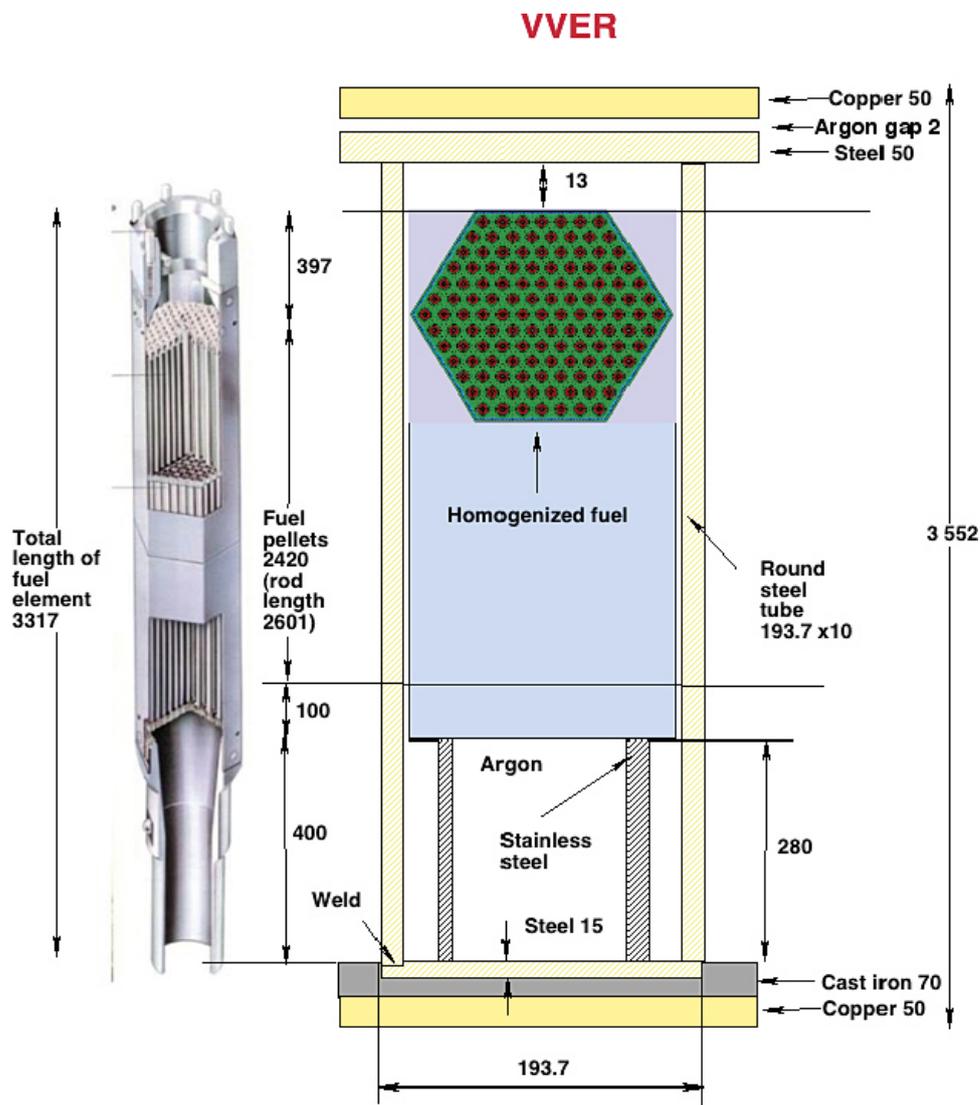
Figure 6-19. *VVER-type fuel assembly and surrounding structures in canister (principal drawing, dimensions not to scale).*

6.3 Effective conductivity of fuel assemblies in longitudinal direction

The effective longitudinal thermal conductivity of a fuel assembly is calculated by weighting the thermal conductivities of UO_2, zirconium and argon by their relative cross-sectional areas, giving the curves in Figure 6-20. The fittings of these curves were formed for the longitudinal thermal conductivity of the homogenized fuel rod array area and are used in the analysis (λ in W/m/K and T in Celsius < 300 °C). The fittings are

$$\lambda_{BWR,\ longitudinal} = 2.85 + 3.67 \times 10^{-4}T$$

$$\lambda_{VVER,\ longitudinal} = 3.67 + 1.14 \times 10^{-4}T$$

$$\lambda_{PWR,\ longitudinal} = 2.94 + 8.87 \times 10^{-4}T \tag{6-1}$$

In the fuel assembly active area, the effective longitudinal (axial) conductivity is approximately 30 times greater than the effective conductivity in the transverse direction (Figures 4-12 and 4-14).
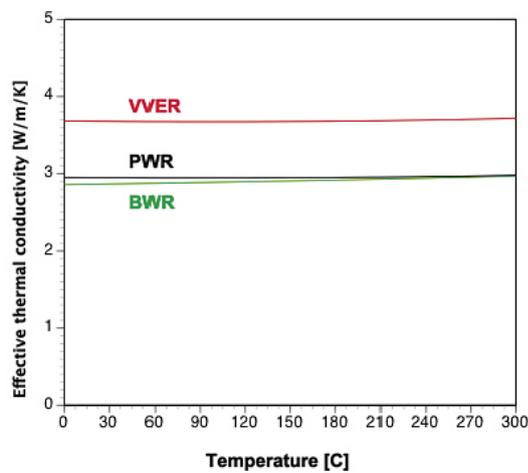
Figure 6-20. *Effective thermal conductivity of the fuelled area in the longitudinal direction.*

6.4 Effective longitudinal heat conduction of lower and upper end of fuel assemblies

Heat transfer in the longitudinal direction in the lower end of the fuel assembly is modelled using the effective thermal conductivity (Equation 3-7)

$$\lambda_{eff} = \lambda_{argon} + 4\,\varepsilon_{tot}\,\sigma T_{mean}^3 h_{argon} \tag{6-2}$$

where T_{mean} is the mean temperature of the argon (the average of the surface temperatures in Kelvin) and h_{argon} is the length of the argon space. In the transverse direction, only the thermal conductivity of argon is applied.

Posiva-VVER fuel assembly

The lower end of the fuel assembly is a cylindrical stainless steel tube, which is located inside the circular compartment tube. The effective thermal conductivity in the vertical direction is calculated by applying Equation (6-2):

$$\lambda_{eff} = \frac{A_{tot} - A_{steel}}{A_{tot}}\left(\lambda_{argon} + 4\,\varepsilon_{tot}\,\sigma T_{mean}^3 h_{argon}\right) + \frac{A_{steel}}{A_{tot}}\lambda_{steel}. \tag{6-3}$$

The inner diameter of the circular tube is 174 mm (Figure 2-2) and the corresponding area $A_{tot} = \pi\,(17.4\text{ cm}/2)^2 = 237\text{ cm}^2$. The cross-sectional area of the stainless steel tube is $A_{steel} = 14\text{ cm}^2$, and its height $h_{argon} = 0.5$ m. The thermal conductivity of stainless steel is $\lambda_{steel} = 15$ W/m/K. By weighting with proportional cross-sectional areas the effective vertical heat conductivity is for instance at 100 °C (emissivity 0.6, Table 2-5).

$$\lambda_{eff} = \frac{237 - 14}{237}\left[0.02\text{ W/m/K} + 4 \cdot 0.5\text{ m} \cdot 0.6 \cdot 5.67 \cdot 10^{-8}\text{ W/(m}^2\text{K}^4) \cdot (373\text{ K})^3\right]$$
$$+ \frac{14}{237} \cdot 15\text{ W/m/K} = 0.021\text{ W/m/K} + 2.4\text{ W/m/K} + 1.1\text{ W/m/K} = 3.5\text{ W/m/K}. \tag{6-4}$$

The effect of conduction in gas (argon) is small.

SKB-PWR fuel assembly

The inner area of the rectangular compartment steel tube is (Figure 2-2) $A_{tot} = (23.5\text{ cm})^2 = 552\text{ cm}^2$. The cross-sectional area of the stainless steel is estimated to be 70 cm^2, and its height is 5 cm. At 100 °C the effective vertical heat conductivity is approximately

$$\lambda_{eff} = \frac{552 - 70}{552}\left[0.02\text{ W/m/K} + 4 \cdot 0.05\text{ m} \cdot 0.6 \cdot 5.67 \cdot 10^{-8}\text{ W/(m}^2\text{K}^4) \cdot (373\text{ K})^3\right]$$
$$+ \frac{70}{552} \cdot 15\text{ W/m/K} = 0.019\text{ W/m/K} + 0.2\text{ W/m/K} + 2.3\text{ W/m/K} = 2.6\text{ W/m/K}. \tag{6-5}$$

Posiva-BWR fuel assembly

The lower end of the BWR fuel assembly includes a weakly conducting triangle (Figure 6-21), which lowers the vertical conductivity. First, the effective conductivity in the vertical direction of the cylindrical area inside the outer radius of the stainless steel tube is determined.

From the continuity of the heat flux, it follows that (Figure 6-21)

$$\lambda_{steel}\frac{\Delta T_1}{\Delta h_1} A_1 = \lambda_{steel}\frac{\Delta T_2}{\Delta h_2} A_2 = \lambda_{tube}\frac{\Delta T_1 + \Delta T_2}{\Delta h_1 + \Delta h_2} A_1. \tag{6-6}$$
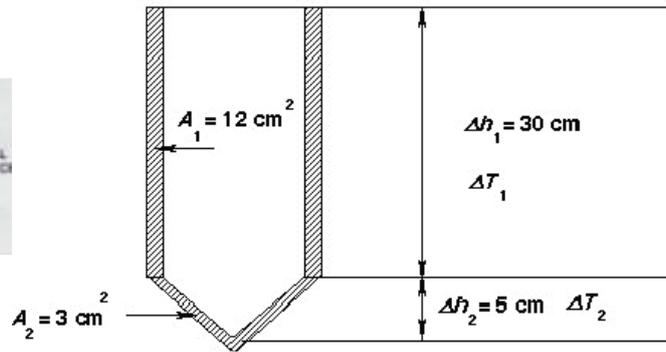
Figure 6-21. *Lower end of the Posiva-BWR fuel assembly.*

This gives, for the effective conductivity,

$$\lambda_{tube} = \lambda_{steel} \frac{1 + \dfrac{\Delta h_1}{\Delta h_2}}{\dfrac{\Delta A_1}{\Delta A_2} + \dfrac{\Delta h_1}{\Delta h_2}} = 0.7 \ \lambda_{steel} \ , \qquad (6\text{-}7)$$

when $\Delta A_1 = 12$ cm², $\Delta A_2 = 3$ cm², $\Delta h_1 = 300$ mm and $\Delta h_2 = 50$ mm. The internal area of the compartment tube is $A_{tot} = (16 \text{ cm})^2 = 256$ cm². At 100 °C, the effective vertical heat conductivity is approximately

$$\lambda_{eff} = \frac{A_{tot} - A_{steel}}{A_{tot}} (\lambda_{argon} + 4 \, \varepsilon_{tot} \, \sigma T^3_{mean} h_{argon}) + 0.7 \frac{A_{steel}}{A_{tot}} \lambda_{steel}$$

$$= \frac{256 - 12}{237} \ [0.02 \text{ W/m/K} + 4 \cdot 0.30 \text{ m} \cdot 0.6 \cdot 5.67 \cdot 10^{-8} \text{ W/(m}^2\text{K}^4) \cdot (373 \text{ K})^3] \qquad (6\text{-}8)$$

$$+ 0.7 \frac{12}{237} \cdot 15 \text{ W/m/K} \ = 0.021 \text{ W/m/K} + 1.4 \text{ W/m/K} \ + 0.6 \text{ W/m/K} = 2.1 \text{ W/m/K} \ .$$

Polynomial fittings

The effective longitudinal thermal conductivity curves of the fuel assemblies at varying temperature are presented in Figure 6-22. The fittings of these curves used in the analysis are (λ in W/m/K and T in Celsius < 300 °C)

$$\lambda_{BWR, \ effective \ at \ bottom \ area} = 1.08 + 5.26 \times 10^{-3} T + 3.53 \times 10^{-5} T^2$$

$$\lambda_{VVER, \ effective \ at \ bottom \ area} = 1.83 + 8.71 \times 10^{-3} T + 5.80 \times 10^{-5} T^2$$

$$\lambda_{PWR, \ effective \ at \ bottom \ area} = 1.88 + 2.60 \times 10^{-3} T + 5.38 \times 10^{-6} T^2 \qquad (6\text{-}9)$$

The curves in Figure 6-22 are only approximate. A considerable amount of heat is transferred in the longitudinal direction also along the compartment steel tubes ($\lambda = 57$ W/m/K) and cast iron ($\lambda = 35$ W/m/K).
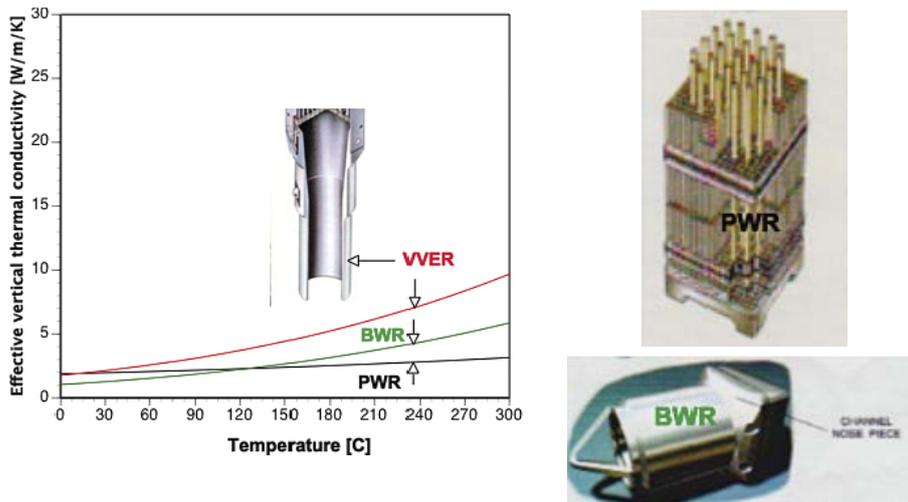
***Figure 6-22.** Effective thermal conductivity of fuel assembly bottom end structure in longitudinal (vertical) direction.*

6.5 Generation of 3D model of the canisters in the repository

The 3D meshes for various fuel canisters are generated by duplicating 2D meshes as shown earlier in Chapter 5 in the longitudinal direction of the canister. The layers are fitted with the cross-sections where some of materials changes or where decay heat generation starts or finishes (Table 6-2). Figure 6-23 shows an example of a 3D mesh and a visualisation of the material types. Heat generation is integrated over the heated volume, and whether it corresponds to the total decay heat power generated in the canister is verified.

Figure 6-24 illustrates parts of a 3D mesh. There are nearly 100 000 control volumes in a canister model.

For the 3D analyses, the location of the fuel pellets is an input parameter. Table 6-2 presents the location of the fuel pellets in the canisters.

Table 6-2. Location of the fuel pellets length in the canisters (Tables 2-1 and 2-2, Figures 6-17 to 6-22).

	SKB-BWR	SKB-PWR	Posiva-BWR	Posiva-VVER
Lower end of fuel pellets from lowest point of canister [mm]	502	350*)	419	620
Upper end of fuel pellets from uppermost point of canister [mm]	665	827	633	512
Active length of fuel rod [mm]	3680	3658	3700	2420
Total length of canister [mm]	4835	4835	4752	3552

*) Estimated.

Figure 6-23. *Visualization of the material types in the SKB-PWR canister.*
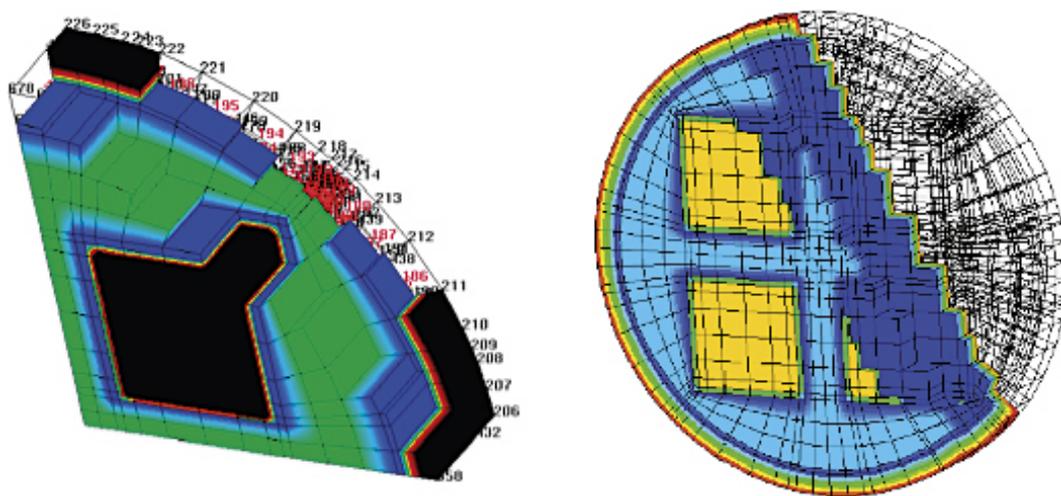
Figure 6-24. *Examples of parts of 3D meshes.*

The thermal conductivity of the homogenized fuel rod array area in the transverse (horizontal) direction for different assemblies is calculated from the polynomial fittings in (11) and in the longitudinal (vertical) direction from the fittings in (13). In the gas gaps, the effective conductivity, considering thermal radiation, is calculated from (10).

Prior to the 3D analyses, for checking purposes, only two layers of 20 cm from the fuel rod array area at the location, where the longitudinal decay heat profile of a fuel assembly obtains its maximum value was modelled and compared to the earlier analysed temperature of the 2D analyses (Table 5-1). The average decay heat power density distributions were multiplied by the peak values of 1.183, 1.06 and 1.125 in Table 2-8 and used for the Posiva-BWR, SKB-PWR and Posiva-VVER fuel assemblies. The temperature along the outer radius was kept as 100 °C, as in the 2D analyses, and the total power was kept as the initial power of 1700 W for the Posiva-BWR and SKB-PWR fuel-type canisters and of 1370 W for the Posiva-VVER fuel-type canister. Table 6-3 shows the results. Small temperature differences (maximum of 0.2 °C) are caused by numerical reasons. This was a comparison-testing case for the 2D and 3D programmes, therein eliminating the possibilities of many malfunctions or errors in the respective codes.

Table 6-3. Maximum temperature in the cast iron and fuel pellets. In all cases the temperature on the outer surface of the canister is 100 °C. In the 3D model the length of the model is 20 cm and there are only two layers of control volumes in the longitudinal direction.

Case ( )	2D model		3D model	
	$T_{Max,\ cast\ iron}$ [°C]	$T_{Max,\ in\ fuel}$ [°C]	$T_{Max,\ cast\ iron}$ [°C]	$T_{Max,\ in\ fuel}$ [°C]
Posiva-BWR (0)	115.2	143.4	115.1	143.4
Posiva-BWR (1)	116.5	161.9	116.4	161.8
Posiva-BWR (2)	114.1	149.4	114.1	149.5
SKB-PWR (1)	112.7	165.4	112.8	165.5
SKB-PWR (2)	113.1	203.0	113.2	203.1
SKB-PWR (3)	113.6	193.8	113.8	193.9
Posiva-VVER (0)	117.1	148.9	117.1	149.0
Posiva-VVER (1)	116.1	154.8	116.0	155.0
Posiva-VVER (2)	118.1	164.0	118.1	164.2

6.6   Evolution of maximum bentonite temperature

For the long-term 3D thermal analyses of the canisters one input quantity is the maximum buffer temperature evolution of the contact point below the canister. Figure 6-25 demonstrates disposing of BWR canisters in a panel consisting of 900 canisters (Ikonen and Raiko 2012). A panel of 900 canisters is a reference case for the Posiva repository basic dimensioning, a very large panel that should obtain the highest canister temperature in the central area.

The temperature evolution in Figure 6-26 was calculated earlier in Ikonen and Raiko (2012), in which the canister was simplified to be composed only of copper, and the decay heat was assumed to be uniformly distributed. The calculation was repeated with the detailed model and approximately the same curves for the buffer temperature were obtained. The temperature distribution at a time of 1.3 years is presented in Figure 6-9.
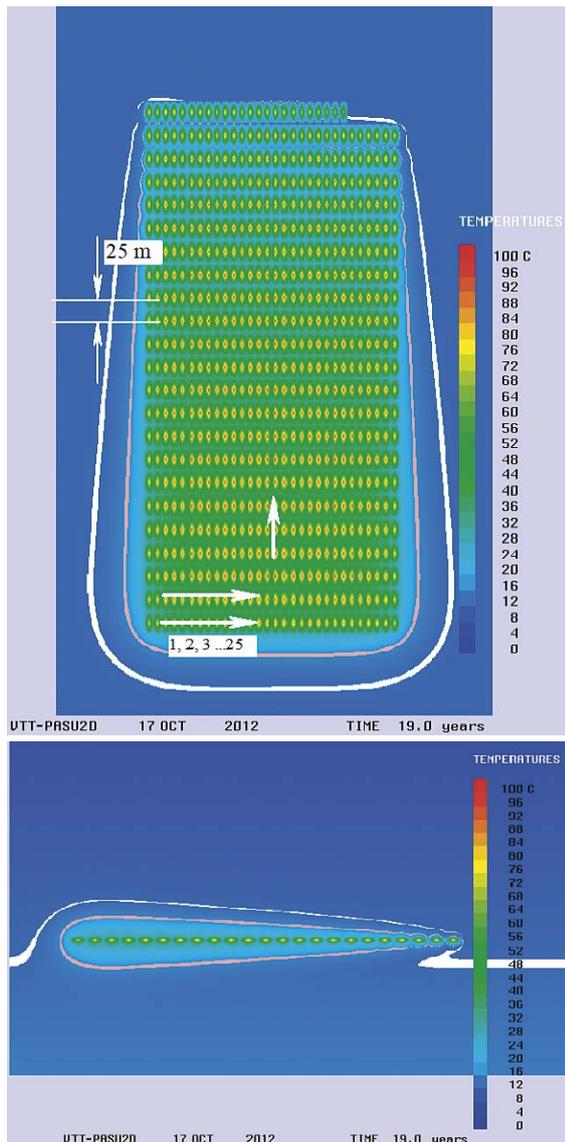
Figure 6-25. *Temperature distribution of the repository in the horizontal cross-section (left) and in the vertical cross-section (right) after 19 years of operation, when the highest temperature of 95 °C is obtained on the hottest BWR canister surface. The tunnel spacing is 25 m, and the canister spacing is 8.9 m. The rate of canister deposition is 36 canisters per year.*
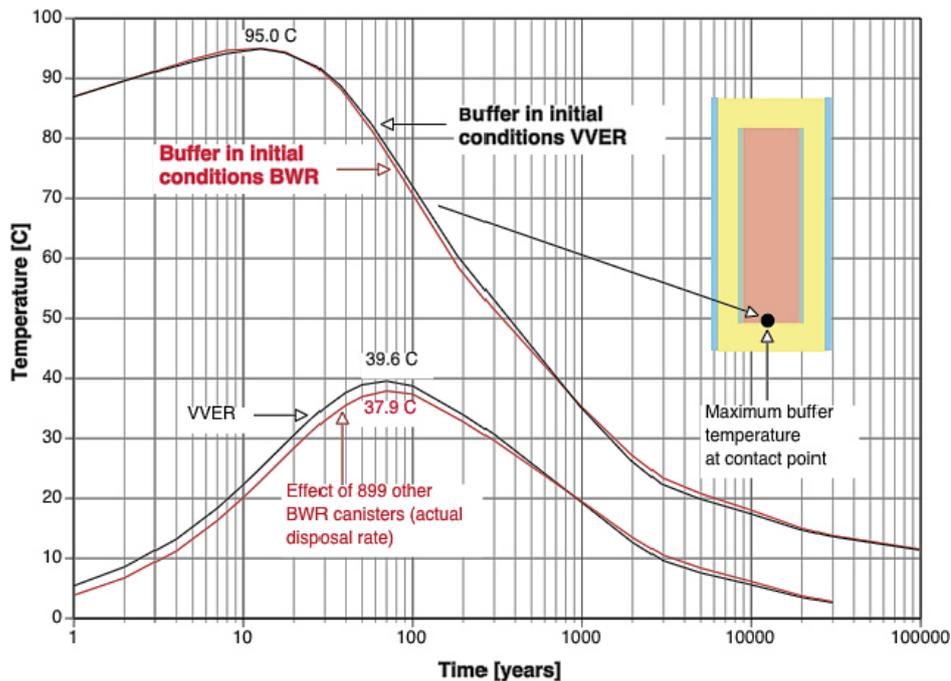
Figure 6-26. *Maximum temperature evolution in the bentonite buffer of the Posiva-BWR canister (the spacing is 8.9 m) and of the Posiva-VVER canister (the spacing is 7.5 m). Contribution of the other canisters in a repository panel is summed in the curves. Upper curves also include initial ambient rock temperature of 10.5 °C of Olkiluoto repository. Lower curves give the contribution of the other canisters in the repository.*

The maximum buffer temperature evolution of the KBS-3 V Posiva-BWR and Posiva-VVER canisters in the initial condition case is presented in Figure 6-26 (Ikonen and Raiko 2012). To solve the problem, the numerical and analytical solutions were combined, as presented in Ikonen and Raiko (2012). The tunnel spacing is 25 m, and the canister spacings for the Posiva-BWR and for the Posiva-VVER are 8.9 m and 7.5 m, respectively. These spacings were determined for when the maximum allowable canister surface temperature was limited to 95 °C.

The contribution of the 899 canisters cause nearly constant temperature distribution at the considered hottest canister in the central area of the repository panel. This was studied in the following way by the analytic global model. The volume of the considered hottest Posiva-BWR canister location was assumed to be without the heat generating canister and consisting only of the host rock. On the radius of 0.875 m of the disposal hole and in the mid-height of the canister location the rock temperature varied 0.05 °C in the circumferential direction. On the axis of the disposal hole the temperature at the mid-height of the canister was 0.16 °C higher than at the lower end of the canister, in the contact point between the bentonite and the canister. It was further studied the case, in which the canister is located on the edge of the repository panel. In the case that the canister locates in the middle of the long edge of the panel the temperature varied 0.46 °C in the circumferential direction around the canister location. Secondly, in the case that the canister locates in the middle of the short edge of the panel the temperature varied 0.66 °C in the circumferential direction. In the third case that the considered canister locates in the corner of the panel the temperature varied 0.90 °C in the circumferential direction. The conclusion of these studies is that the temperature variation around the copper cylinder caused by the effect of the other canisters of the repository panel is negligible small in all areas of the panel. The temperature differences are small also in the vertical direction at all canister locations in the repository panel.

Figure 6-27 gives the evolution of the maximum bentonite buffer temperature for the SKB-BWR and PWR case. Table 6-4 gives the evolution of the maximum bentonite buffer temperature for the SKB-BWR and PWR and for a Posiva-BWR panel. The temperatures are close to each other due to similar planning criteria (the maximum calculated bentonite buffer temperature is 95 °C in the global thermal dimensioning analyses). The repository dimensioning gives the maximum temperature evolution of the bentonite buffer and that equals the temperature of the bottom of the canister in the centre of a large panel of canisters in a repository in Forsmark and Olkiluoto.
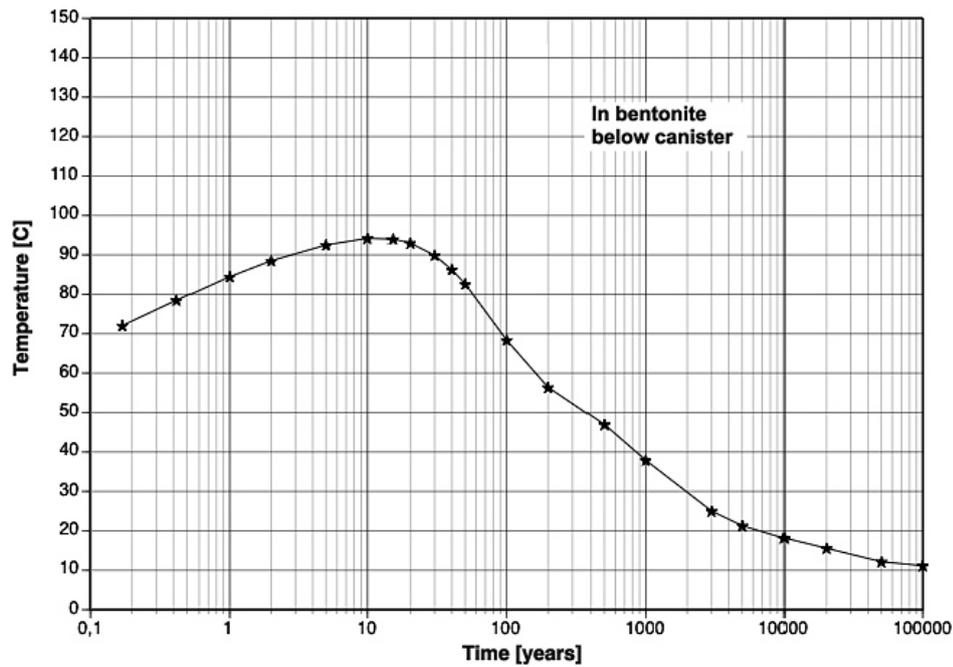
Figure 6-27. *Evolution of the maximum bentonite buffer temperature in a SKB-BWRandPWR repository case (Hökmark et al. 2010).*

The maximum bentonite buffer temperature evolution in the SKB repository is given in Figure 6-27.

The evolution of the maximum bentonite buffer temperature in Table 6-4 is applied separately for the SKB and Posiva cases in long-term 3D analysis as an input quantity of the lowest point of a canister, which is always in contact with the buffer.

Table 6-4. Evolution of the maximum bentonite buffer temperature in the SKB repository (Hökmark et al. 2010, Figure 5-15) and in a Posiva-BWR and Posiva-VVER panel with 900 canisters (Ikonen and Raiko 2012).

SKB		Posiva		
Time [years]	Temperature [°C]	Time [years]	BWR temperature [°C]	VVER temperature [°C]
0.2	72.1	1	87.0	87.2
0.4	78.6	2	89.6	89.9
1	84.5	4	92.2	92.5
2	88.5	7	94.3	94.5
5	92.6	10	94.7	95.6
10	94.1	12	94.8	96.0
15	94.1	15	94.6	95.8
20	93.0	20	93.5	95.2
30	89.9	25	92.1	94.1
40	86.3	30	90.5	92.7
50	82.6	40	86.9	89.6
100	68.4	50	83.4	86.3
200	56.4	70	77.1	80.1
500	47.0	100	70.5	73.5
1000	38.0	200	57.3	60.1
3000	25.1	300	51.3	53.7
5000	21.4	1000	35.1	35.0
10 000	18.1	2000	27.0	26.1
		3000	23.3	22.3

6.7   Pre-cooling times

The decay heat for the fuels was presented in Section 2.4 (Table 2-6). The decay power between two points can be interpolated by a linear fitting in a log-log coordinate system as

$$\ln P = a + b \ln t .$$ (6-11)

By setting the powers P_1 and P_2, between which the known power P exists, and the corresponding times t_1 and t_2, the fitting coefficients a and b are solved, and the interpolation for the pre-cooling time t is solved from

$$\ln \frac{t}{t_1} = \frac{\ln \dfrac{P}{P_1}}{\ln \dfrac{P_1}{P_2}} \ln \frac{t_1}{t_2} .$$ (6-12)

This fitting is sufficiently accurate, if the points are given after sufficiently short time increments, for instance, after every 10 years, as in Table 2-6. Table 6-5 shows the pre-cooling times in the cases presented in Chapter 5. In the reference cases, the pre-cooling time is 33.0, 21.24 and 28.3 years for the Posiva-BWR, SKB-PWR and Posiva-VVER reference case, respectively, when burn-ups and decay heat are given in Table 2-6. In the 3D analyses, the decreasing rate of the decay heat for the fuel assemblies having varying burn-ups is set inside the programme.

Table 6-5. Decay heat power versus pre-cooling time.

Case	Fuel assembly power [W]	Pre-cooling time [years]
Posiva-BWR (0)	1700/12	33.0
Posiva-BWR (1)	92.5 and 240.0	58.4 and 9.50
Posiva-BWR (2)	182.1 and 60.71	20.0 and 88.7
SKB-PWR (1)	1700/4	21.24
SKB-PWR (2)	800 and 300	4.1 and 36.5
SKB-PWR (3)	700 and 150	5.8 and 79.4
Posiva-VVER (0)	1370/12	28.3
Posiva-VVER (1)	142.71 and 57.08	16.3 and 76.4
Posiva-VVER (2)	85.63 and 171.25	46.2 and 9.8
Additional analyses		
SKB-BWR (0)	1700/12	32.7
SKB-BWR (1)	92.5 and 240.0	58.1 and 9.39
SKB-BWR (2)	182.1 and 60.71	20.0 and 88.3

6.8   Results of 3D temperature analyses of the whole repository

In the following analyses, the steps are as follows. The temperature evolution of the outer surface of a canister is known input data for these 3D analyses and was determined earlier for the SKB and Posiva canisters in a repository. At some moment, the maximum buffer temperature (Table 6-4 and Figures 6-26 and 6-27) is set to be at the lower end of the canister, and the longitudinal temperature distribution along the outer copper surface is set according to Figure 6-14. In the circumferential direction, the outer copper temperature is approximately constant, as was shown in Section 6.1.2. The stationary state is searched by iteration. The iteration is stopped when the maximum temperature difference between two consecutive iteration cycles is 0.001 °C. The decay heat power from the considered moment is taken from Table 2-8.

Figures 6-28 to 6-30 show the maximum cast iron temperature evolutions in the same cases as were studied in the 2D analyses in Chapter 5. The maximum temperature appears after approximately 10–12 years from the disposal of the hottest canister. The highest temperature of 108.9 °C is encountered in the Posiva-VVER reference case 0. The conclusion that can be drawn from Figures 6-28 to 6-30 is that different decay heat powers in individual fuel assemblies in a canister have only a small effect on the maximum cast iron temperature although larger effects are found in the fuel pellets themselves.
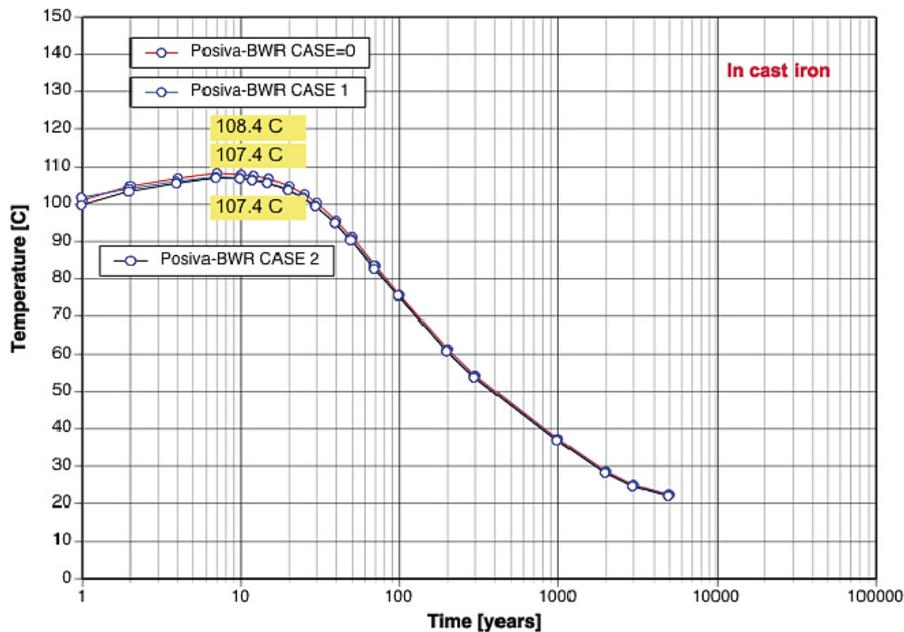
Figure 6-28. *Maximum cast iron temperature evolution for the Posiva-BWR canister.*
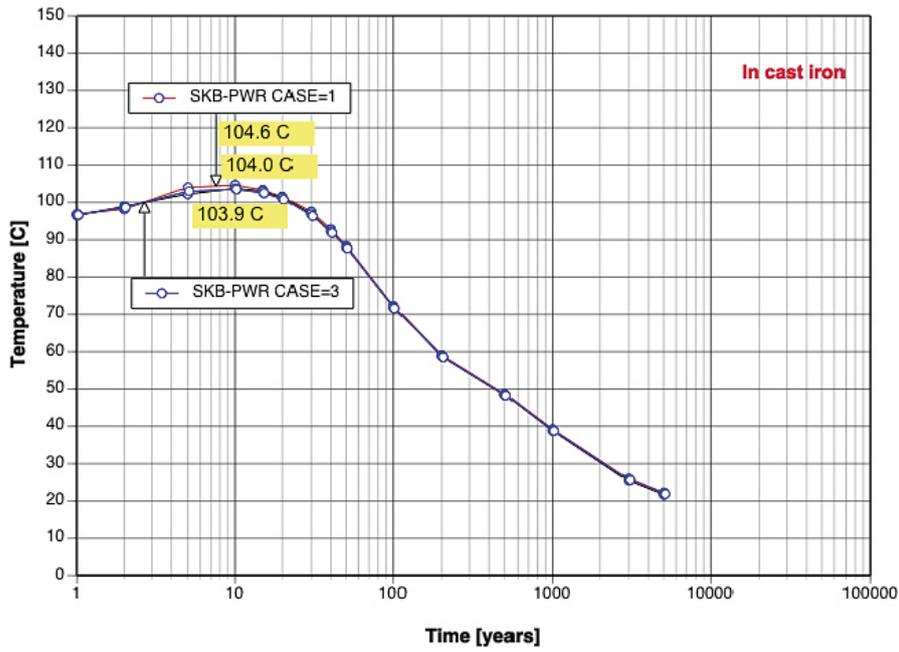
Figure 6-29. *Maximum cast iron temperature evolution for the SKB-PWR canister.*
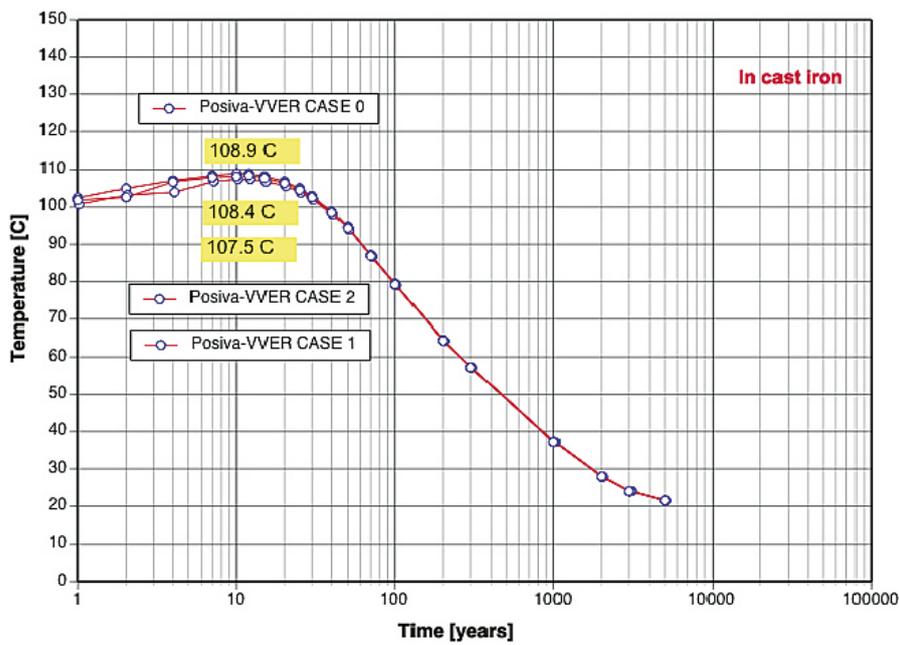
Figure 6-30. *Maximum cast iron temperature evolution for the Posiva-VVER canister.*

Figures 6-31 to 6-33 show the maximum fuel pellets temperature evolutions in the respective cases studied in the 2D analyses in Chapter 6. The maximum temperature appears after approximately four years or fewer from the disposal of the hottest canister. The highest temperature of 182.7 °C is encountered in the 2nd case for the SKB-PWR canister.

It should be emphasized that the curves in Figures 6-28 to 6-33 concern dry installation conditions, whereas, in reality, groundwater may fill the gaps in the buffer, and temperatures decrease over time. That case has not been calculated here.
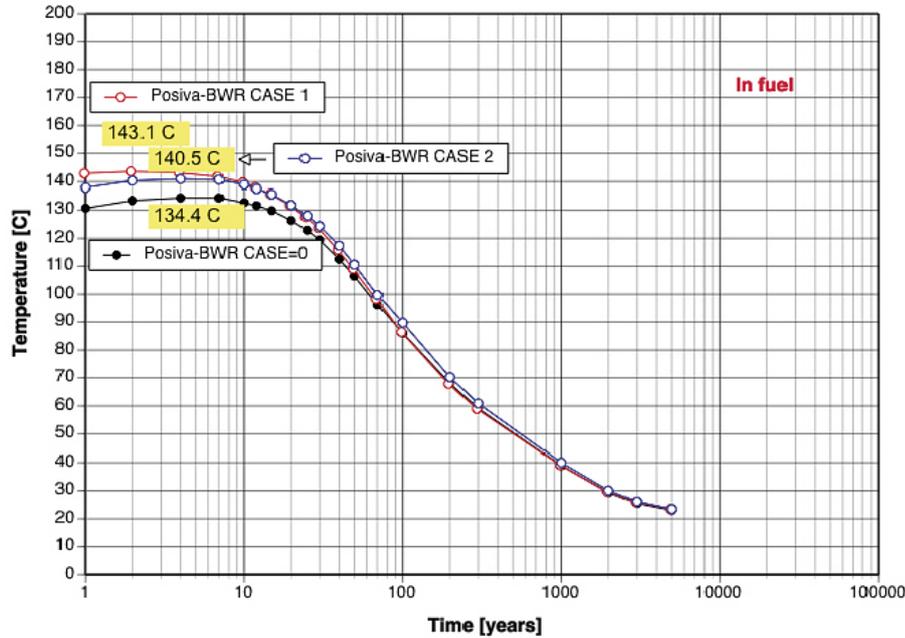
Figure 6-31. Maximum fuel pellet temperature evolution for the Posiva-BWR canister.
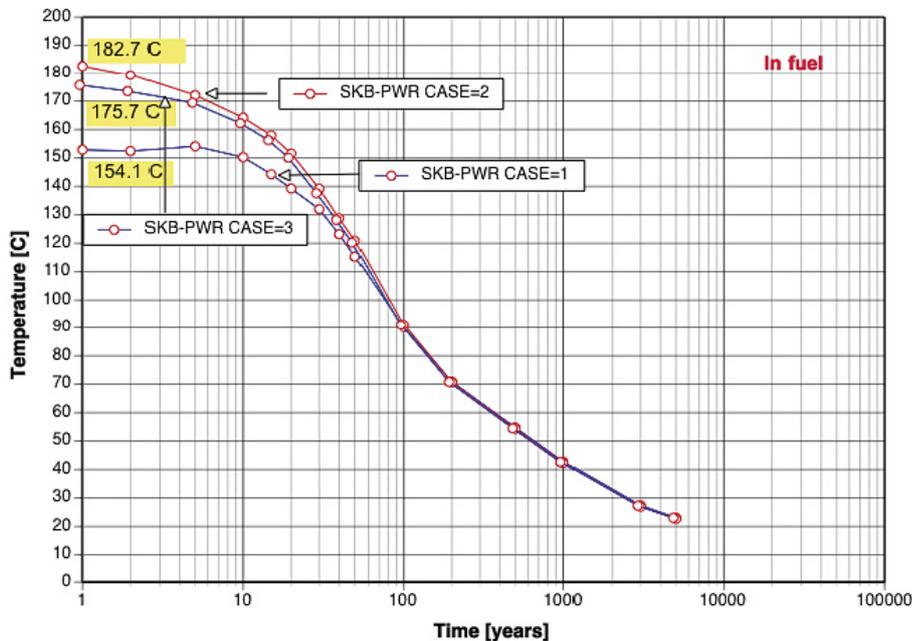
Figure 6-32. Maximum fuel pellet temperature evolution for the SKB-PWR canister.
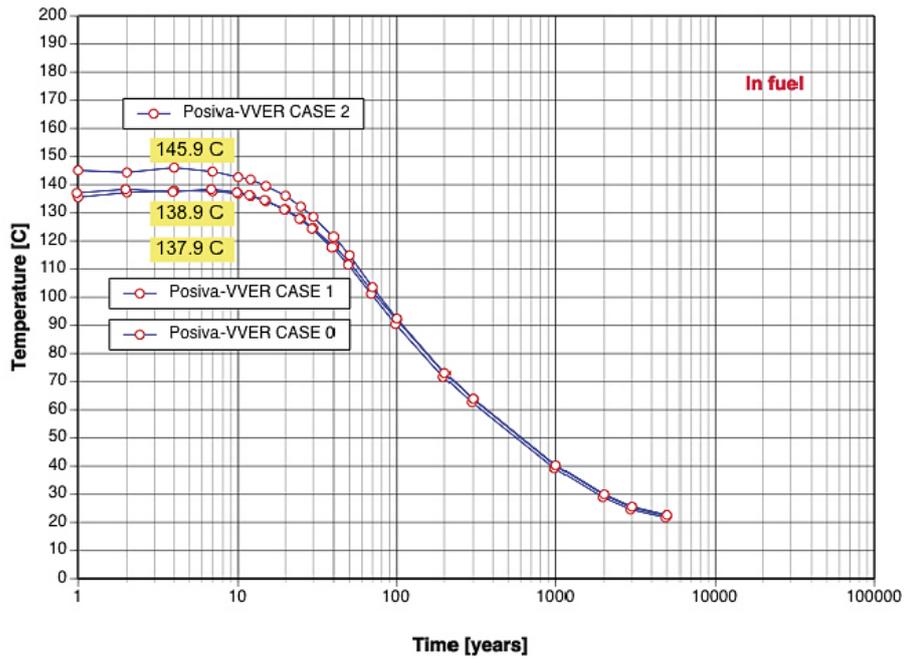
Figure 6-33. *Maximum fuel pellet temperature evolution for the Posiva-VVER canister.*

Figures 6-34 and 6-35 demonstrate the temperature distributions in the longitudinal cross-section passing through the centres of the fuel assemblies.
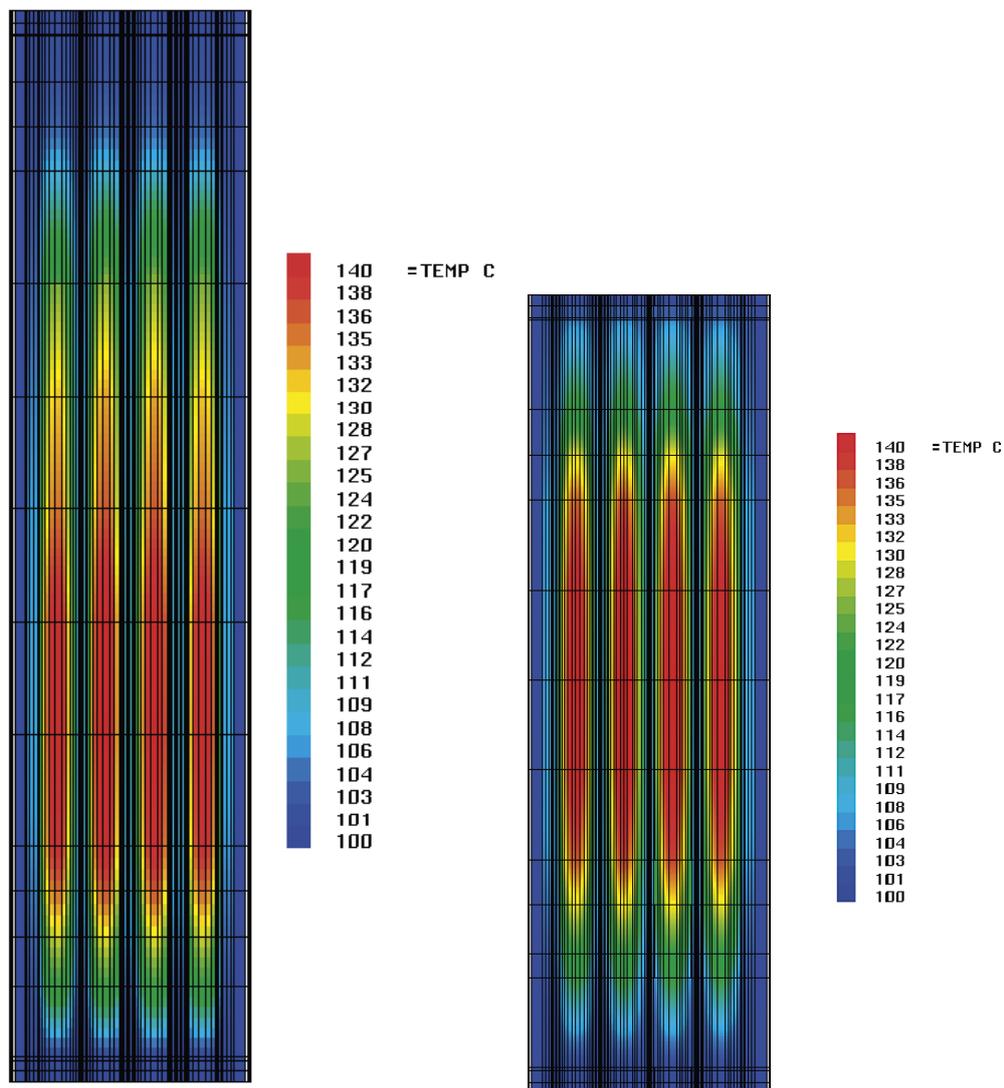
Figure 6-34. *Left figure: temperature distribution of the Posiva-BWR-type canister in the longitudinal cross section passing through the centres of the fuel assemblies. Right figure: Posiva-VVER-type canister.*
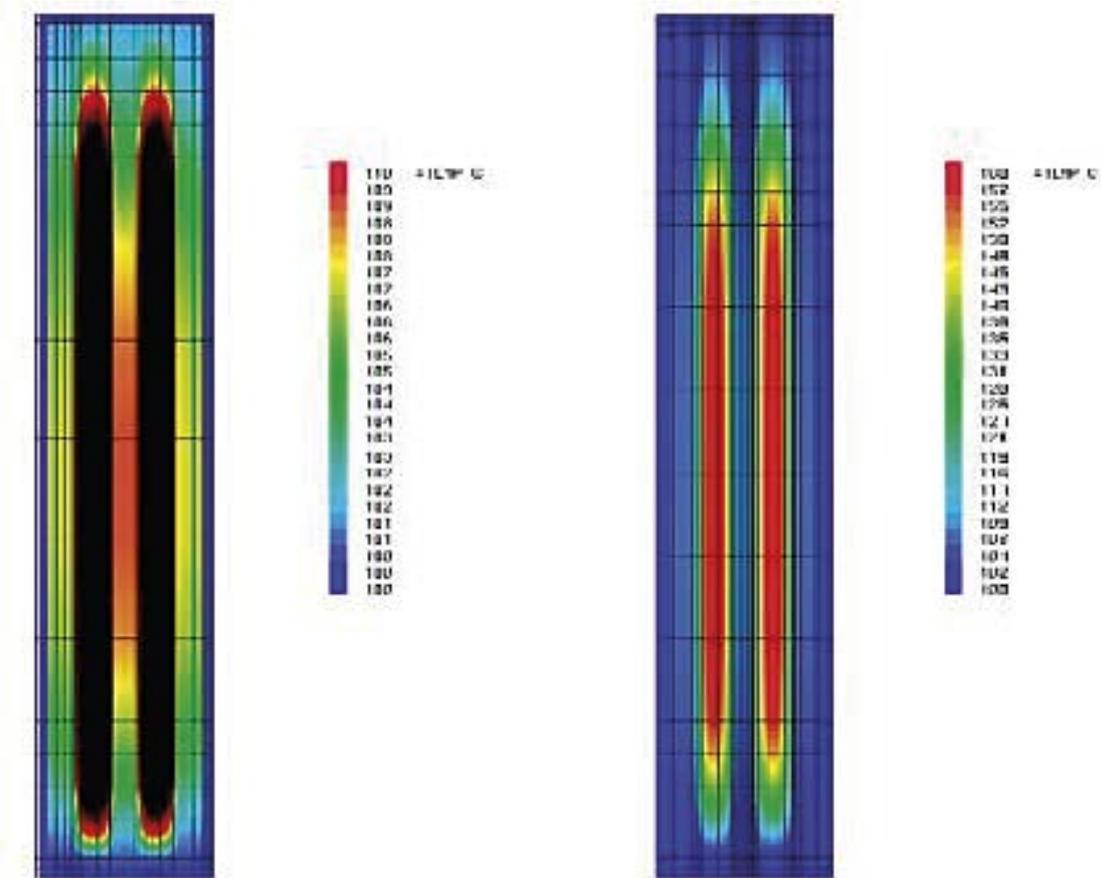
Figure 6-35. *Example of the temperature distribution of the SKB-PWR-type canister cross section. Two scales are used to better visualize the temperature of the cast iron (left) and of the fuel pellets (right).*

Figures 6-36 to 6-38 show the maximum temperature distributions for the cast iron in the longitudinal direction from the moment (10–12 years) at which the highest temperature is encountered. The maximum temperature of the cast iron in different planes perpendicular to the axis of the canister is searched and plotted in Figures 6-36 to 6-38.
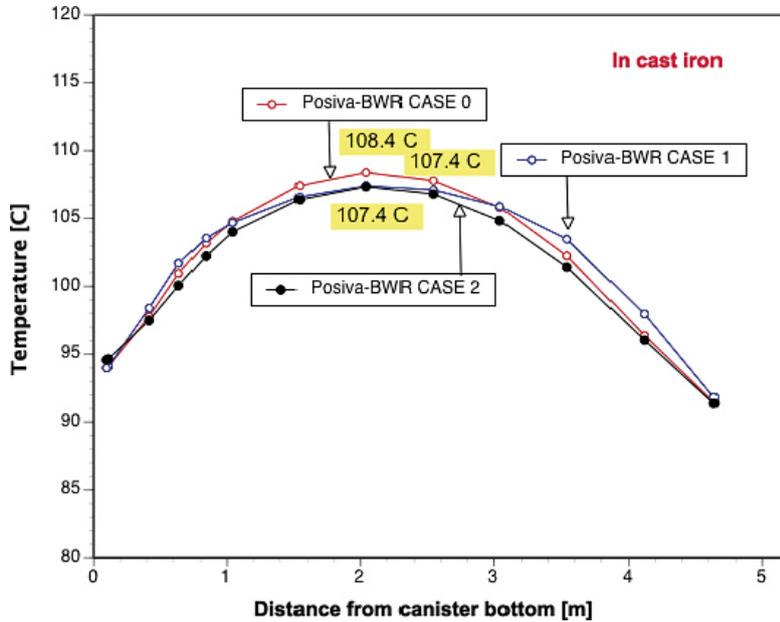
Figure 6-36. *Temperature profile of the cast iron of the Posiva-BWR canister after 10–12 years.*
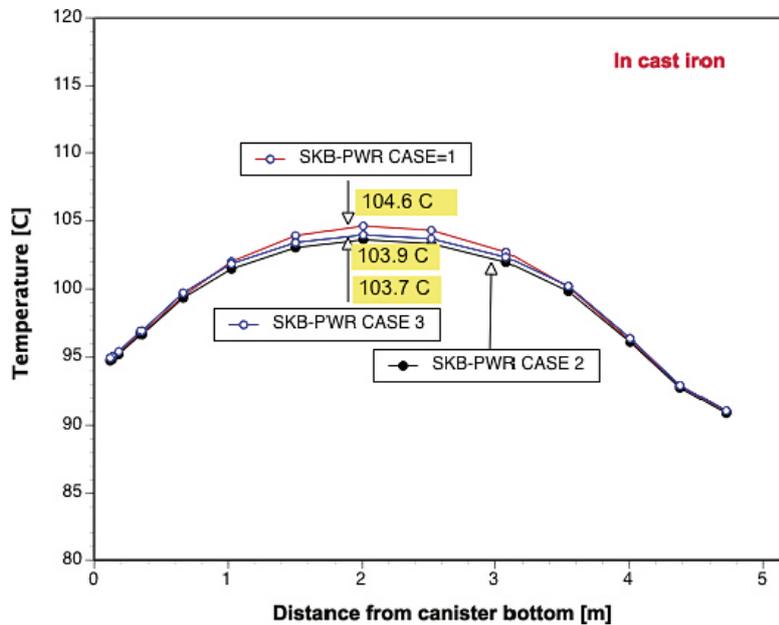
Figure 6-37. *Temperature profile of the cast iron of the SKB-PWR canister after 10–12 years.*
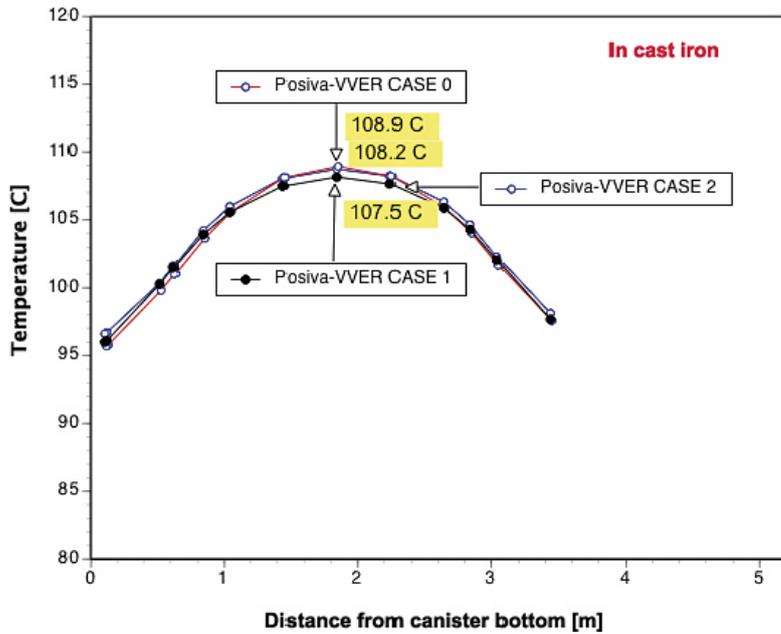
Figure 6-38. Temperature profile of the cast iron of the Posiva-VVER canister after 10–12 years.

Figures 6-39 to 6-41 show the temperature distribution in the fuel pellets in the longitudinal direction from the moment (4 years or earlier) at which the highest temperature is encountered. The maximum temperature of the fuel pellets in different planes perpendicular to the axis of the canister is searched and plotted in Figures 6-39 to 6-41.

In the lower end of the fuel assemblies, the temperature increases, and the density of the shield gas decreases in the upwards direction (Figures 6-39 to 6-41). Thus, natural circulation flows are not formed in the lower end area. In the upper end, the situation is reversed; however, the canister space is closed, gaps are narrow and convective flows are small and the convection effect can be conservatively ignored.
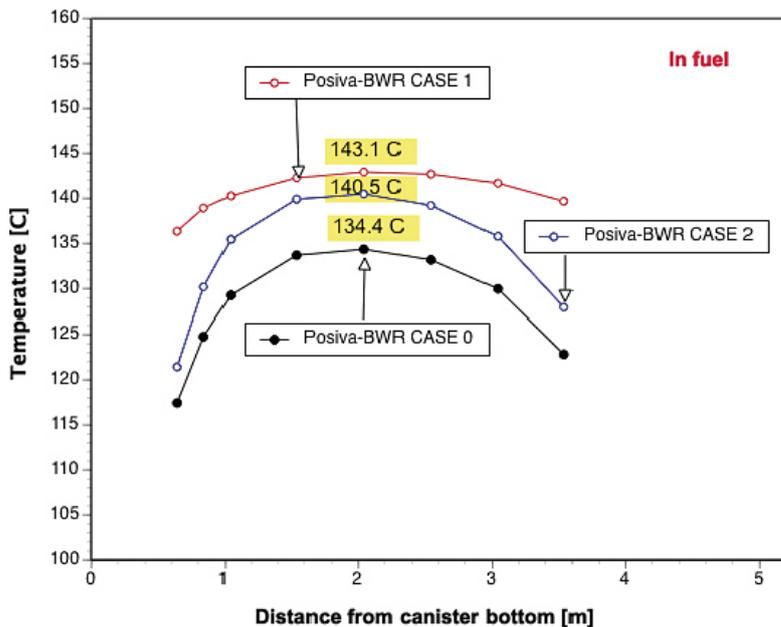
Figure 6-39. Temperature profile of the fuel pellets of the Posiva-BWR canister after 1–4 years.
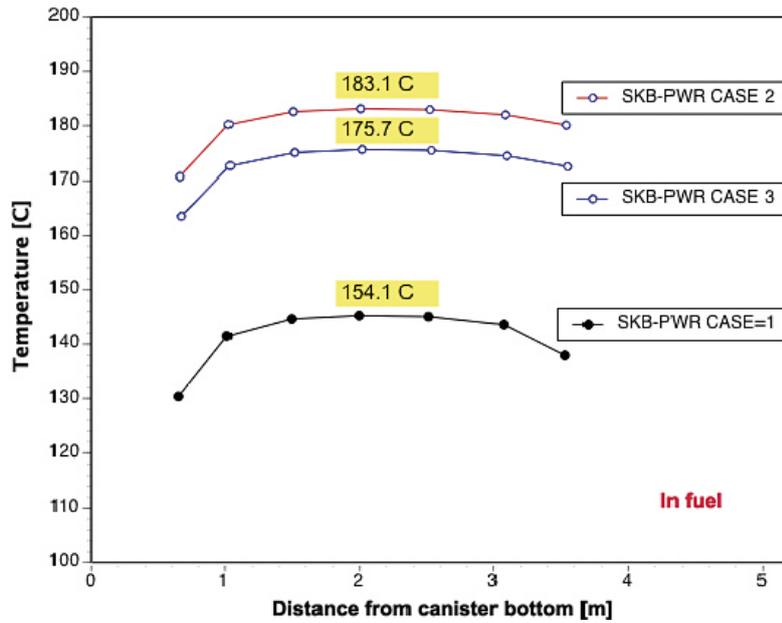
Figure 6-40. *Temperature profile of the fuel pellets of the SKB-PWR canister after 1–2 years.*
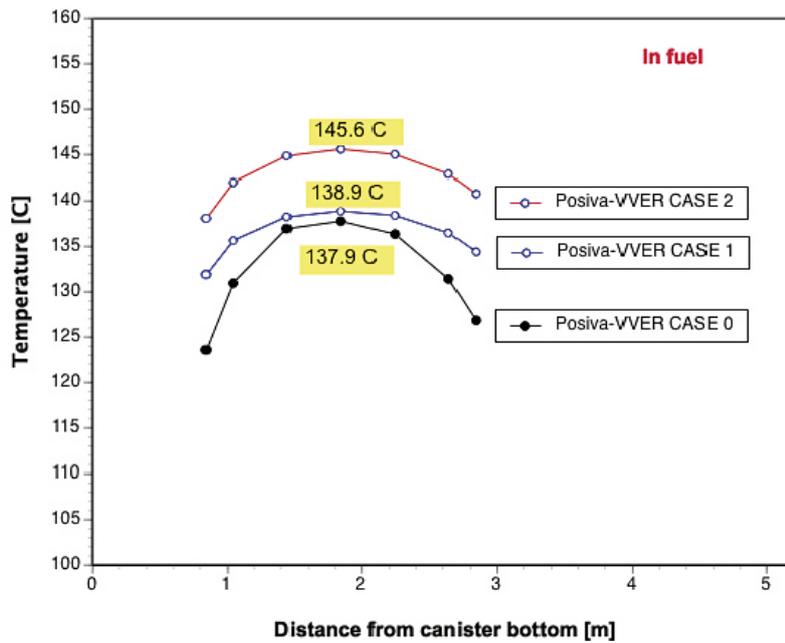
Figure 6-41. *Temperature profile of the fuel pellets of the Posiva-VVER canister after 1–4 years.*

6.9 Summary of analysed 3D cases

Table 6-6 summarizes the maximum temperatures of the cast iron and fuel for different cases.

Table 6-6. Summary of 3D analyses showing the maximum temperature of the cast iron and of the fuel pellets. The maximum temperature exists in the cast iron after approximately 10–12 years and in the fuel pellets after approximately 4 years or earlier following the disposal of the considered canister having the maximum buffer temperature (limited to 95 °C).

Case	Maximum temperature in cast iron [°C]	Maximum temperature in fuel pellets [°C]	Maximum fuel assembly heat power [W]
Posiva-BWR (0)	108.4	134.4	141.7
Posiva-BWR (1)	107.4	143.1	240
Posiva-BWR (2)	107.4	140.5	182
SKB-PWR (1)	104.6	154.1	425
SKB-PWR (2)	103.9	182.7	800
SKB-PWR (3)	104.0	175.7	700
Posiva-VVER (0)	108.9	137.9	114.2
Posiva-VVER (1)	108.4	138.9	142.7
Posiva-VVER (2)	107.5	145.9	171.2

The temperature increase above the ambient temperature in the fuel is approximately proportional to the square root of the fuel assembly heat power.

The differences between the times at which the maximum temperature of the fuel pellets and of the cast iron is encountered, are caused by the interaction of many canisters in a repository panel, the decreased decay heat power and the heat transfer conditions inside a canister.

According to Table 6-6, the highest temperature in the cast iron is approximately 109 °C. The maximum target temperature is set to 125 °C. Thus, the margin is 16 °C. One sensitive parameter is the average gap width between the insert and the cylindrical copper wall. The nominal average gap width is 1.5 mm. The temperature change over the gap is approximately 12 °C (Equation 5-1). The gap width resulting in a temperature of 125 °C in the cast iron is approximately (12 °C + 16 °C)/12 °C × 1.5 mm = 3.5 mm.

6.10 Comparison of 2D and 3D results

The Posiva-BWR reference case (0) is considered first. The maximum temperature in the cast iron occurs after approximately 10 years. The decay heat power at that time is 1430 W. The decreased factor is 1430 W/1700 W = 0.84. The maximum of the axial decay heat profile is 1.183 (Table 2-8). The aforementioned effects partially compensate each other, giving a total coefficient for the maximum decay heat density of 0.84 × 1.183 = 0.993. The maximum local temperature on the outer copper surface is (Figure 6-20 for the Posiva-BWR canister) 1.0071 × (95.0 °C + 273 °C) − 273 °C = 97.6 °C. Using this canister surface outer temperature and a heat power of 0.993 × 1700 W = 1688 W, the 2D analysis gives 110.5 °C for the maximum temperature in the cast iron cross-section. This is 2.3 °C higher than the 108.2 °C obtained by the 3D analysis.

For SKB-PWR reference case (1), the corresponding 2D study gives 109.3 °C, 4.7 °C higher than the 104.6 °C obtained by the 3D analysis. For Posiva-VVER reference case (0), the corresponding 2D study gives 112.2 °C, 3.3 °C higher than the 108.9 °C obtained by the 3D analysis.

The 3D analyses give lower temperatures because a considerable amount of heat is removed through the canister ends, which cannot be modelled in 2D.

7　Sensitivity studies

The purpose in this chapter is to study the sensitivity of some geometric factors to the temperature field.

7.1　Effect of a geometric eccentricity of the annular gap

This section studies to what extent the temperatures deviate from axisymmetric in the cast iron and in the copper cylinder if the insert is displaced inside the copper cylinder such that the insert and the cylinder come into contact. In the symmetric case, the width of the gas gap is 1.5 mm. In the asymmetric case, the width of the gap varies between 0 and 3 mm. For this study, the asymmetric case of the SKB-PWR canister was chosen; the canister is characterized by fuel assembly decay heat powers of 800 W + 3 × 300 W. Initially, the gap is closed near the hottest (800 W) fuel assembly (up and left in Figure 7-1) to cause the highest temperature difference in the copper wall. The geometric eccentricity is caused by reducing the gap between the copper cylinder and the cast iron close to zero (1 % from 1.5 mm), corresponding in practice to a line contact.

A slice of the canister is separated from the hottest location in the longitudinal place. The 2D model is extended over a 10 mm air gap, a 290 mm bentonite layer, a 50 mm pellet slot and 875 mm to the host rock; thus the total radius is 1750 mm (half the tunnel above the canister) from the canister centre line. The outer radius is so great that a constant temperature along the outer radius can be set. The temperature at this radius was chosen to produce a temperature of approximately 100 °C in the copper cylinder.
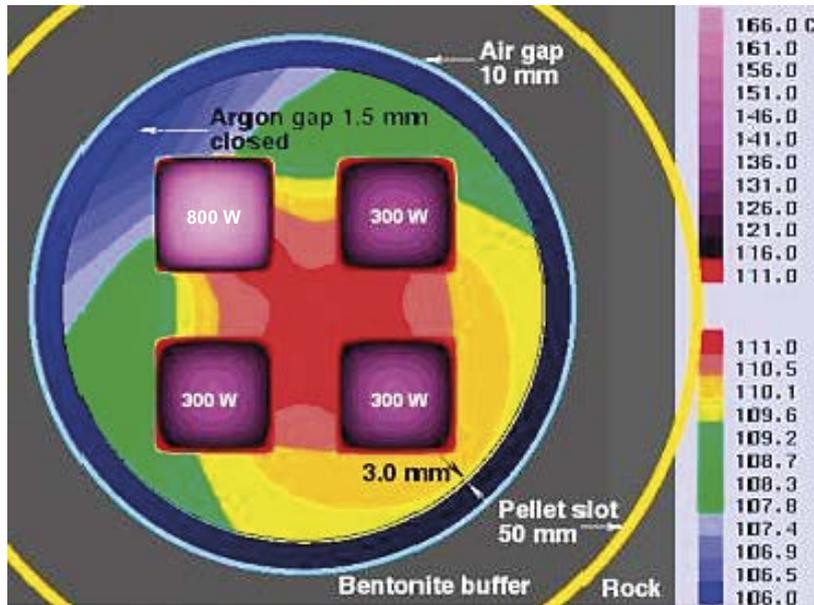
Figure 7-1. *Asymmetric decay heat power of the SKB-PWR fuel assemblies and the gas gap of 1.5 mm closed near the hottest (800 W) fuel assembly.*

Figure 7-2 shows that the temperature variation along the external copper wall along the circumference is 3.1 °C for a power of 4 × 425 W and 3.6 °C for a power of 800 W + 3 × 300 W. In addition, the concentric case, the same case as discussed in Section 6.1.2 (Figures 6-21 and 6-22), where one of the fuel assemblies is hotter than the other three assemblies, is plotted in Figure 7-2. The conclusion is that the temperature distribution in the circumferential direction is substantially more sensitive to the geometric eccentricity than to the varying heat powers of the fuel assemblies. The conclusion from Figure 7-2 is that the assumption of the concentric geometry is not conservative when evaluating the copper wall temperatures. The eccentricity can increase the copper wall temperature by approximately 2 °C.

Figure 7-3 shows the temperature along the outer radius of the cast iron. The eccentricity causes a temperature variation of approximately 6–7 °C along the outer radius and decreases the mean temperature by approximately 4 °C when compared to the concentric case. The conclusion drawn from Figure 7-2 is that the assumption of the concentric geometry is conservative when evaluating the temperature of the cast iron.

Figure 7-4 compares the symmetric and asymmetric heat powers in the geometrically eccentric case.
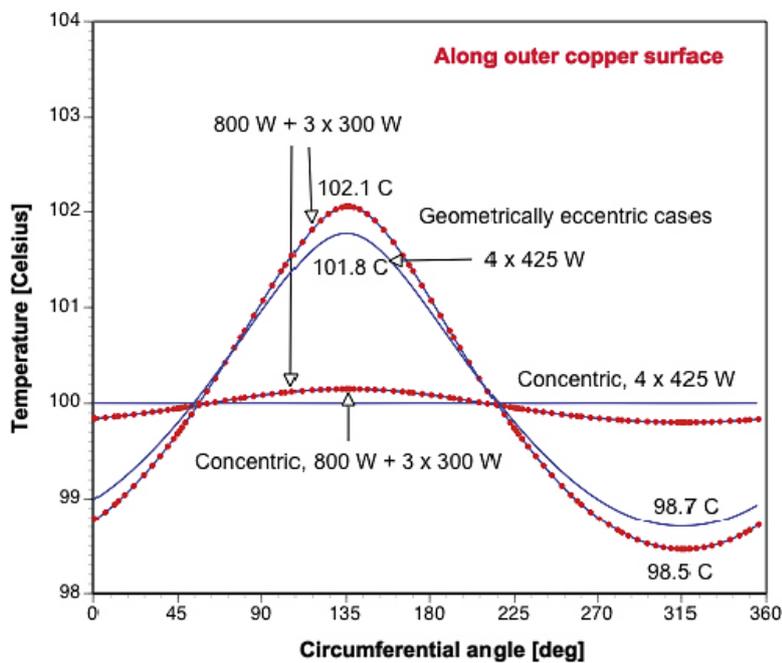
Figure 7-2. *Temperature variation in the circumferential direction of the external copper wall in different cases.*
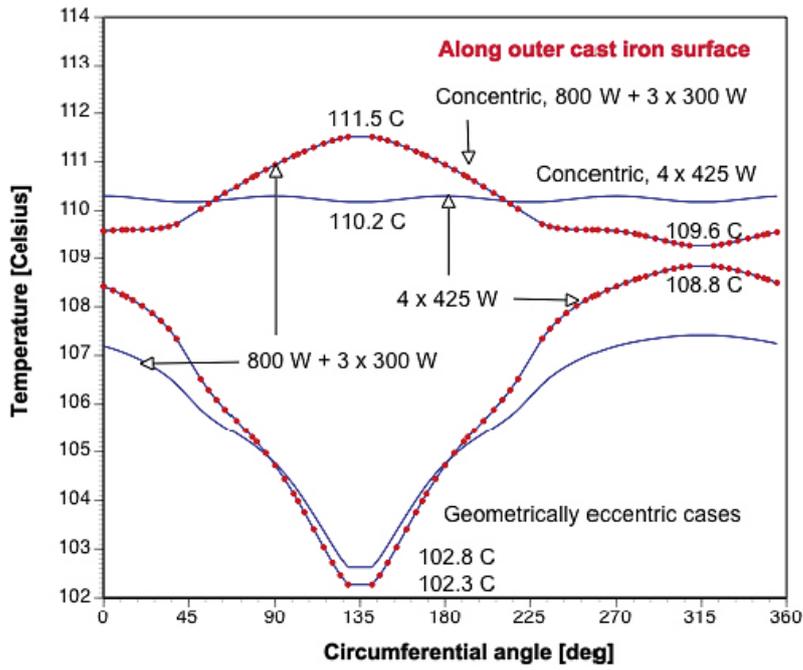
Figure 7-3. *Temperature variation in the circumferential direction along the outer radius of the cast iron in different cases.*
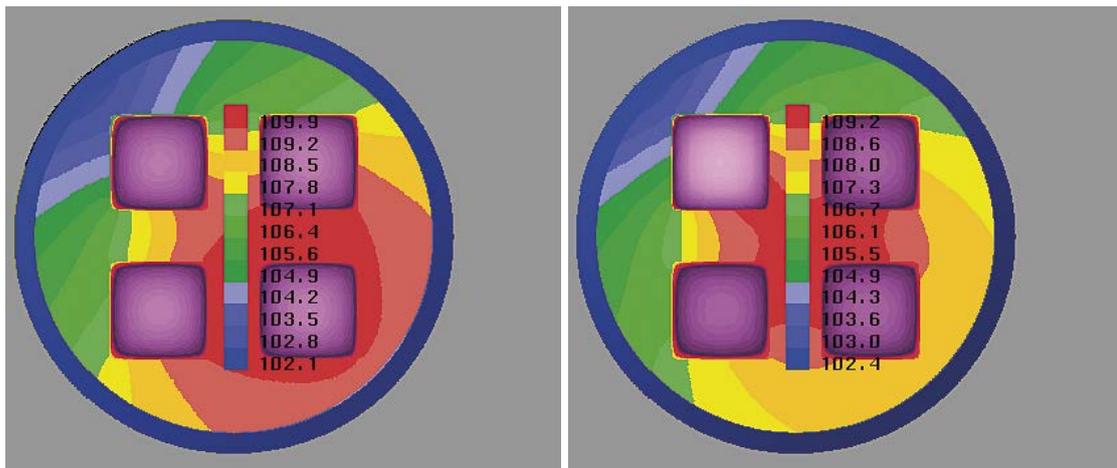
Figure 7-4. *Gas gap of 1.5 mm closed with symmetric decay heat powers (left) and asymmetric (right) decay heat power for the SKB-PWR fuel assemblies (right).*

Furthermore, the case where the contact is on the opposite side of the hottest fuel assembly (right and down) was studied to obtain the highest temperatures in the cast iron. Figures 7-5 and 7-6 show the cases in which the gap is closed on the opposite side to obtain the highest temperature difference in the cast iron. The maximum temperature difference in the cast iron is 8.6 °C.
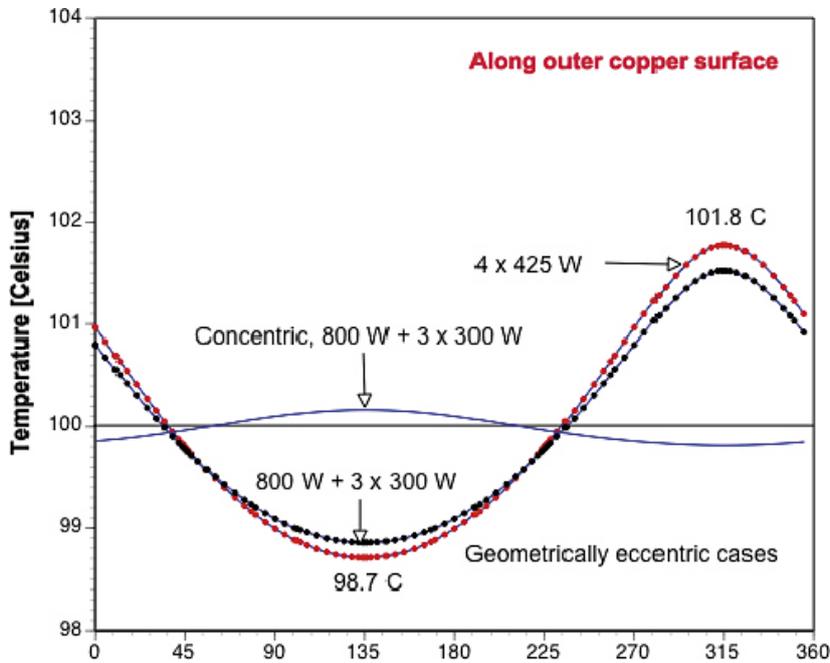
Figure 7-5. Temperature variation in the circumferential direction along the external copper wall when the gap is closed on the opposite side for different cases.
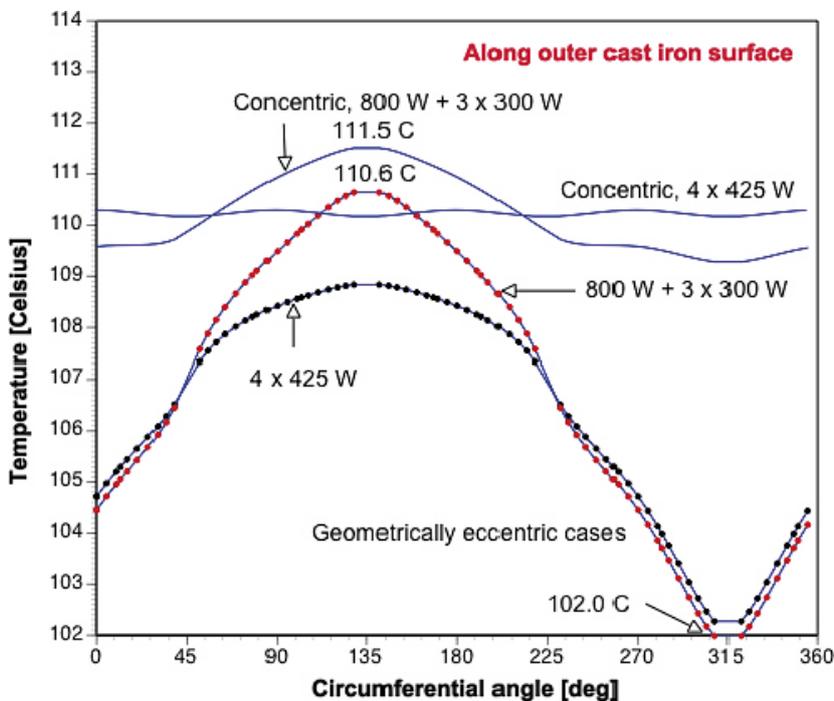
Figure 7-6. Temperature variation in the circumferential direction along the outer radius of the cast iron when the gap is closed on the opposite side for different cases.

The conclusion to be drawn from the above studies is that the geometric eccentricity and contact between the cast iron insert and copper have a much larger influence (approximately five times) on the temperature variations in the cast iron than does the asymmetric decay heat power of the fuel assemblies. The possible eccentricity lowers the maximum temperature in the cast iron, and the assumption of concentricity is conservative. The average temperature of the copper wall is not changed; however, the maximum temperature of the outer surface is increased by nearly 2 °C (Figures 7-2 and 7-5). The simultaneous eccentricities between the cast iron and copper and between the copper and bentonite buffer (10 mm air-filled gap) were not studied.

7.2 Effect of geometric eccentricity between the fuel assembly and the compartment steel tube

In this section the case in which a fuel assembly does not locate centrally inside the compartment steel tube is studied. The nominal gap in the Posiva-BWR fuel canister between the steel tube and the fuel channels is (160 mm − 139 mm)/2 = 10.5 mm (Tables 2-1 and 2-2). The fuel assembly locating in the compartment shown in Figure 7-7 (right) was moved 10 mm to the left so that the gap width is only 0.5 mm and the surfaces are practically touching each other. On the opposite side, the gap width is 20.5 mm. 2D analyses in the concentric and eccentric case, and assuming a constant temperature of 100 °C on the outer surface of the canister, gave the maximum temperatures in the cast iron of 115.18 °C and 115.28 °C, in the steel tube of 115.18 °C and 115.29 °C and in the fuel pellets of 143.43 °C and 143.49 °C, respectively. Thus the eccentricity increases the maximum temperatures very little. In 3D cases with inclined or curved fuel assemblies inside a compartment, it can be expected that the temperature changes will be lower than those of the 2D analyses.
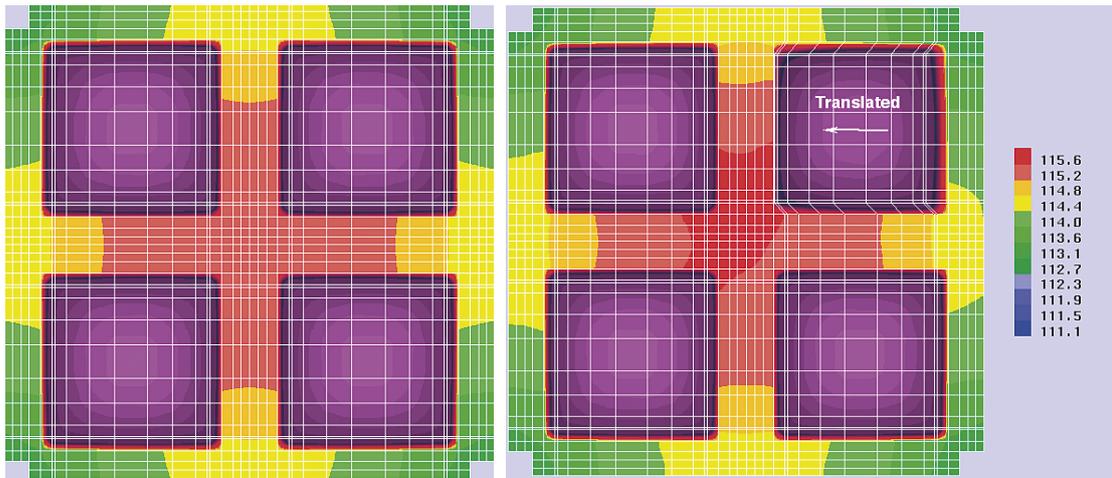
Figure 7-7. *Enlargements of the central area of the Posiva-BWR canister (12 fuel assemblies) in reference case 0, showing the temperature distributions of the case in which all fuel assemblies are concentric in the compartment steel tubes (left) and in which one fuel assembly is moved to the left against the edge of the steel tube (right).*

7.3 Effect of an unintended hollow in the cast iron insert

In manufacturing the insert, a situation may occur in which the cast iron material does not fully fill the voids between the compartment steel tubes. The Posiva-BWR canister reference case was studied. Figure 7-8 shows the cross-section of the canister, where cast iron between steel tubes is substituted by gas. The cast iron thickness between the channel tubes is 30 mm (Table 2-2).

The hollow locates in the middle of the canister in the longitudinal direction, and its length is 18.6 cm (this measure is based on the respective strength analysis study (Alverlind 2016, p 14)). The effective conductivity over the 30 mm gap was calculated from (10) using an emissivity of 0.6 (Table 2-5) for the steel surfaces. This value was also used in the opposite direction of the gap, although this is theoretically not fully correct.

According to a 2D analysis, the maximum obtained temperature in the cast iron was 112.7 °C at point A with the hollow, and the maximum temperature of the fuel pellets was 150.3 °C. A constant temperature of 100 °C on the outer surface of the canister was assumed. Without the hollow, the corresponding temperatures became 115.6 °C and 146.5 °C (Table 5-1). With the hollow, the temperature of the cast iron decreased by 2.9 °C because cast iron does not exist in the hot middle area between the fuel assemblies. The temperature of the fuel was increased by 3.8 °C. This 2D analysis corresponds to the case in which the length of the hollow equals the length of the canister.

Then, a 3D analysis was performed with the actual hollow length of 18.6 cm. The effective conductivity in the longitudinal direction was calculated in two ways, omitting thermal radiation and calculating the value over the gap thickness of 186 mm from (10), therein using the emissivity value of 0.6 (Table 2-5) of the cast iron surfaces. Both models gave practically the same result because, in the middle of the canister, the temperature is maximized and the longitudinal heat flow is close to zero. A constant temperature of 100 °C and the varying temperature profile along the outer surface of the canister was assumed, and the actual axial decay heat profile was used. Temperature profiles were plotted in Figure 7-9 with and without the hollow in the cast iron along the axial line at the locations A and B in Figure 7-8. The maximum temperature in the cast iron without the hollow is 116.3 °C, and that with the hollow is 116.5 °C with the varying temperature profile along the outer surface. The corresponding temperatures of the fuel pellets are 141.1 °C and 141.1 °C (Figure 7-10). Thus, the hollow increases the maximum temperatures of the cast iron by only approximately 0.2 °C, which is insignificant.

The conclusion of the analysis is that the effect of the hollow is negligible and more variations were abandoned.
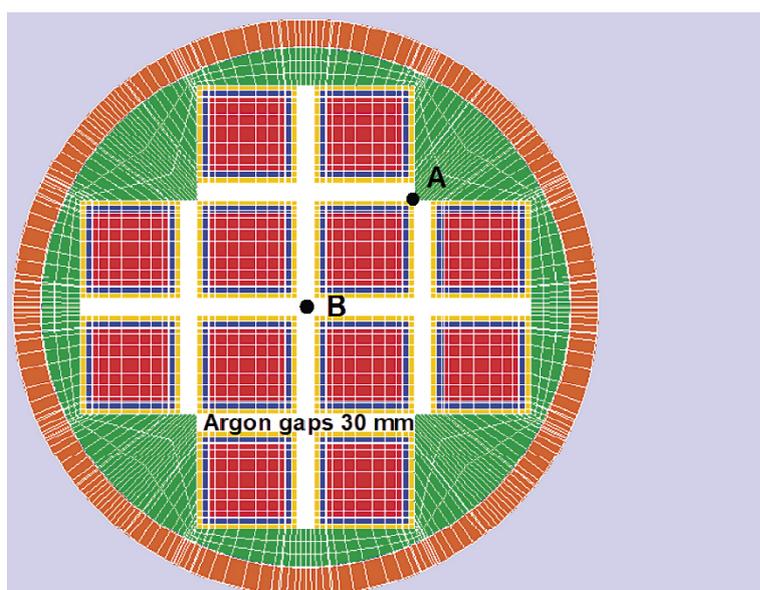
Figure 7-8. *White colour shows areas in which cast iron does not fill the spaces between the steel channel tubes (Posiva-BWR canister).*
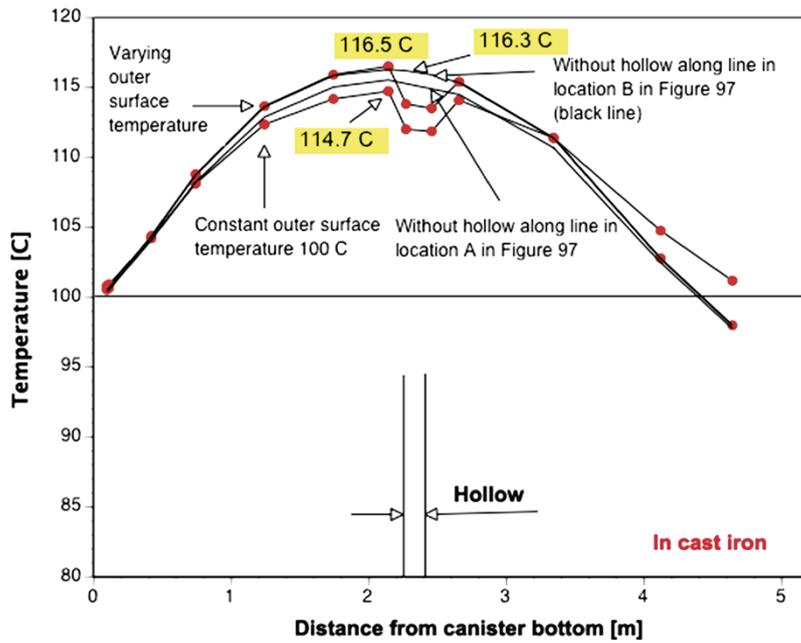
Figure 7-9. *Longitudinal temperature profiles of the cast iron of the Posiva-BWR canister.*
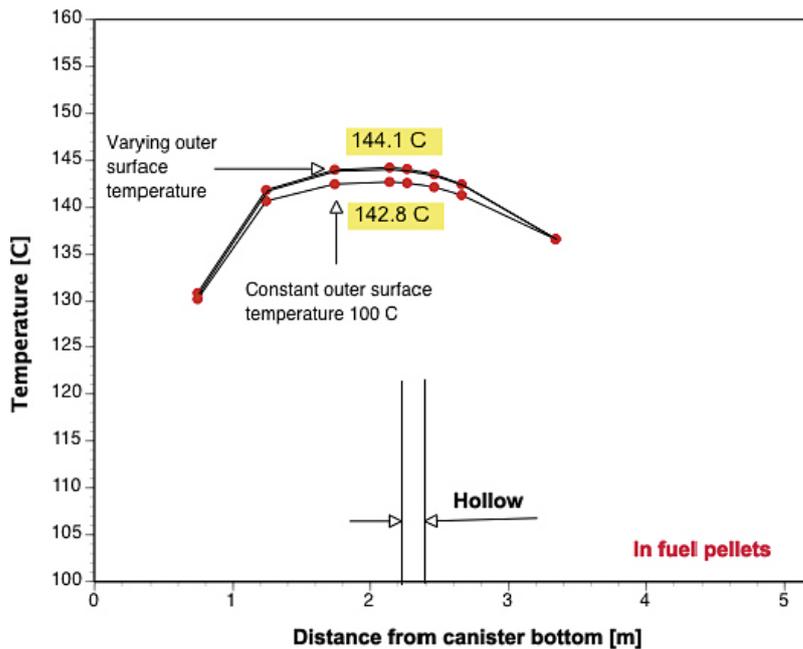
Figure 7-10. *Temperature profiles of the fuel pellets of the Posiva-BWR canister with and without a hollow in the cast iron (actual longitudinal decay heat profile).*

7.4 Curvature of the cast iron insert due to asymmetric decay heat power and eccentricity

Temperature differences in the cross-section cause curvature (thermal bending deformation) of the cast iron insert; this is estimated in the next study.

Through a geometric study (Figure 7-11), a formula for the displacement d can be derived as follows:

$$\delta = \frac{\alpha\, \Delta T\, H^2}{8D}\,.$$
(7-1)

The parameters have the following values:

* $\alpha = 11.5 \times 10^{-6}$ 1/K thermal expansion coefficient of cast iron (Raiko 2012)
* $\Delta T = 8.6\ °C$ temperature difference between edges in the cast iron
* $H \approx 4.7$ m height of the SKB-PWR insert
* $D = 0.949$ m outer diameter of the cast iron

By applying these values the displacement becomes $\delta = 0.29$ mm. This displacement is small when compared to the 1.5 mm gas gap between the copper cylinder and the cast iron insert. Thus, the temperature difference between the opposite edges of the cast iron insert does not cause a remarkable deformation or forced contacts.
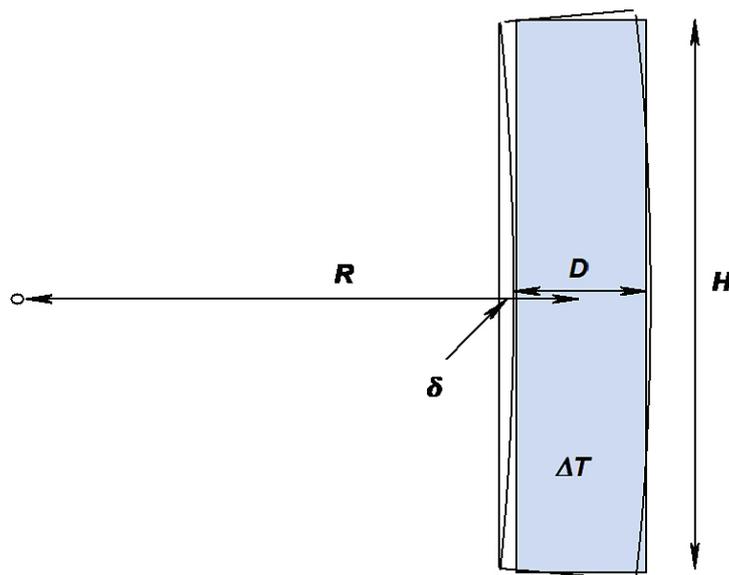
Figure 7-11. Curving of the cast iron insert.

7.5   Convective heat transfer in air-filled gap

To estimate the effect of convective heat transfer in a narrow vertical gap, the natural circulation flow of gas was briefly studied using a 2D model between two vertical walls in Figure 7-12. The width of the air-filled gap between the canister and the bentonite is 10 mm (in the Posiva-BWR canister the gap between the compartment steel tube and the fuel channel is 10.5 mm). The height of the gap in the model is the length of 4.752 m of the Posiva-BWR canister. The gap is close-ended, and the so-called "chimney effect" of gas flow through a pipe is not encountered. In the upper and lower ends, the velocities are zero, as the left panel of Figure 7-12 shows. Heat transfer across the gap occurs via conduction, radiation and convection. The temperature of the copper surface was assumed to be 95 °C, and the temperature of the bentonite surface was assumed to be 84 °C. The temperature difference over the gap is thus 11 °C. The kinematic viscosity of air is 2.2×10^{-5} m/s. The left panel of Figure 7-12 shows the velocity in the boundary layers near the walls, and the right panel shows the velocity profile across the gap at mid-height obtained by a laminar natural circulation CFD model by modelling conduction, thermal radiation (air and argon transparent gases) and convection. The maximum natural circulation velocity was found to be 1.1 cm/s. This velocity is so small that laminar flow may be expected.

The thermal power that the flow conveys upwards through the gap is estimated. The volumetric thermal capacity of air is 0.00095 J/cm³/K. The circumferential length of the gap is $\pi \times 105$ cm = 330 cm. The thermal power is 0.5 cm × 330 cm × 1 cm/s × 0.00095 J/cm³/K × 11 K = 1.6 W. This is very small compared to the thermal power of 1700 W of the canister. Actual flows inside the canister are three-dimensional and more complicated than in this example.

At mid-height, heat is transferred in the horizontal direction by conduction and radiation but not by convection because there is no horizontal velocity. There is convective heat transfer in the upper and lower ends, but the horizontal velocity component is small. The convective heat transfer effect at the lower and upper ends of the gap is small due to the lower velocity near the ends. The effect of heat transfer by convection is small compared to conductive heat transfer in this example.

Inside the canister, the conditions are different from ideal due to the complicated structures. In the lower parts, temperature increases in the upward direction and driving forces for natural circulation flows do not exist. In the analyses, the convective heat transfer in the gas-filled gaps was assessed to be very low and the mechanism was conservatively omitted in the analyses.
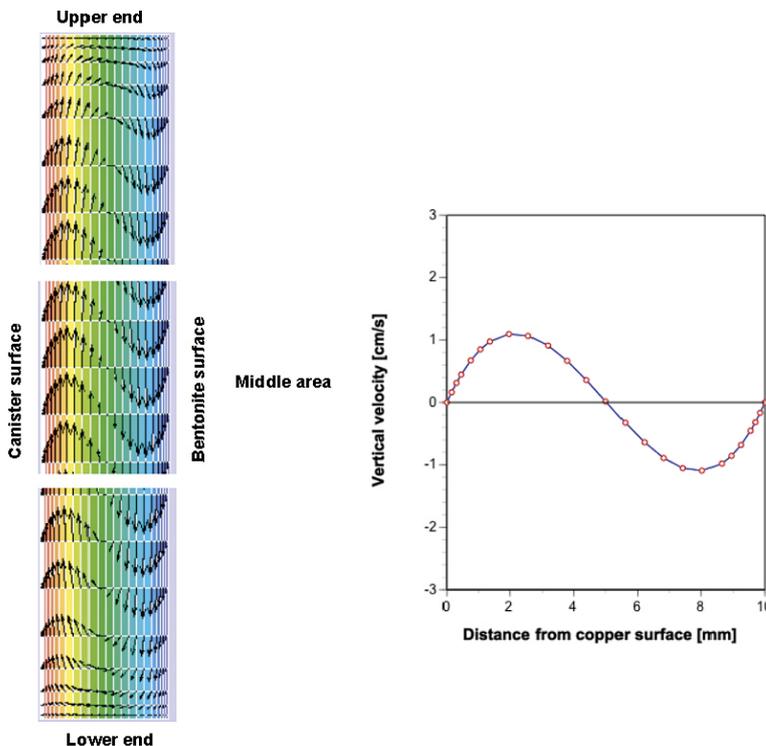
Figure 7-12. *Natural circulation flow in high, narrow, 10 mm air-filled gap between the canister and the bentonite buffer (left) and the velocity profile at mid-height (right).*

8 Conclusion

The objective of this study was to evaluate the temperature inside spent fuel canisters, when they are disposed of in the vertical KBS-3 V-type spent nuclear fuel repository in Forsmark, Sweden or in Olkiluoto, Finland in the crystalline bedrock. Four canister types, SKB-BWR, SKB-PWR, Posiva-BWR and Posiva-VVER-440, were studied. The main goal of the study was to determine the temperatures in the cast iron inserts; however, the analyses also provided the temperatures of the spent fuel assemblies and pellets. The target maximum temperature of the cast iron was set to 125 °C because of the availability of existing material test data.

The main target of the study was to investigate the effect of varying decay heat powers of fuel assemblies in a canister on the temperatures of cast iron and fuel pellets. This was first studied with 2D models in the full cross-section of a canister at the location at which the longitudinal decay heat profile of a fuel assembly is maximized and using the effective thermal conductivity for the homogenized fuel. The total power was 1700 W in the BWR and SKB-PWR fuel-type canister and 1370 W in the VVER-440 fuel-type canister, corresponding the heat powers at the moment of disposal. These 2D analyses gave the maximum temperatures of the cast iron inserts of 112.7–118.1 °C in the nine analysed cases, and for those of the fuel pellets were 143.4–203.0 °C. The highest fuel temperatures naturally occurred only in those assemblies that greatly exceeded the average heat power. For uniform decay power assemblies, the temperatures varied between 143.5 °C and 165.4 °C. The temperatures inside a canister were also calculated in such cases when the canister surface temperature varies between 60 °C and 140 °C.

The 3D analyses corresponding to circumstances in the repositories for long times gave a maximum temperature for the cast iron inserts of 103.9–108.9 °C for different canister types and varying decay heat powers of the fuel assemblies in a canister, and that for the fuel pellets was 134.4–182.7 °C. The maximum temperatures of the cast iron appear after 10–12 years, and those of the fuels appear after 4 years or earlier after the disposal of the canister at the repository. The 3D analyses obtained clearly lower temperatures than did the 2D analyses. The main reason for this is that, in the 2D analyses, the temperature along the outer radius of the canister was conservatively set to a constant, 100 °C, and the decay heat was set to correspond to the power at the canister disposal moment; in contrast, in the 3D analyses, the actual evolution of the outer surface temperature and decreasing decay heat power of the individual fuel assemblies were considered. In addition, in the 3D modelling, some of the decay heat escapes through the top and bottom ends of the canister.

If the temperature of the fuel assembly greatly increases, one could expect that some of the nuclides of fission products might be more easily released from the canister. At high temperature and with some water and steam inside the canister, the corrosion rate of metal parts may increase.

Various sensitivity analyses were performed, e.g., concerning the geometric eccentricity between the copper shell and the cast iron insert, the eccentricity of the fuel assembly in the compartment and the effect of an unintended hollow in the cast iron insert material. These studies showed that the target maximum temperature of 125 °C in the cast iron is not reached in any investigated case. One sensitive parameter is the average gap width between the insert and the cylindrical copper wall. The nominal average gap width is 1.5 mm; however, if the average gap width was approximately 3.5 mm, the target maximum temperature of 125 °C in the cast iron could be reached. This emphasizes the importance of keeping strict tolerances in gap measures.

One conclusion to be drawn from the analyses is that the varying decay heat powers of the fuel assemblies in a canister do not change the temperatures of the cast iron remarkably as long as the total decay heat power in the canister remains constant. Further, the simulation of the evolution of the temperatures in the repository showed that the temperatures of 104–109 °C in the cast iron remain below the target maximum temperature of 125 °C in the analysed cases under given assumptions. The maximum temperature in the copper shell is about 97 °C.

Acknowledgement

References

SKB's (Svensk Kärnbränslehantering AB) publications can be found at www.skb.com/publications.
SKBdoc-documents will be submitted upon request to document@skb.se.
Posiva's reports and publications can be found at https://www.posiva.fi/en/index/media/reports.html.

Alverlind L, 2016. Isostatic pressure load on BWR and PWR canisters using a scaled iron material model. Report 5000484-1, rev 4, Inspecta Technology AB. SKBdoc 1089758 ver 3.0, Svensk Kärnbränslehantering AB.

Anttila M, 2005. Radioactive characteristics of the spent fuel of the finnish nuclear power plants. Posiva Working Report 2005-71, Posiva Oy.

Bejan A, Kraus A D (eds), 2003. Heat transfer handbook. New York: Wiley.

DeHart M D, 2005. TRITON: A two-dimensional depletion sequence for characterization of spent nuclear fuel. In SCALE: A modular code system for performing standardized computer analyses for licensing evaluations. ORNL/TM2005/39, Version 5, Vols. I-III (CD-ROM), Oak Ridge National Laboratory, TN, Vol. I, Book 3, Sect T1.

Fletcher C A J, 1991. Computational techniques for fluid dynamics. Volume II. 2nd ed. Berlin: Springer.

Gauld I C, Hermann O W, Westfall R M, 2005. ORIGEN-S: SCALE system module to calculate fuel depletion, actinide transmutation, fission product buildup and decay, and associated radiation source terms. In SCALE: A modular code system for performing standardized computer analyses for licensing evaluations. ORNL/TM2005/39, Version 5, Vols. I-III (CD-ROM), Oak Ridge National Laboratory, TN, Vol. II, Book 1, Sect. F7.

Gauntt R O, Cash J E, Cole R K, Erickson C M, Humphries L L, Rodriguez S B, Young M F, 2005. MELCOR computer code manuals. Vol. 2: Reference manual, version 1.8.6. NUREG/CR 6119, Vol. 2, Rev. 3; SAND2005 5713, Sandia National Laboratories.

Howell J R, 2001. A catalog of radiation heat transfer configuration factors. 2nd ed. The University of Texas at Austin.

Hökmark H, Lönnqvist M, Kristensson O, Sundberg J, Hellström G, 2009. Strategy for thermal dimensioning of the final repository for spent nuclear fuel. SKB R-09-04, Svensk Kärnbränslehantering AB.

Hökmark H, Lönnqvist M, Fälth B, 2010. THM-issues in repository rock. Thermal, mechanical, thermo-mechanical and hydro-mechanical evolution of the rock at the Forsmark and Laxemar sites. SKB TR-10-23, Svensk Kärnbränslehantering AB.

Ikonen K, 2006. Fuel temperature in disposal canisters. Posiva Working Report 2006-19, Posiva Oy.

Ikonen K, 2009. Thermal dimensioning of spent fuel repository. Posiva Working Report 2009-69, Posiva Oy.

Ikonen K, 2013. Säteilylämmönsiirron laskennasta (Analysis of thermal radiation). Espoo: VTT Technology. (In Finnish.)

Ikonen K, Raiko H, 2012. Thermal dimensioning of Olkiluoto repository for spent fuel. Posiva Working Report 2012-56, Posiva Oy.

Jonsson M, Junéll H, 2017. SKB fuel data for heat transfer analysis. SKBdoc 1519860 ver 1.0, Svensk Kärnbränslehantering AB.

MATPRO, 2014. Material property correlations: Comparisons between FRAPCON-3.5, FRAPTRAN-1.5, and MATPRO. NUREG/CR-7024, United States Nuclear Regulatory Commission.

Mills A E, 1999. Basic heat and mass transfer. 2nd ed. Upper Saddler River, NJ: Prentice Hall.

Nuclear Engineering International, 2011. Uranium after Fukushima. Nuclear Engineering International 56, 686.

ORNL, 2005. SCALE: A modular code system for performing standardized computer analyses for licensing evaluations. ORNL/TM2005/39, Version 5, Vols. I-III (CD-ROM), Oak Ridge National Laboratory, TN. (Available from Radiation Safety Information Computational Center at Oak Ridge National Laboratory as CCC-725.)

Raiko H, 2012. Canister design 2012. Posiva 2012-13, Posiva Oy.

Raiko H, Sandström R, Rydén H, Johansson M, 2010. Design analysis report for the canister. SKB TR-10-28, Svensk Kärnbränslehantering AB.

Rautaruukki, 1996. Rautaruukin terästuotteet: suunnittelijan opas Raahe, Finland: Rautaruukki. (In Finnish.)

SKB, 2004. RD&D-Programme 2004. Programme for research, development and demonstration of methods for the management and disposal of nuclear waste, including social science research. SKB TR-04-21, Svensk Kärnbränslehantering AB.

SKB, 2010. Spent nuclear fuel for disposal in the KBS-3 repository. SKB TR-10-13, Svensk Kärnbränslehantering AB.

Viertel M, Runevall O, 2014. Aktivitetsinventarier och källstyrkor för använt kärnbränsle i det svenska avfallsprogrammet. SKBdoc 1198314 ver 2.0, Svensk Kärnbränslehantering AB. (In Swedish.)

Some verification cases for axisymmetric code

The objective of this appendix is to calibrate the analytical line heat source model using the analytical model to use it for analysing the whole spent fuel repository. The canister maximum surface temperature is the most important output quantity. The calibration is based on a comparison of the results obtained using the control volume solution of a single canister. The gaps are considered as described in Section 3.2.1. Figure A-1 shows the grid of the numerical axisymmetric model of the BWR canister area and the surrounding rock. The colours represent different materials.

Different verification cases are performed in the computer programme KAPSEL, which was developed and applied at VTT for axisymmetric analysis. The programme is based on the control volume method. In the following, three verification cases are presented. In these cases, the exact solution is known.

Verification case 1: Line segment heat source

The analytical solution for the temperature of a line segment heat source is

$$T(x,y,z,t) = \frac{Q/H}{\rho c\, 4\pi\, v\, t}\, e^{-\frac{x^2+y^2}{4\, v\, t}}\, \frac{1}{2}\, \left\{ \mathrm{erf}\left[\frac{1}{2\sqrt{vt}}\left(\frac{H}{2}+z\right)\right] + \mathrm{erf}\left[\frac{1}{2\sqrt{vt}}\left(\frac{H}{2}-z\right)\right] \right\}, \qquad \text{(A-1)}$$

where x and y are co-ordinates in the horizontal plane, the height of the heat source is $H = 5.0$ m, and z is measured from the mid-height of the heat source. In (A1), $v = \lambda/(\rho c)$ is the thermal diffusivity. Thermal energy of $Q = 10^{12}$ J is released during the first 30 s uniformly in a cylinder, whose radius is 10 cm and whose height is 5.0 m. This cylinder is divided in the radial direction into three element layers and in the vertical direction into 16 element layers. The height of the model is 70 m, and diameter is 60 m (Figure A-1). Figure A-2 compares the temperature evolutions for a heat pulse and continuous heat power of 2000 W obtained using the analytical and numerical solutions.
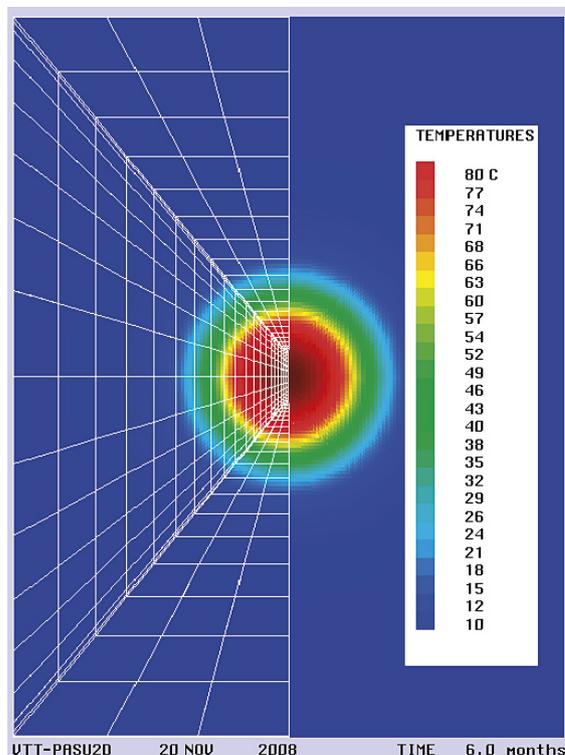
Figure A-1. Mesh and temperature distribution of a line heat source after ½ year.
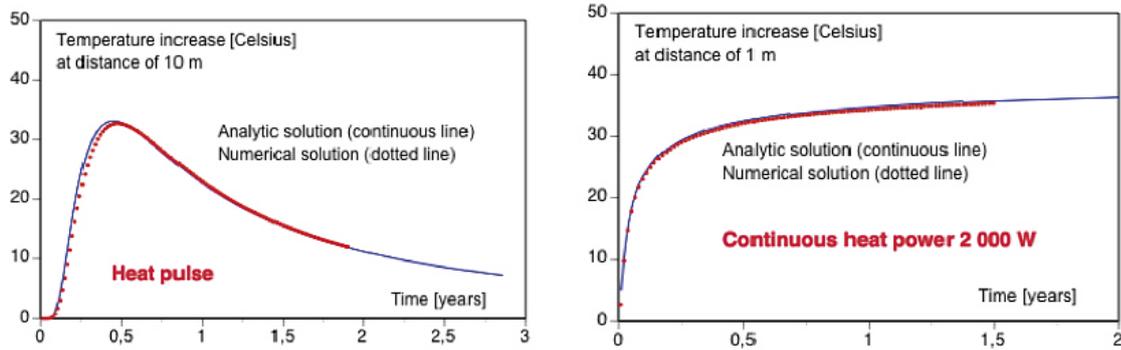
Figure A-2. *Temperature evolutions in first verification case.*

Verification case 2: Uniform heat generation in a homogenous cylinder

In the axisymmetric canister model all materials were changed to the host rock, whose conductivity is $\lambda = 2.82$ W/m /K. For the whole volume of the model (Figure A-3), uniform heat generation $\Phi = 1$ W/m^3 was applied. The temperature along the outer cylindrical surface of radius $R = 30$ m was set to 0 °C and adiabatic boundary conditions were applied at the upper and lower ends of the model shown in Figure A-3. In the stationary state, the radial temperature profile is parabolic, and the temperature on the axis of symmetry is calculated as

$$T_{On\ axis} = \frac{\Phi}{4\lambda} R^2 = \frac{1\ \text{W/m}^3}{4\lambda} (30\ \text{m})^2 = 79.787\ ^{\circ}\text{C} . \tag{A-2}$$

The model in Figure A-3 gives 79.711 °C. Figure A-3 also demonstrates that the unstructured "distorted" mesh performs correctly.
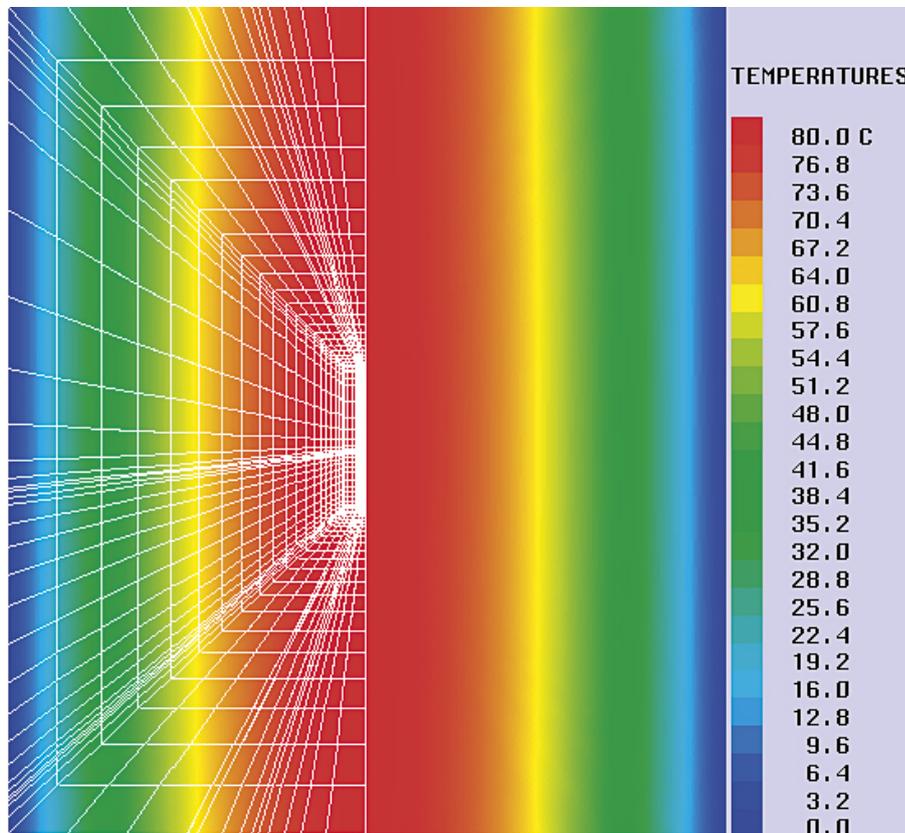
Figure A-3. *Uniform heat generation in a homogenous cylinder.*

Verification case 3: Canister, air gap, bentonite, pellet slot and part of host rock between insulated walls

All the dimensions, the thermal properties of the materials, the emissivities and the radial mesh (basic mesh) are identical to those used in the repository analyses when using the solid model. The thermal conductivity of the rock is $\lambda = 2.82$ W/m/K, that of bentonite is $\lambda = 1.0$ W/m/K and that of the pellet slot is $\lambda = 0.2$ W/m/K.

In this test case, a Posiva-BWR canister is set between two thermally insulated walls (Figure A-4) perpendicular to the axis of the cylinder. The canister is solid and composed of only copper. A decay power of 1700 W is assumed to be distributed uniformly in the canister volume. The thermal flux at the canister surface is

$$\phi_0 = \frac{P}{H\,2\pi\,r_0} = \frac{P}{4.752\ \text{m} \cdot 2\pi \cdot 0.525\ \text{m}} = 108.45\ \text{W/m}^2 \ . \tag{A-3}$$
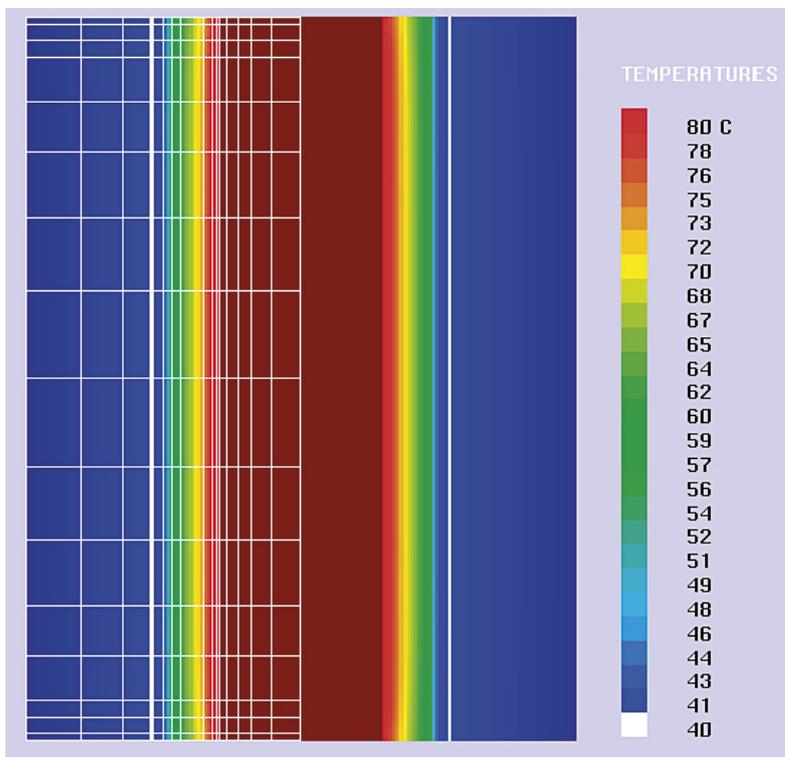
Figure A-4. *A BWR canister is set between two thermally insulated walls.*

The temperature T_{0b} along the external surface of the air gap (i.e., along the internal surface of the bentonite) is calculated by adding the temperature increments formed at the pellet slot and bentonite layers to the temperature T_{rock} at a point in the host rock:

$$T_{bentonite\,surface} = T_{rock\,wall} + \Delta T_{pellet\,slot} + \Delta T_{ben}$$

$$= T_{rock\,wall} + \frac{\phi_0\,r_0}{\lambda_w}\,\ln\frac{r_{rock}}{r_{rock}-\delta_{pel}} + \frac{\phi_0\,r_0}{\lambda_{ben}}\,\ln\frac{r_{rock}-\delta_{pel}}{r_0+\delta_{air}}\,,$$

(A-4)

where $\delta_{air} = 10$ mm and $\delta_{pel} = 50$ mm are the widths of the air and pellet gaps, respectively. Due to the continuity of heat flux over the air gap, the heat flux can be written as ($\varepsilon_1 = \varepsilon_{copper} = 0.3$, $\varepsilon_2 = \varepsilon_{bentonite} = 0.8$)

$$\phi_0 = \lambda_{air}\frac{T_0-T_{0b}}{r_0\ln(1+\delta_{air}/r_0)} + \frac{\sigma\,(T_0^4 - T_{0b}^4)}{\dfrac{1-\varepsilon_1}{\varepsilon_1} + \dfrac{1}{F_{12}} + \dfrac{1-\varepsilon_2}{\varepsilon_2\,(r_2/r_1)}}$$

(A-5)

$$= [\frac{\lambda_{air}\,\delta_{air}}{r_0\ln(1+\delta_{air}/r_0)} + \delta_{air}\varepsilon_{tot}\sigma(T_0+T_{0b})\,(T_0^2+T_{0b}^2)]\frac{T_0-T_{0b}}{\delta_{air}}\,.$$

The outer radius of the model was set as 1.75 m and the temperature there was 27.820 °C.

In the canister area in the stationary state the radial temperature profile is parabolic and the temperature on the axis of symmetry is calculated as

$$T_{On\,axis} = T_{On\,surface} + \frac{1\,700\text{ W}}{4\,\pi\,H\,\lambda} = 100.729\,^{\circ}\text{C}$$

$$+ \frac{1\,700\text{ W}}{4\,\pi\cdot 4.752\text{ m}\cdot 2.82\text{ W/m/K}} = 100.802\,^{\circ}\text{C}$$

(A-6)

A separate small programme was made to perform analytical calculations under steady-state conditions by applying the above equations. Table A-1 shows that the numerical result is very accurate, although the mesh is very course.

Table A-1. Results of the analyses using the analytical and numerical model.

Point in Figure A-5 below	Distance from rotation axis [m]	Analytical temperature [°C]	Numerical temperature [°C]	Difference in temperatures [%]
1	1.75	27.820	27.820	
2	0.875	41.815	41.811	0.01
3	0.825	58.566	58.607	0.07
4	0.535	69.571	83.290	0.08
5	0.525	100.729	100.837	0.11
6	0	100.802	100.910	0.11

This test case shows the following:

- Operations related to the air gap with thermal radiation and the outer pellet slot work correctly in the numerical programme KAPSEL.

- Large differences between "element" sizes do not cause numerical inaccuracies. This means that control volume operations are programmed precisely over different materials and air and pellet gaps. An implicit approach is applied everywhere concerning, e.g., material-temperature-dependent properties and thermal radiation.

- A course mesh produces accurate results.

- Radial temperature gradients are accurate.

- This test case, with the two previous test cases, shows that the axisymmetric programme KAPSEL performs correctly.
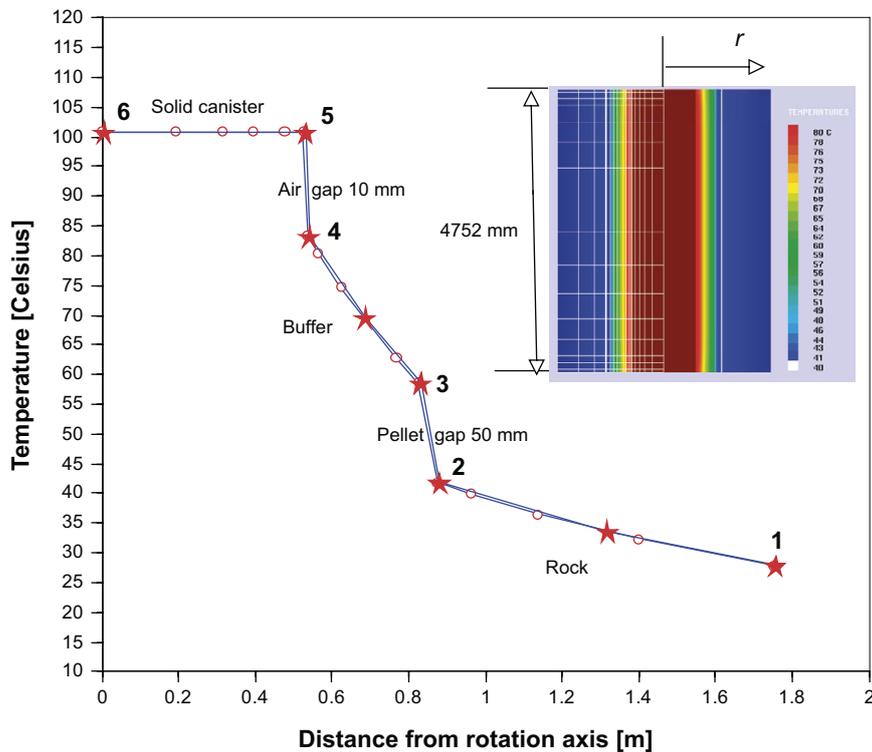
Figure A-5. *Uniform heat generation in a homogenous cylinder.*

A CO-OPERATION REPORT BETWEEN SVENSK KÄRNBRÄNSLEHANTERING AB AND POSIVA OY

SKB's and Posiva's programmes both aim at the disposal of spent nuclear fuel based on the KBS-3 concept. Formal cooperation between the companies has been in effect since 2001. In 2014 the companies agreed on extended cooperation where SKB and Posiva share the vision "Operating optimised facilities in 2030". To further enhance the cooperation, Posiva and SKB started a series of joint reports in 2016, which includes this report.